MODELING TRACE ELEMENTS OVER ATHABASCA OIL SANDS REGION IN ALBERTA, CANADA USING WRF-CHEM

JINGLIANG HAO

A DISSERTATION SUBMITTED TO THE FACULTY OF GRADUATE STUDIES IN PARTIAL FULFILLMENT OF THE REQUIREMENTS FOR THE DEGREE OF

DOCTOR OF PHILOSOPHY

GRADUATE PROGRAM IN EARTH AND SPACE SCIENCE

YORK UNIVERSITY

TORONTO, ONTARIO

June 2024

Abstract

The Athabasca Oil Sands Region (AOSR) in northern Alberta, Canada serves as a significant source of trace elements, potentially leading to adverse impacts on the human and ecosystem health. In this study, the Weather Research and Forecasting model coupled with chemistry (WRF-Chem) is modified to predict the transport and deposition of eight elements (Al, Ca, Fe, K, Mn, Si, Ti, and Zn) in the AOSR in 2016 and 2017. A recently developed regional-scale element emission database in the AOSR is used. The surface meteorological observations at a weather station in the center of the studied area are used for the model validation. The model has a good performance on the air temperature, wind at surface, and precipitation. Comparing with observed element concentrations at three monitoring sites, the percentage differences in the annually averaged concentrations of the eight elements between the model and the measurement are in the range of -6.9% to 76% (23% for eight elements together) at AMS1, -48% to 72% (25%) at AMS17, and -165% to 5.8% (-56%) at AMS18. Among the eight elements, the model simulations at the three sites have the smallest percentage difference for Ca (17%), followed by Al (31%), Si (37%), Fe (46%), K (58%), Ti (63%), Mn (66%), and Zn (92%). Modeled annually averaged concentrations and atmospheric deposition of individual elements range from 0.016 to 2.67 μg m^{-3} and 2.62 to 385 mg $m^{-2}yr^{-1}$ in the central region of the oil sands industry, respectively. The corresponding total annually averaged concentration and deposition for all eight elements are 5.98 μg m^{-3} and 862 mg $m^{-2}yr^{-1}$, respectively. Modeled element concentrations and deposition show a rapid decline by around three orders of magnitude from the central region to the remote region in a distance of around 150 km. Splitting the whole year into cold and warm seasons, the modeled total concentrations of the eight elements at three sites are overestimated by 82% in the cold season but underestimated by 38% in the warm season mainly due to the use of constant element emissions. The atmospheric stability also contributes to those seasonal variations.

In order to study how the model performance depends on the emissions and deposition mechanisms, two sensitivity tests over one full year period are conducted. In the first sensitivity test, the annual

emissions for all eight elements are reallocated to 30% in the cold season and 70% in the warm season. The seasonally varying emissions impose small impacts on the modeled annually averaged concentration and deposition either for each element or for eight elements in total. But it leads to a reduction in the bias for the modeled total concentrations of eight elements from 45% to 13% in the cold season and from 45% to 24% in the warm season. It suggests that seasonal varying emissions should be used in seasonal predictions of trace elements. In the second sensitivity test, Zhang et al. (2001)'s dry deposition scheme and Wang et al. (2014)'s wet deposition scheme are used instead of the original Binkowski's and Shankar (1995)'s and Slinn (1984)'s schemes in WRF-Chem. The modeled annual total dry and wet depositions of all elements are decreased by 56% and increased by 33%, respectively. The total dry&wet deposition is decreased by 31%. Given the significant change in deposition, direct measurement of depositions shall be considered in future field experiments. The measurements can be utilized to validate the numerical deposition schemes.

Acknowledgements

I would like to thank my supervisor, Prof. Yongsheng Chen, for his careful guidance, kind encouragement, and continuous suggestions in the four years of my PhD study. His wide tolerance and open-minded approach provided me a relax atmosphere, allowing me to transform my thoughts into the outcomes. During the revision of my thesis, he carefully read my whole thesis word by word and offered constructive comments and suggestions, which greatly improved my thesis.

Many thanks to my committee members, Dr. Mark Gordon and Dr. Leiming Zhang, for their valuable comments and suggestions throughout my study. In every committee meeting, they always gave me many insightful advice and critical feedbacks, freeing me out of confusions and ensuring my PhD progress smoothly.

I am grateful to my parents and wife for their unwavering understanding, patience, love, and support over the years. Their steadfast standing behind me became the significant power driving me to overcome the challenges and complete the PhD journey.

Table of Contents

2. Data and Model Description

3. Validation of Modeling Results

4. Temporal and Spatial Distributions

List of Abbreviation

Ag:	silver
Al:	aluminum
AMS:	air monitoring station
AOSR:	the Athabasca Oil Sands Region
As:	arsenic
Ba:	barium
Ca:	calcium
Cd:	cadmium
Co:	cobalt
Cr:	chromium
Cu:	copper
Fe:	iron
Ga:	gallium
In:	indium
K:	potassium
La:	lanthanum
Mg:	magnesium
Mn:	manganese
Mo:	molybdenum
Na:	sodium
Ni:	nickel
OS:	oil sands
P:	phosphorus
Pb:	lead
PBL:	planetary boundary layer
Pd:	palladium
PM:	particulate matter

$PM_{2.5}$:	particulate matter with diameters smaller than 2.5 um
$PM_{2.5-10}$:	particulate matter with diameters larger than 2.5 um and smaller than 10 um
PM_{10}:	particulate matter with diameters smaller than 10 um
Rb:	rubidium
S:	sulfur
Sb:	antimony
Se:	selenium
Si:	silicon
Sn:	tin
Sr:	strontium
SWE:	snow water equivalent
Ti:	titanium
V:	vanadium
WRF:	the Weather Research and Forecasting model
WRF-Chem:	the Weather Research and Forecasting model coupled with chemistry
Zn:	zinc
Zr:	zirconium

List of Statistical Quantities

1. the percentage difference

$$\text{percentage difference} = \frac{(\text{modeling}-\text{observation})}{0.5*(\text{modeling}+\text{observation})} * 100\% \quad (1)$$

2. the absolute percentage difference

$$\text{absolute percentage difference} = \left|\frac{\text{modeling}-\text{observation}}{0.5*(\text{modeling}+\text{observation})}\right| * 100\% \quad (2)$$

3. the percentage error (bias)

$$\text{percentage error} = \frac{\text{modeling}-\text{observation}}{\text{observation}} * 100\% \quad (3)$$

4. the root-mean-square error (RMSE)

$$\text{error} = \sqrt{\frac{\sum_{i=1}^{N}(\text{mod}-\widehat{\text{obs}})^2}{\text{N}}} \quad (4)$$

List of Tables

List of Figures

1. INTRODUCTION

1.1 Trace elements

There has been growing interest in air quality research on atmospheric particulate matter (PM), because of the potential effect of PM on the environment and human health. Atmospheric particulate matter is defined as a mixture of organic and inorganic chemicals, including major and trace elements, with emission from both natural and anthropogenic sources. These elements are metals, metalloids, or nonmetals. Elements emitting from natural processes, such as sea spray, biomass burning, and volcanic activity, are concentrated in the coarse PM ($PM_{2.5\text{-}10}$ with diameters of 2.5-10 μm) and giant PM (PM_{10+} with diameters > 10 μm), while elements originating from anthropogenic activities, such as fuel combustion, vehicle exhaust, and industrial production, are accumulated in the fine PM ($PM_{2.5}$ with diameters < 2.5 μm). The deposition of PM from the atmosphere to the surface leads to the accumulation of PM-bound elements in ecosystems. Despite the function of some elements (Co, Cu, and Mn) in the plant growth (Nagajyoti et al., 2010), other elements have detrimental impacts on human and ecosystem health (Wright et al., 2018). Impacts on humans include damage to the lungs and nervous system by Al (Krewski et al., 2007), damage to the kidneys and bones by Cd (Trzcinka-Ochocka et al., 2010), and damage to the lungs, nasal passages, and cardiovascular by Ni (Denkhaus and Salnikow, 2002). Risks to the health of ecosystems include effects on metabolic, reproductive, and breathing processes of mammals and birds by Al (Rosseland et al., 1990), effect on growth and reproduction of biota by Cd (Gallego et al., 2012), effect on metabolism, bone densities, growth, and survival of birds by Cr (Outridge and Scheuhammer, 1993).

Many trace elements are identified as toxic by government and international air quality agencies, such as the US Environmental Protection Agency (USEPA). The USEPA listed 13 metals or metalloids as priority pollutants, namely Sb, As, Be, Cd, Cr, Cu, Pb, Hg, Ni, Se, Ag, Tl, and Zn. Apart from these toxic elements, some other elements are also useful for air quality studies because of their use for pollutants source apportionment (Al-Momani et al., 2005; Mamun et al., 2020).

1.1.1 Source and distribution

Particulate elements originated from natural and anthropogenic sources have a wide range of particle sizes as soon as they are released. The coarse mode and fine mode of elements are from natural sources and anthropogenic emissions, respectively. Natural sources include sea spray (such as Na and Cl), biomass burning (such as Cd and K), volcanic activity (such as Si and Fe), and crustal erosion (such as Al and Ti) (Harrison and Yin, 2000; Bilos et al., 2001; Birmili et al., 2006; Makkonen et al. 2010; Charlesworth et al., 2011; Mooibroek et al., 2011). Anthropogenic emissions include fuel combustion (such as Cu and Ni), vehicle exhaust (such as As and Be), industrial sources (such as Cr and Se), and waste incineration (such as Pb and Tl) (Balasubramanian and Qian 2004; Al-Momania et al., 2005; Ioannidou, 2011; Moreno et al., 2011; Duan et al., 2012; Wang et al., 2016; Fomba et al., 2018). Many elements have been treated as tracers in environmental studies to identify their corresponding sources because of the uniqueness of those elements from different emissions, such as Cu and Sb from traffic related sources, Al from the crustal sources, Na from the sea spray, and V from oil combustion sources (Al-Momani et al., 2005; Mamun et al., 2020).

The size differentiated composition of PM provides information on the sources of particles, and on the effect of the sources on the atmospheric elements concentration (Al-Momania et al., 2005). The information of mass concentration in different size ranges is also important for air quality modeling researchers who make use of it to estimate dry deposition flux from the atmosphere to the surface. In the atmosphere, the concentration of elements is often a log-normal distribution rather than a normal distribution (Balasubramanian and Qian, 2004; Al-Momania et al., 2005). According to the mass concentration of elements in different size ranges of PM, Mamun et al. (2020) grouped elements into three groups, (1) elements in fine mode and from anthropogenic sources, (2) elements in coarse mode and from natural sources, and (3) elements in variable mode and from multiple competing sources. In the fine mode group, many elements have a tremendous part of their mass in the range of fine mode regardless of the locations, such as urban, suburban, and rural. Most of the 13 USEPA toxic elements, including Sb, As, Cd, Pb, Ni, Se, Ag, Tl, and Zn, are dominant in the fine mode and they mainly come from anthropogenic

emissions. Some elements are concentrated even in the submicron range, such as As, Be, Cd, Pb, and Se (Allen et al., 2001; Harrison et al., 2003; Samara and Voutsa, 2005). Some elements have a bimodal size distribution with the first peak at the fine mode and the second peak at the coarse mode, such as Ni and Zn (Mamun et al., 2020). It is reported that some elements of this group, such as Cd, Ni, and Zn, have higher accumulation in the fine mode during the cold season, but their overall size distribution does not have a seasonal variation (Song and Gao, 2011; Fomba et al., 2018). Although none of the 13 USEPA toxic elements is in the coarse mode group, elements (such as Al, Ca, Fe, Mg, and Na) belong to this group (Mamun et al., 2020). They primarily originate from the crustal source and they dominate in large particles. In addition, these coarse elements also come from combustion sources and industrial sources, such as the steel production and the metal refining. Elements in the coarse mode group may have a minor distribution in the fine mode, as a result of some anthropogenic emissions. For example, Pan et al. (2015) found that Al and Fe were concentrated in the coarse mode, but more than 10% of their masses were still in the submicron range.

In the variable mode group, the size distribution of elements has a significant variation over different sampling sites under the impact of various emission sources and under the seasonal impacts. Elements in this group come from both anthropogenic emissions and the crustal origin. Four of the 13 USEPA toxic elements, namely Be, Cr, Cu, and Hg, are categorized into this group (Mamun et al., 2020). Harrison et al. (2003) found that more than 70 % of the Be mass is in particles smaller than 2 μm in United Kingdom. However, Wang et al. (2016) reported that more than 60% of the Be mass is in particles larger than 2.1 μm based on four rural sites in China. The peak size distribution of Cr is throughout fine and coarse modes depending on the source. Oil combustions, metal industries, and the soil dust re-suspension process contribute to Cr in submicron, fine mode, and both fine and coarse modes, respectively (Samara and Voutsa, 2005). The size distribution of Cu also relies on sources, including brake and tire wear, fuel combustions, and soil dust re-suspension processes. Cu associated with soil dust re-suspension in suburban areas accumulates in the coarse mode, whereas Cu related with fuel combustion in urban and industrial areas

concentrates in the fine mode (Allen et al., 2001; Samara and Voutsa, 2005; Toscano et al., 2011; Malandrino et al., 2016; Zwozdziak et al., 2017). The size distribution of Hg is affected by particle partitioning, ambient particle concentrations, meteorological conditions (Kim et al., 2012). Many studies found that Hg was concentrated in the fine mode during winter time due to anthropogenic productions like the coal combustion for heating (Tsai et al., 2003; Gildemeister et al., 2005; Wang et al., 2006; Xiu et al., 2009; Arruti et al., 2010; Chen et al., 2016). On the contrary, Hg accumulates in the coarse mode during summer time, resulting from the transport of sea salt aerosols (Kim et al., 2012; Zhu et al., 2014). Apart from Be, Cr, Cu, and Hg, other major elements also have a variable size distribution for various sites, such as Cl, Mn, and K (Mamun et al., 2020).

1.1.2 Concentrations

The ambient concentration of elements is crucial to assess the immediate influence on environment and humans (Balasubramanian and Qian, 2004). The concentration of elements are closely related to their residence time and dry deposition. The residence time and dry deposition of elements are determined by their size distribution. Mamun et al. (2020) conducted a review of element concentrations in PM in North America, Europe, and Asia. Generally, they found that ambient element concentrations are higher in urban, industrial, and high-traffic areas than in the nonurban areas. The concentration of Zn was the highest among the 13 USEPA toxic elements, followed by Pb and Cu, in both $PM_{2.5}$ and PM_{10} ($PM_{2.5}$ + $PM_{2.5-10}$). The concentrations of Be, Tl, and Hg were the lowest. Among major elements, the concentration of S was the highest in both $PM_{2.5}$ and PM_{10}, and that of Co, V, and Ba were much lower. Si, Al, Ca, and Fe were enriched in PM and they are primarily originated from the crustal source.

Although the location of emission sources, the duration of emission, and the amount of elements emitted play a key role in element concentrations, the variation of element concentration on the daily and seasonal basis is attributable to the change of meteorological conditions. Diurnal and seasonal variations of element concentrations are different among different elements as a result of various sources and

meteorological conditions (Singh et al., 2002; Lim et al., 2006). Even when emission rate is relatively constant, a wide variation of element concentration from nighttime to daytime may be observed under different atmospheric stability. Mamun et al. (2020) concluded that the concentration of crustal elements, such as Fe, Mn, and Ca, was higher during daytime, whereas that of some elements, such as Pb, Cu, and Cd was higher during nighttime. Elevated element concentrations during daytime are caused by re-suspension of soil dust, while enhanced concentrations during nighttime are attributable to weaker pollutant dispersion under lower atmospheric boundary layer and stable atmospheric condition (Bilos et al., 2001; Chandra et al., 2017). Chandra et al. (2017) observed 1.3 and 1.9 times higher concentrations during daytime for Fe and Mn, respectively, and 2.4, 1.9, and 4.5 times higher concentrations during nighttime for Pb, Cu, and Cd, respectively. Singh et al. (2002) found that the diurnal variation of element concentrations in the coarse mode was dominant by wind speed, whereas that in the fine mode depended on sources and meteorological conditions. Wind speed had a stronger impact on the variation of elements from one stationary source and these elements were diluted more easily with increased wind speed (Al-Momania et al., 2005). However, Odabasi et al. (2002) found that there was no statistically significant relationship between measured element concentrations and wind direction. They also reported that the relationship between element concentrations and wind speed was not statistically significant for most of anthropogenic elements, whereas it was statistically significant for crustal elements. Wind speed accounted approximately 20–40% for the variation of ambient concentrations of crustal elements. Higher crustal elements concentration, such as Al, K, and Br, during summer was attributed to higher temperature and subsequent drier soil and more particle re-suspensions (Masri et al., 2015). Moreover, the seasonal variation is more obvious for anthropogenic elements than crustal elements (Al-Momania et al., 2005; Chandra et al., 2017; Mamun et al., 2020). Elevated anthropogenic element concentrations, such as Pb, are owing to more fossil fuel combustion for heating and thermal inversion near atmospheric boundary layer in winter (Moreno et al., 2011; Toscano et al., 2011; Duan et al., 2012).

1.1.3 Dry deposition

The impact of atmospheric PM on human health is evaluated by concentration, while that on the environment is evaluated by dry deposition rate and dry deposition flux. The dry deposition flux of elements in PM relates to emission source characteristics, the distance between receptor and source, the size distribution of elements, and meteorological conditions (Shahin et al., 2000; Sabin and Schiff, 2008). In general, dry deposition fluxes of trace elements tend to be higher in the industrial and urban areas than that in the rural and non-urban areas (Lim et al., 2006). Dry deposition rates of crustal elements are usually higher than that of anthropogenic elements, due to the size distribution of crustal elements concentrated in the coarse mode (Lim et al., 2006). Larger particles correspond to larger dry deposition velocity. Even with low concentrations, particles in the coarse mode dominate the dry deposition flux of the full size range because of the large size and large dry deposition velocity.

Diurnal variations of dry deposition flux are mostly in consistence among different elements and observation sites (Mamun et al., 2020). Enhanced dry deposition flux during daytime is caused by large wind speed and high concentration (Fang et al., 2004; Lim et al., 2006). The fluctuation of dry deposition flux is also stronger during the daytime because of larger variation of wind speed under unstable atmospheric conditions (Yi et al., 2001). The effect of wind speed and wind direction on dry deposition flux varies among different elements (Mamun et al., 2020). Unlike diurnal variations, seasonal variation of dry deposition flux for elements is inconsistent among different sampling sites, likely because of different concentrations and size distributions (Mamun et al., 2020). Odabasi et al. (2002) found that there was no significant seasonal variation in element dry deposition fluxes. There was no statistically significant relationship between flux and wind direction. The relationship between flux and wind speed was not statistically significant for anthropogenic elements, while it was statistically significant for crustal elements. Guo et al. (2017) reported that dry deposition fluxes of some elements, such as Cr, Co, and Ni, were larger in winter than that in summer. Cd and Pb had greater dry deposition fluxes in summer, whereas Zn and As had similar seasonal dry deposition flux. The difference in seasonal dry deposition flux among elements was attributable to meteorological conditions and emission sources.

At sampling sites, dry deposition flux of elements is directly measured through surrogate surfaces, including polyvinyl chloride (PVC) plates (Sabin and Schiff, 2008; Fang et al., 2011; Zhang et al., 2012), greased Mylar strips (Shahin et al., 2000; Yi et al., 2001), and water surface (Sakata and Asakura, 2011; Shi et al., 2012). However, the measurement of dry deposition flux using surrogate surfaces leads to many uncertainties. The surface roughness, the geometry of the surface, and the nature of used substrates have an impact on the wind profile and local turbulence around the surface, and thereby affect the actual flux (Shahin et al., 2000). Additionally, the presence of organic pollutants has an influence on the accumulation of elements on the surface (Mamun et al., 2020). As a result, large uncertainties can not be avoided among dry deposition flux measurements, even for the same observation site (Tasdemir and Kural, 2005).

The dry deposition rate of elements is also obtained from various dry deposition models. Dry deposition rate of one element is a product of measured concentration and modeled dry deposition velocity. Elements in wide ranges of size distribution have different dry deposition velocities (Shahin et al., 2000). The dry deposition velocity is related with meteorological conditions, such as atmospheric stability, ambient temperature, wind speed, and wind direction (Odabasi et al., 2002; Zheng et al., 2005; Tasdemir and Kural, 2005). The dry deposition velocity is also estimated by the ratio of measured dry deposition flux and measured concentration (dry deposition velocity = dry deposition flux/ concentration). Mamun et al. (2020) reported that the overall ranges of dry deposition velocity obtained from this ratio were consistent among different sampling times and regions. The anthropogenic elements, such as Pb, Cd, and V, whose size distributions concentrate in the fine mode, have a lower range of dry deposition velocity than crustal elements. It is anticipated that there are discrepancies between a measurement-derived dry deposition velocity and modeled one, because of large uncertainties in both measurements using surrogate surfaces and simulations using models. Their difference could be more than one order of magnitude (Odabasi et al., 2002).

1.1.4 Wet deposition

Wet deposition is another way to remove particulate elements from the atmosphere to the surface through precipitation scavenging. The precipitation scavenging includes in-cloud and below-cloud scavenging processes. The process where elements in the cloud become cloud condensation nuclei or are captured by cloud water, and then deposited to the surface is in-cloud scavenging. Below-cloud scavenging means that elements below the cloud are captured by falling raindrops and snow, and then deposited to the surface. Atmospheric wet deposition flux of elements has been measured in North America (Landing et al., 2010; Gratz et al., 2013), Europe (Montoya-Mayor et al., 2013; Cerro et al., 2020), the Middle East (Muezzinoglu and Cizmecioglu, 2006; Özsoy and Örnektekin, 2009), and Asia (Cong et al., 2010; Pan and Wang, 2015). The measurements of wet deposition for elements are limited in other regions. Generally, wet deposition fluxes of elements were highest in the Middle East, followed by Asia, Europe, and North America. Cheng et al. (2021) concluded that more than half of the wet deposition was contributed by crustal elements, compared with anthropogenic elements. The uncertainties in wet deposition monitoring of elements are caused by spatial and temporal data availability, precipitation type, and relative importance of in-cloud and below-cloud scavenging (Cheng et al., 2021).

In modeling studies, wet deposition flux of elements is calculated as a summation of in- and below-cloud scavenging processes. Current chemical transport models estimate the wet deposition flux from different size-resolved scavenging coefficients for rain and snow. The scavenging coefficient for only a few types of snow crystals are available because of limited experimental or field data. The uncertainties in wet deposition modeling of elements include scavenging ratios, airborne concentrations, and modeled precipitation rates (Cheng et al., 2021). There is not a large variability in the scavenging ratio of an element between different field studies measuring long-term averages. The scavenging ratios of different elements are strongly related to their particle sizes. There are also uncertainties on whether element concentrations in the surface are the same as those entering or below the cloud where precipitation scavenging is initiated (Cheng et al., 2021).

1.2 Modeling elements

There have been numerous observation campaigns for particulate elements in terms of their concentrations (Arruti et al., 2010; Subhash et al., 2017; Fomba et al., 2018) and deposition (Kyllönen et al., 2009; Cooke et al., 2017; Guo et al., 2017). The modeling without the limitation of monitoring locations and observation durations is another tool used for the study on the fate of elements in the atmosphere, and for the assessment of atmospheric elements deposition and subsequent environmental impacts. However, there have been limited applications of dispersion models and Eulerian air quality models on the simulation of elements. Diaz-De-Quijano et al. (2016) used a simplified geomatic model of particulate matter dispersion to identify the source of four elements (Cd, Zn, Pb, and Cu) and the distance of their dispersion to the emission sources in the peatlands of France. They suggested that the modeling performance of element estimations could be increased with some corrections to the dataset, such as using a dataset of diffuse element emissions. A Lagrangian dispersion model, CALPUFF, was used by Yang et al. (2023) to simulate 29 particulate elements and the modeled element concentrations were evaluated by comparing the modeling results with measured element concentrations at three sites locating at the oil sands region in Canada. The discrepancies between the simulations and the measurements were more pronounced in winter than that in summer because of a lack of temporal variations in the element emissions.

The Eulerian air quality models with more complicated physical and chemical algorithms are also used to study spatial and temporal changes of elements with size distributions by solving mass continuity equations, including emission, advection, diffusion, chemical reaction, and wet & dry deposition processes. A local air quality model, the Surface Meteorology and Ozone Generation (SMOG) air pollution modeling system, was used by Lu et al. (2003) to assess geographical distributions and deposition rates of 10 elements in Los Angeles Basin, United States. They showed a similar spatial pattern between the concentration and the deposition. There is no significant seasonal variation in spatial patterns in winter and summer. Hutzell and Luecken (2008) modified a regional off-line model, the Community Multiscale Air Quality (CMAQ) model, to include five elements, and simulated them over the continental United States.

The off-line model is computationally efficient because the simulations of meteorology and chemistry are separated. The simulation of meteorology is conducted prior to the simulation of chemistry, and the simulated meteorological results are used to drive the chemistry simulations. Through the comparison of simulated element concentrations with observed element concentrations, Hutzell and Luecken (2008) found that the model underestimated the elements and had a weak ability to produce the time dependence of element concentrations. Appel et al. (2013) simulated elements in the dust for the continental United States by CMAQ, and compared modeling results to the observation. The model performance in element concentrations was good in the western United States. But the model overestimated element concentrations in the eastern United States. Liu et al. (2019) reported the simulation of 11 elements in $PM_{2.5}$ over northern China by using CMAQ. By comparing with the observations, their simulations indicated that the model had the ability to generate the trend of concentrations, but underestimated the values of concentrations. The Goddard Earth Observing System coupled with Chemistry (GEOS-Chem), a global model, was used to simulate trace elements (Xu et al., 2019; Yan et al., 2022). The evaluation of modeled element concentrations against observations showed a spatial consistency and a discrepancy in values within a factor of two (Xu et al., 2019).

Among all the above modeling studies, only Appel et al. (2013) considered the sulfate chemistry with elements (Fe and Mn) in the atmosphere. They reported that particulate sulfate concentration in January was lower in the eastern US, but it only had small changes in the summer, after they updated concentrations of Fe and Mn into the sulfate chemistry. Other modeling studies assumed that there is no chemical reaction for elements due to limited knowledge of atmospheric chemistry for elements. The atmospheric chemistry may change the solubility of elements, and affect the subsequent atmospheric deposition (especially wet deposition) of elements. Thus the lack of considering atmospheric chemistry may impact model accuracy, but this impact is expected to be small.

1.3 Research in oil sands region

The Athabasca oil sands region in northern Alberta, Canada is one of the largest oil sand bitumen reserves in the world. The oil sands industry benefits Canada financially while it leads to potential environmental impacts. The oil sands in Alberta consist of sand, water, clay, and bitumen. Bitumen is a form of heavy crude oil and is comprised of particulate organic material, hydrocarbons, metals, and sulfur compounds. Development of the oil sands industry, including mining, processing, and tailings pond leakage, has caused concerns about the pollution. A substantial part of extracted bitumen is upgraded from heavy sour to light sweat synthetic crude at facilities in Alberta. The upgrading byproducts, such as petroleum coke and sulfur, are consolidated and stored in large stock piles on the ground of sites. Emissions from bitumen mining, upgrading, and storage of byproducts have been identified as sources of ambient PM in surrounding communities. The emissions from shovel and mine heavy hauler fleet operations consist of emissions from raw oil sands, haul road fugitive dust, and diesel engine combustion exhaust (Landis et al., 2019).

The Oil Sands Monitoring (OSM) project, a collaborative research by the government of Canada, the government of Alberta, and indigenous communities and industries, has initiated many studies with aim at understanding potential environmental impacts to the Athabasca Oil Sands Region (AOSR) by various pollutants, such as acidic chemicals (Shephard et al., 2015; Griffin et al., 2019; McLinden et al., 2020), polycyclic aromatic compounds (Galarneau et al., 2014; Cheng et al., 2018; Schuster et al., 2019), and mercury (Kirk et al., 2014; Willis et al., 2018; Wasiuta et al., 2019). Some studies have been conducted for elements in the AOSR with focus on the source apportionment (Phillips-Smith et al., 2017; Mamun et al., 2021), concentrations (Landis et al., 2017), and deposition (Bari et al., 2014; Shotyk et al., 2016; Cooke et al., 2017; Gopalapillai et al., 2019; Mamun et al., 2022).

The synthetic crude oil production from the bitumen in the AOSR is completed by using a combination of surface mining and in-situ manufacture. The elements emitted during these processes are dispersed in the atmosphere and subsequently removed through dry deposition and wet scavenging from the atmosphere to the surface, potentially resulting in side effects to the health of human and ecosystem.

Thus measuring element concentrations in the ambient air, identifying the relative contribution by different oil sands productions to observed element concentrations, and quantifying the atmospheric deposition are critical to the emission mitigation and locally environmental impact management. Landis et al. (2017) studied the observed elements in the AOSR during 1999-2015, and stated that crustal elements, such as Al, Ca, Fe, and Si, were less in winter when the ground was frozen and often covered with snow and were more in spring and fall when the wind speed were high. Elements used as markers of oil productions and oil combustions, such as V and Ni, were relatively steady in the whole year because of the continuous emission from the mining fleet and upgrading operations. Through the source apportionment, they found that the contribution from fugitive dust was minimal in winter when the ground, haul roads, overburden and byproduct stockpiles, and mine faces were frozen and covered by snow. The contributions of oil combustion and heavy hauler emission showed no significant seasonal trend. The biomass combustion impacts were highest in summer during wild fire season, but they also contributed significantly during winter when brush burning operations and residential wood heating was common.

Mamun et al. (2021) studied a total of 48 major and trace elements in $PM_{2.5}$ and $PM_{2.5-10}$ at the four air monitoring sites in the AOSR during 2016-2017. The most abundant element in $PM_{2.5}$ was S followed by crustal elements (Si, Ca, and Fe), whereas crustal elements Si, Al, and Ca were higher in $PM_{2.5-10}$ than other elements. In general, concentrations of most elements were comparable to or lower than their concentrations in other industry and urban sites in North America. In addition, the most of the 13 USEPA toxic elements in $PM_{2.5}$ were below detection limits. Concentrations of crustal elements, such as Si, Al, Ca, and Fe, in both $PM_{2.5}$ and $PM_{2.5-10}$ were generally higher during spring and summer, and lower in winter. The higher concentration of crustal elements in summer was related with the high summer temperature that led to enhanced particle re-suspension from the dust. Contrary to the crustal elements, most anthropogenic elements did not have any consistent or significantly seasonal variations. A few anthropogenic elements, such as Pb and Cd, showed higher concentrations in $PM_{2.5}$ during winter than during summer, possibly due to the increased biomass burning during winter, the winter temperature

inversion supporting the accumulation of anthropogenic emissions near the surface, and the seasonal transport of pollutants. Mamun et al. (2021) concluded that the oil sands industry had a clear impact on the element concentrations in the ambient air.

There is only one dispersion model called CALPUFF that has been used to study the spatial and temporal distribution of elements in the AOSR. CALPUFF is an advanced and integrated Lagrangian puff modeling system for the simulation of atmospheric pollution dispersion adopted by the USEPA in its Guideline on Air Quality Models (Yang et al., 2023). Yang et al. (2023) found that CALPUFF model underestimated elements in $PM_{2.5}$ during both summer and winter at Stoney Mountain. At Fort McKay and Wapasu Creek, the model overestimated Si, Ca, Al, Ti, Mn, Ba, and Sr in $PM_{2.5}$ by more than 50% during winter, but it underestimated these elements during summer. The model performance difference between winter and summer was partially due to a lack of seasonal variations in the element emissions input for the model. Yang et al. (2023) also plotted the spatial distribution of modeled As, Mn, and Ni concentrations. The maximum concentrations of these three elements were located around 15 km northwest of the center of the AOSR, and elevated concentrations of these three elements were restricted to the oil sands industry activities, indicating contributions by the oil sands industry to ambient air element concentrations.

Mamun et al. (2023) calculated annual element deposition fluxes through combining modeled element concentrations by CALPUFF (Yang et al., 2023) and the deposition framework in Mamun et al. (2022). The annual wet deposition was larger than the annual dry deposition for the elements. The deposition fluxes peaked around the center of the AOSR where the surface mining and oil sands industry activities took place, and then decreased by three orders of magnitude outward. About half of elements (Al, Ca, Cr, Co, Cu, Fe, Ni, K, Rb, Si, Sr, S, Ti, and Zn) had higher dry deposition during the warm season due to the elevated concentrations during the warm season. For most of the elements, the wet deposition was higher during the cold season or nearly the same in both seasons because wet scavenging of the particulate element by snow was approximately three times more efficient than by rain.

Elements enter aquatic ecosystem by surface runoff, atmospheric deposition, wastewater, and ground

water, in which elements interact with dissolved and particle organic matters. Gueguen et al. (2016) reported that the maximum element loadings were along river stations and northern transects. Approximate 60-70% of sampling stations along river and northern transects had the highest loading. This is because north-south prevailing winds of the oil sands region in winter caused effects on element deposition. Based on six samplings at tributaries, Kelly et al. (2010) found that concentrations of 13 USEPA priority toxic elements in water did not significantly increase from upstream sites to midstream and stream mouth sites, regardless of summer and winter. However, the concentrations of some priority toxic elements in tributary water significantly increased near oil sands development, and they were related with overall land development for oil sands. In winter, concentrations of some priority toxic elements, such as Hg and Tl, were two times greater in watersheds with more oil sands development. In summer, concentrations of priority toxic elements in more developed watershed were eight times greater than that in less developed watershed. At all midstream and stream mouth sites, Hg concentrations were greater in summer, whereas Sb, Cd, Cr, Pb, Ni, Ag, and Zn concentrations were greater in winter. Phillips-Smith et al. (2017) stated that the average concentrations of some elements measured in the Athabasca River region of Alberta was equal to or greater than that measured in urban and industrial sites in Canada. Huang et al. (2016) found that, in the Athabasca River during summer, concentrations of all priority toxic elements near developed areas were greater than that in upstream. At sites within the Athabasca Delta and downstream of development, concentrations of all priority toxic elements, except Be and Se, were greater than that in upstream. The most of Co and Pb were in the particulate phase (55-62%), while Cu and Ni were in the dissolved phase (63-72%) for all samples in summer including flood events. There was an elevated Hg concentrations in Athabasca River and it was attributable to expanding oil sands developments.

Spatial analysis indicated that some element deposition masses, such as Pb, Ni, and Be, decreased exponentially with distance from upgrading facilities (Gueguen et al., 2016). Some element deposition masses, such as As, Cd, and Cr, decreased exponentially with distance from the oil sands development and also increased locally near oil sands development because of emissions from land cleaning, mining, and

road dust. Some element deposition masses, such as Hg and Cd, were only from local sources. Gueguen et al. (2016) found that some element concentrations had a high level within a 60-80 km radius before they exponentially decreased to a relatively constant value. These elements included Al, Sb, As, Ba, Fe, Ni, Tl, Ti, and Zn. Some elements, such as Cd, Cl, Cr, and Sr, had no significant trend of concentration with distance, reflecting that they did not originate from oil sands operation facilities. Huang et al. (2016) stated that there were three main elemental groups, including oil sands mining source (Al and Fe), oil processing source (Ni), and biogeochemical processes (Pb and Zn). The concentrations of oil sands mining group had an exponentially decrease with distance from the mining sites. The concentrations of oil processing group were more spatially homogeneous than that of oil sands mining group because elements in the oil processing group were related with emission of fine particles.

Hg is released to the atmosphere during oil sands processing and deposits to water and land, where Hg is methylated by bacteria to more biological accessible methyl-Hg. Methyl-Hg is a neurotoxin that bioaccumulates through food chain, and thereby reaches toxic levels in higher trophic level, such as fish. The deposition of total Hg was up to 1000 ng m^{-2} with most of it bound to particles, and its loading was larger with increased proximity to oil sands region (Huang et al., 2016). The maximum deposition of Methyl-Hg and total Hg was primarily located at the north of Alberta oil sands region. Huang et al. (2016) also found that Hg concentration was similar to background values observed in previous studies from remote areas, and was much smaller than values measured from industrial sources. The overall spatial distribution of Hg was not significantly affected by oil sands development. On the contrary, the three-month averaged deposition of some priority elements at the near sites was higher than that at the distant sites.

Phillips-Smith et al. (2017) found that average concentrations of some elements from a long-term campaign covering two years were lower than that from one specific observation at one site. This is because a specific measurement is affected by many anthropogenic activities, such as traffic and industry. From a long-term campaign, S, K, Zn, Br, Cd, and Pb are all associated with biomass burning. Landis et al. (2018)

stated that some elements, such as Zn, As, Cd, and Pb, were significantly enhanced during wildfire. The effect of wildfire on Sb, Cd, and Pb was more than doubled their respective annual time-weighted concentrations, suggesting that the annual variability of these elements might be driven by local and regional wildfire.

1.4 Objectives of this research

The literature review above mentions many observation campaigns over the AOSR for the research on particulate elements in terms of their source apportionment, concentrations, and deposition. However, the measurements of element concentrations were limited at monitoring stations, and the element deposition was investigated for the limited temporal scale with only wintertime or the limited spatial coverage at some sampling sites. In addition, there was only one dispersion model that has been used to simulate elements over the AOSR to assess the environmental impacts by oil sands industry. Therefore, a comprehensive element modeling study by using an air quality model over the AOSR and its surroundings on a yearly basis is necessary to reveal spatial and temporal effects of industrial activities on the ecosystem. In this study, a regional on-line air quality model, the Weather Research and Forecasting model coupled with chemistry (WRF-Chem), was used for the simulation of eight trace elements (Al, Ca, Fe, K, Mn, Si, Ti, and Zn) over the AOSR. The emission, transport, and dry & wet deposition processes in WRF-Chem were modified to include these elements, and the stack and area emissions of elements in $PM_{2.5}$ and $PM_{2.5-10}$ over the AOSR were prepared. The goals of present study were to (1) validate modeled meteorological conditions with meteorological observations, (2) evaluate the modeling performance on modeled element concentrations against in-situ observations, (3) investigate the spatial and seasonal distribution of modeled element concentrations and deposition in the AOSR, (4) explore the sensitivity of modeled concentrations to the seasonally varied element emissions, and (5) assess the uncertainty of modeled deposition using different deposition schemes.

2. Data and Model Description

In this chapter, the reason for the selection of eight elements for simulations is discussed. In order to simulate elements, some modifications to WRF-Chem are made to include elements for their emission, transport, and deposition. The WRF-Chem configurations, meteorological and chemical input data, and element emission database are presented. To validate modeling results, observations of meteorological data at a weather station and element concentrations at air monitoring sites are discussed. Two sensitivity tests are designed to investigate the sensitivity of modeled concentration and deposition to emission database and deposition schemes.

2.1 Element species

The element emissions inventory for 33 elements (Al, Ag, As, Ba, Ca, Cd, Co, Cr, Cu, Fe, Ga, In, K, La, Mg, Mn, Mo, Na, Ni, P, Pb, Pd, Rb, S, Sb, Se, Si, Sn, Sr, Ti, V, Zn, and Zr) over the AOSR (Yang et al., 2023) is considered in this study. Fig. 2.1 shows the total emission rate for each of the 33 elements in $PM_{2.5}$ and $PM_{2.5-10}$. Eight trace elements, namely Al, Ca, Fe, K, Mn, Si, Ti, and Zn, are selected for the simulation because of their highest emission rates among the 33 elements. S is not considered because it is a major element. In order to facilitate the evaluation of modeled element concentrations against observations, Mg, Ba, and P are not chosen due to their unavailability of observed concentrations in the database for $PM_{2.5-10}$. The emission rates for the eight elements in $PM_{2.5}$, $PM_{2.5-10}$, and PM_{10} are show as Table 2.1. Among the eight elements, the total emission rate of Si is the highest at 144 g/s, followed by Ca, Al, Fe, K, Ti, Mn, and Zn. The emission rates of the eight elements in $PM_{2.5}$ are comparable to some industrial areas in the United States, around 10 times larger than the eastern United States, and around 100 times larger than the western United States (Reff et al., 2009). The emission rates of the six elements (Ca, Al, Fe, K, Ti, and Mn) in PM_{10} are comparable to their emission rates in the dust source region in East Asia (Xuan, 2005), and emission rates of Mn and Zn in PM_{10} are similar to that from industrial sources in Greater Mumbai, India (Bhanarkar et al., 2005).

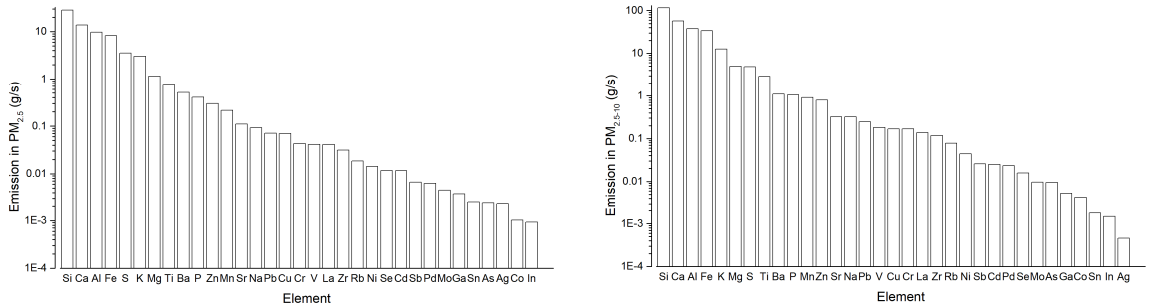

Figure 2.1 Total emission rate (g/s) for 33 elements in $PM_{2.5}$ and $PM_{2.5-10}$ in the AOSR.

Table 2.1 The emission rate (g/s) for the eight elements in $PM_{2.5}$, $PM_{2.5-10}$, and PM_{10}.

Particle size	Si	Ca	Al	Fe	K	Ti	Mn	Zn
$PM_{2.5}$	28.16	13.76	9.68	8.25	3.03	0.74	0.22	0.3
$PM_{2.5-10}$	116.17	56.92	37.43	33.59	12.66	2.9	0.92	0.8
PM_{10}	144.33	70.68	47.11	41.84	15.69	3.64	1.13	1.1

2.2 WRF-Chem model

The Weather Research and Forecasting model coupled with chemistry (WRF-Chem) is a regional on-line air quality model that simulates various processes relevant with meteorology and chemicals in the atmosphere across scales from tens of meters to thousands of kilometers. Contrary to off-line models, WRF-Chem is an on-line model that requires initial & boundary condition data for both meteorology and chemistry as model input. WRF-Chem predicts meteorology and chemistry simultaneously, reflecting the interaction between meteorology and chemistry, such as the direct and indirect effects on the cloud by aerosols. WRF-Chem is a flexible model with multiple choices for gaseous phase chemistry, aerosol

chemistry, dry deposition schemes, photolysis schemes, biogenic emissions, and anthropogenic emissions. The application of WRF-Chem includes the prediction of local and regional weather and climate, the simulation of release and dispersion of pollutants, and the analysis of aerosol direct and indirect forcing for global climate change issues.

The mass conservation dynamics equation for aerosols in WRF-Chem is

$$\frac{\partial}{\partial t}M = -\nabla \cdot (vM) - \frac{\partial}{\partial \sigma}(\sigma M) + \left(\frac{\partial M}{\partial t}\right)_{diff} + Cond + Coag + E\,, \tag{2.1}$$

where M is the mass of aerosols, t is the time, v is the horizontal wind, and σ is vertical coordinate (Binkowski and Shankar, 1995). The first three terms on the right side of Eq. (2.1) stand for the transport by horizontal wind, the transport by vertical wind, and turbulence diffusion, respectively. The dry deposition of aerosols near the surface is taken into account as a lower boundary condition in the turbulence diffusion term. The last three terms in the Eq. (2.1) represent condensation growth, coagulation, and source emissions.

2.3 Model modifications

After particulate elements emit from the stack and area emission sources, they move up into the atmosphere through vertical diffusion and advection (Fig. 2.2). They experience transport with other aerosols in the form of air phase (dry particles), and some elements become aqueous phase when aerosols get into the cloud and are attached with cloud droplets. The elements in the cloud are removed by in-cloud wet scavenging when rain droplets or snow particles appear, and elements in the air are either removed by below-cloud wet scavenging when rain droplets and snow particles fall or removed by dry deposition processes.

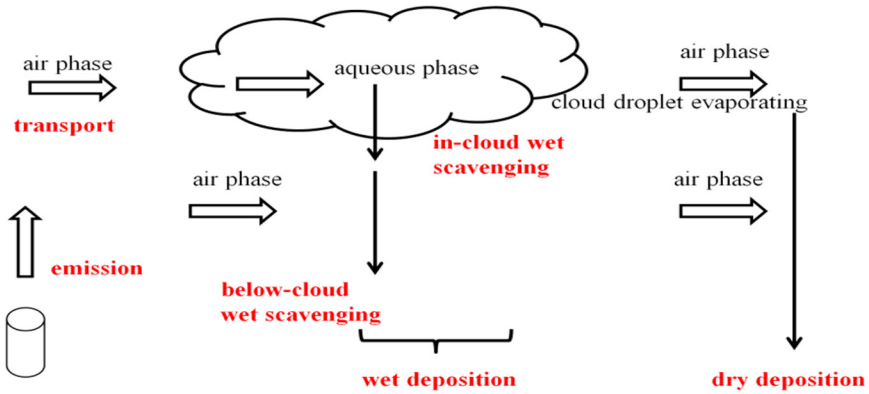

Figure 2.2 Processes related with elements in the atmosphere.

In this study, the Model for Simulating Aerosol Interactions and Chemistry (MOSAIC is selected as the aerosol chemistry module in WRF-Chem. In MOSAIC, the aerosols are separated by their effective diameters into four size bins (0.039–0.156, 0.156–0.625, 0.625–2.5, and 2.5–10 μm) with a log-normal distribution. The eight elements (Al, Ca, Fe, K, Mn, Si, Ti, and Zn) are added into these four bins. MOSAIC requires some constants of aerosol properties (including density, molecular weight, and hygroscopicity) and values of eight elements are set as in Table 2.2. The dry density comes from https://www.angstromsciences.com/density-elements-chart, and the molecular weight is from https://iupac.qmul.ac.uk/AtWt/. The hygroscopicity is defined as the ability to absorb moisture from the environment and is determined based on the solubility of elements, as discussed in Cheng et al. (2021). In addition, emission, transport, dry deposition and wet scavenging processes in WRF-Chem are modified to include eight elements for the simulation. The detailed modifications to WRF-Chem can be found in the Appendix. Due to the limited knowledge on the atmospheric chemistry for these eight elements, the assumption of no chemical reaction is made in this study. The same assumption has been used in other modeling research (Lu et al., 2003; Hutzell and Luecken, 2008; Xu et al., 2019).

Table 2.2 Constants of eight elements in WRF-Chem.

Elements	Dry density (g/cm^3)	Molecular weight (g/mol)	Hygroscopicity (dimensionless)
Al	2.70	26.982	0.068
Ca	1.55	40.078	0.5
Fe	7.87	55.845	0.068
K	0.89	39.098	0.35
Mn	7.21	54.938	0.25
Si	2.33	28.085	0.068
Ti	4.51	47.867	0.068
Zn	7.14	65.38	0.35

2.4 Model configurations

WRF-Chem version 4.2.1 is used for the simulation of eight elements, i.e., Al, Ca, Fe, K, Mn, Si, Ti, and Zn, over the AOSR over a two-year period from January 1, 2016 to December 31, 2017 (2016-01-01_06Z to 2018-01-01_06Z in WRF-Chem). The simulation timestep is set as 30 seconds and the modeling results are output every hour. The initial and boundary meteorological conditions are reinitialized every three months in the simulation, in order to reduce the deviation of simulated meteorological conditions. Fig. 2.3 shows the two nested domains in WRF-Chem. The horizontal resolutions are 9 km for the outer domain covering Alberta and 3 km for the inner domain covering the AOSR. There are 43 vertical levels with the lowest level at around 3 m above the surface. The gaseous and aerosol chemistry modules are the Carbon Bond Mechanism version Z (CBMZ) and the Model for Simulating Aerosol Interactions and Chemistry (MOSAIC) with four bins, respectively. The CBMZ is able to simulate organic and inorganic chemistry for gaseous species, such as nitrogen oxides, sulfur oxides, carbon oxides and volatile organic compounds (Zaveri and Peters, 1999). The MOSAIC deals with the complex physical & chemical behavior

of major aerosols, such as sulfate, nitrate, ammonium, black carbon, organic carbon, and mineral dust (Zaveri et al., 2008).

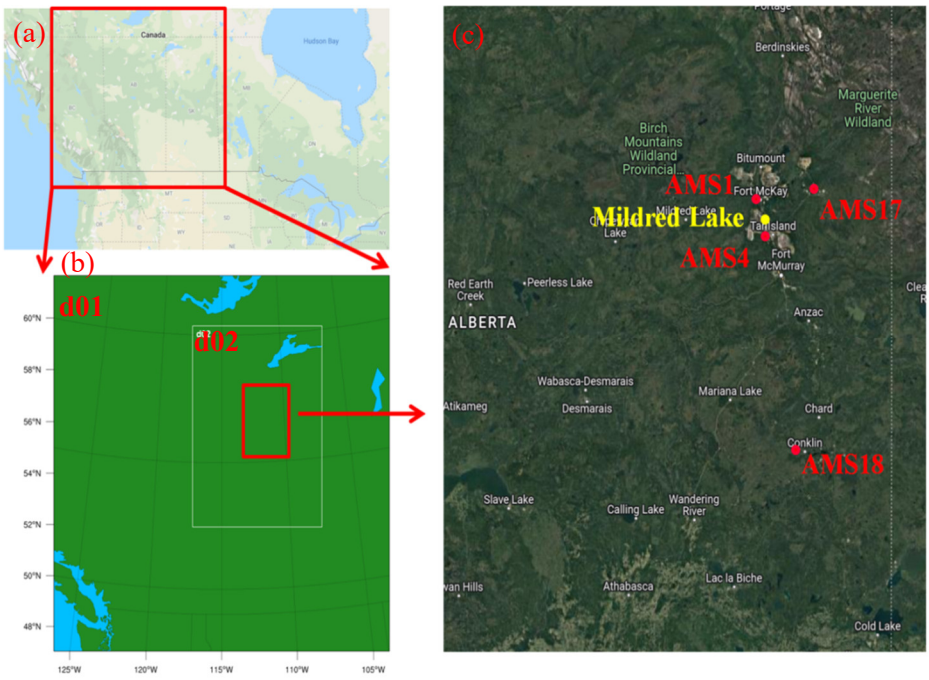

Figure 2.3 The two domains (d01 & d02) in WRF-Chem and observation sites (Mildred Lake, AMS1, AMS4, AMS17, and AMS18) in the AOSR (from Google Maps).

The default below-cloud scavenging scheme by Slinn (1984) and aerosol dry deposition scheme by Binkowski and Shankar (1995) are used in this study. The aerosol dry deposition (F) is a production of aerosol concentration (C) and dry deposition velocity. In Binkowski and Shankar's dry deposition scheme, the dry deposition velocity (V_d) is calculated as

$$F = V_d \cdot C$$

$$V_d = V_g + \frac{1}{R_a + R_s + R_a R_s V_g} \tag{2.2}$$

where V_g is the gravitational settling velocity, R_a is the aerodynamic resistance, and R_s is the surface resistance. The aerodynamic resistance describes the resistance for aerosol particles when they are transported from the atmosphere to the surface by turbulence. It indicates how efficiently particles can

move through the air near the surface. It depends on some factors, such as atmospheric stability, wind speed, and surface roughness. The surface resistance describes the resistance for aerosol particles when they start to interact with the surface. In the surface resistance, Binkowski and Shankar (1995) considered Brownian diffusion, interception and impaction for aerosols. Brownian diffusion means that aerosol particles are collected by the surface due to collisions under random motion. Impaction occurs when aerosol particles deviate from the airflow due to their inertia and impact onto the surface directly. Interception happens when aerosol particles follow the airflow and touch with the surface because of the size of particles. The removal of aerosols by below-cloud scavenging depends on aerosol concentration and scavenging coefficient (Λ) as

$$\frac{\partial n}{\partial t} = -\Lambda \cdot n \tag{2.3}$$

where n is the concentration for aerosols and t is time. Slinn (1984) provided a theoretical formula for Λ as

$$\Lambda(d) = \int_0^\infty A(d, D_p)(V_D - v_d)E(d, D_p)N(D_p)\, dD_p \tag{2.4}$$

where d is the diameter of aerosol, D_p is the diameter of raindrop, A is the effective cross-sectional area of a falling raindrop, V_D and v_d are the terminal velocities of raindrop and aerosol particle, respectively, E is the collection efficiency between an aerosol particle of size d and a raindrop of size D_p, N is the number size distribution of raindrops related with the precipitation rate. In the collection efficiency, Slinn (1984) considered three important collection mechanisms, namely, Brownian diffusion, interception, and impaction. Similar to Eq. 2.2, these collection mechanisms occur between particles and water droplets.

The physical schemes selected in WRF-Chem are given in Table 2.3. The microphysics scheme is from Lin et al. (1983). The longwave and shortwave radiation schemes are RRTM (Mlawer et al., 1997) and Goddard (Chou and Suarez, 1999), respectively. The surface layer follows the Monin-Obukhov Similarity (Monin and Obukhov, 1954). The YSU boundary layer scheme (Hong et al., 2006) and Noah land surface model (Chen and Dudhia, 2001) are selected. The cumulus scheme uses Grell 3D ensemble

(Grell and Freitas, 2014). These physical schemes are selected because of their common usage in the research community (Kalenderski et al., 2013; Fountoukis et al., 2016; Zeng et al., 2020; Ren et al., 2023).

Table 2.3 The physical schemes in WRF-Chem.

Physics description	Schemes	References
microphysics	Lin et al.	Lin et al., 1983
longwave radiation	RRTM	Mlawer et al., 1997
shortwave radiation	Goddard	Chou and Suarez, 1999
surface layer	Monin-Obukhov Similarity	Monin and Obukhov, 1954
land surface	Noah	Chen and Dudhia, 2001
boundary layer	YSU	Hong et al., 2006
cumulus	Grell 3D ensemble	Grell and Freitas, 2014

Table 2.4 shows meteorological and chemical input data for WRF-Chem. The meteorological initial and boundary conditions are produced using the NCEP (National Centers for Environmental Prediction) 6-hourly operational global FNL (Final) analysis data with the horizontal resolutions of 0.25° × 0.25°. The temperature, humidity, horizontal wind, cloud water mixing ratio, and geopotential height over the globe on 26 mandatory vertical levels from 1000 millibars to 10 millibars are interpolated onto the WRF-Chem grid. Details of the data can be found at https://rda.ucar.edu/datasets/ds083.3/. The chemical initial and boundary conditions are generated from the Community Atmosphere Model with Chemistry (CAM-chem) 6-hourly output with the horizontal resolutions of 0.9° × 1.25° (https://www.acom.ucar.edu/cam-chem/cam-chem.shtml). The anthropogenic emission comes from the REanalysis of the TROpospheric chemical composition (RETRO) with the resolutions of monthly and 0.5° × 0.5°. The biogenic emission is from the Model of Emissions of Gases and Aerosols from Nature (MEGAN) with the resolutions of

monthly and 0.5° × 0.5°. The boundary conditions for chemistry and emissions are determined from the above corresponding data. The boundary condition for elements is set as the default background value (extremely small) defined by WRF-Chem, because only element emission database in the AOSR are available.

Table 2.4 The input data for WRF-Chem.

Input data	Sources
meteorological initial & boundary	NCEP FNL (Final) operational global data
chemical initial & boundary	the Community Atmosphere Model with Chemistry (CAM-chem) output
anthropogenic emission	the REanalysis of the TROpospheric chemical composition (RETRO)
biogenic emission	the Model of Emissions of Gases and Aerosols from Nature (MEGAN)

2.5 Element emissions

The element emissions inventory for eight elements (Al, Ca, Fe, K, Mn, Si, Ti, and Zn) over the AOSR is based on $PM_{2.5}$ and $PM_{2.5-10}$ emissions from the Joint Canada-Alberta Implementation Plan for Oil Sands Monitoring (JOSM) air emissions inventory. The PM emissions include stack and area emissions. They are grouped into nine source sectors, including (1) agriculture, (2) biogenic-vegetation and soil, (3) non-OS (non-oil sands) dust, (4) electric power generation, (5) industrial processes and fuel combustion, (6) residential wood burning, (7) OS sources, (8) waste disposal, and (9) other industrial and miscellaneous sources. The elements are extracted from $PM_{2.5}$ and $PM_{2.5-10}$ emissions with a speciation cross reference table and then are gridded by the Sparse Matrix Operator Kernel Emissions tool (Yang et al., 2023). The

total emissions of the eight elements in the AOSR are shown in Fig. 2.1. Because stack and area element emissions belong to the annual emission inventory, they are split equally for each month as the element emissions (hence a constant emission rate). The gridded element emission rates in the unit of ug $m^{-2}s^{-1}$ are input into WRF-Chem. In the simulation at each grid point, WRF-Chem will calculate the element emissions at every model time step (30 seconds). The seasonal variations in element emissions will be considered in Chapter 5.

For anthropogenic stack emissions, the plume rise is not simulated in WRF-chem, potentially leading to the overestimation of elements near the surface. In order to reduce the modeling errors caused by the plume rise, when the stack emission of elements is prepared, the plume-rise algorithm by Briggs (1969) is used as

$$H = (3 \cdot D_S \cdot V_S)/U \tag{2.5}$$

where H is plume-rise, D_S is stack diameter, V_S is plume velocity at stack outlet, and U is horizontal wind speed in climatology. This formula is an empirical equation developed based on the experiment in the wind tunnel. The plume-rise is reasonable under the neutral condition of the atmosphere (Briggs, 1969). This algorithm is also used in the emission processing program called "emiss_v04" developed by NOAA (National Oceanic and Atmospheric Administration, United States) in the WRF-Chem modeling system. The spatial distribution of stack emissions for the eight elements in PM_{10} is shown in Fig. 2.4. There are more stack emissions for Ca, Fe, and Zn. The spatial distribution of stack emissions is different for each individual element. However, the major stack emission is always close to AMS1, AMS4, and AMS17.

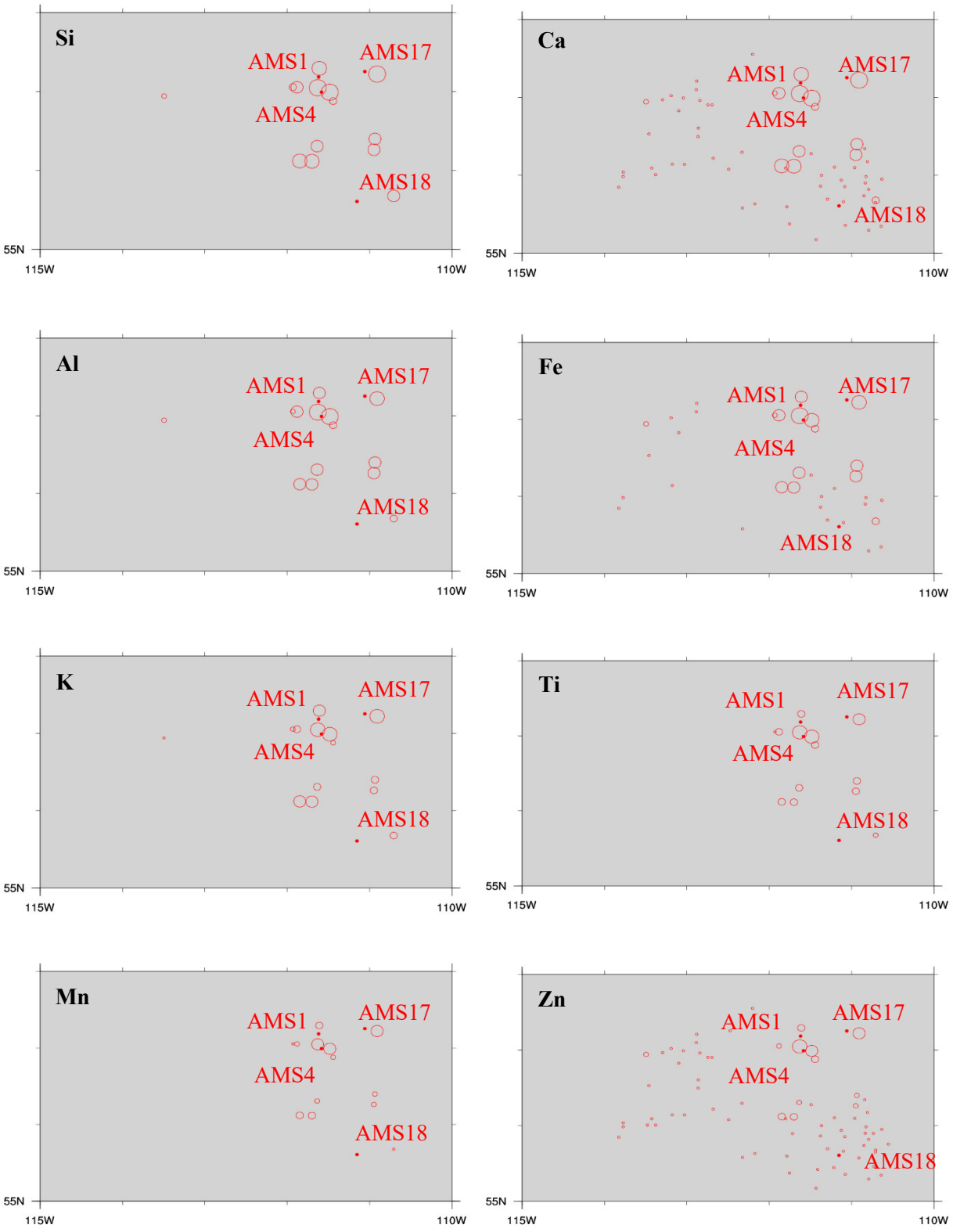

Figure 2.4 The spatial distribution of stack emission for the eight elements in PM_{10} (four red dots for AMS sites; larger circles for higher stack emission rates).

The area emission of Al, as an example, is showed in Fig. 2.5. The emission is restricted in the AOSR because the emission data are extracted from $PM_{2.5}$ and $PM_{2.5-10}$ emission inventory by the JOSM in the AOSR. The spatial distributions of Al emission in $PM_{2.5}$ and $PM_{2.5-10}$ are similar. Both emission rates peak in the center of oil sands industry area with a maximum value of 0.46 ug $m^{-2}s^{-1}$ and 0.83 ug $m^{-2}s^{-1}$, respectively. The emission in $PM_{2.5-10}$ is larger than that in $PM_{2.5}$ by around a factor of two. The emission pattern generally shows the roads with hotspots related to oil sands facilities. All other elements have the similar spatial distribution of area emissions as Al, but their magnitudes of emission rates are different from Al.

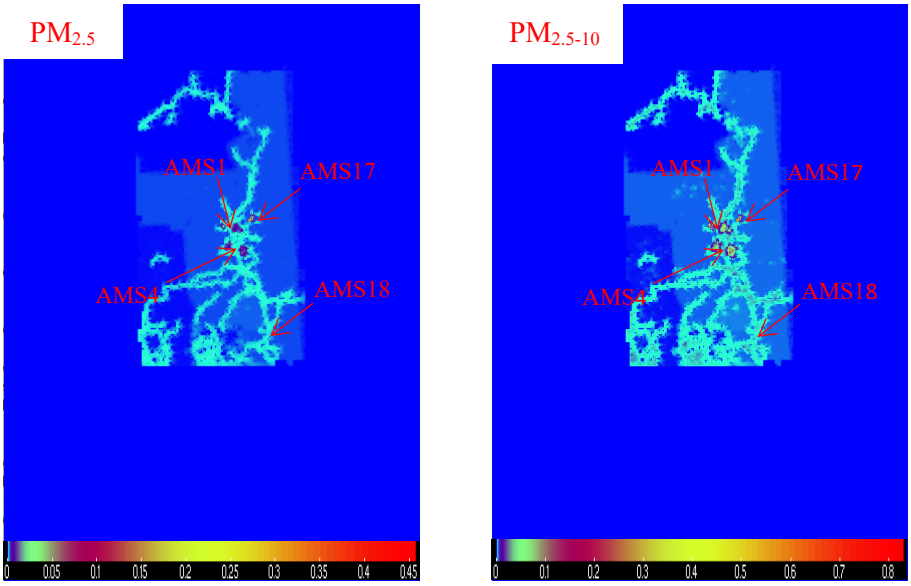

Figure 2.5 The spatial distribution of area emission (ug m^{-2} s^{-1}) for Al in $PM_{2.5}$ and $PM_{2.5-10}$ (maps with domain d02 in Fig. 2.3b).

2.6 Model validations

The model performance on element simulations is evaluated by comparing with the field measurement at air monitoring stations (AMS's, Fig. 2.3c) in the AOSR where only the element concentrations are measured. There are four AMS sites located in the AOSR. At each site, particulate matters were collected by a dichotomous sampler (Partisol 2000-D, Thermo Scientific, Waltham, MA) on 47 mm PTFE filters

(Pall Corporation, New York). The samplers were operated once every 3 or 6 days with a 24-hour sampling time (midnight to midnight) following the National Air Pollution Surveillance (NAPS) program protocol, set by the Environment and Climate Change Canada. In the dichotomous sampler, a virtual impactor splits the incoming PM_{10} into fine ($PM_{2.5}$) and coarse ($PM_{2.5–10}$) fractions. Mass flow controllers maintained the flow rates of the fine and coarse particle streams at 15L/min and 1.7L/min, respectively. All samples were subsequently analyzed for elements using spectrometry (Epsilon 5 EDXRF, Malvern Panalytical Inc., Longmont CO, USA & ICP-MS; AgilentTechnologies, Wilmington, DE, USA). However, the measurement at AMS4 (Buffalo Viewpoint; 56.99667° N, -111.5925° W) is not considered for the comparison because it is available only for a few months. The element concentrations in $PM_{2.5}$ and $PM_{2.5-10}$ at AMS1 (Fort McKay; 57.18941° N, -111.6405° W) and AMS18 (Stoney Mountain; 55.62141° N, -111.1727° W) are observed every 3 days during 2016-2017, while that at AMS17 (Wapasu Creek; 57.26176° N, -111.0370° W) are every 6 days during 2016-2017. The elements in the ambient air at AMS1, AMS17, and AMS18 are observed at a height of roughly 3 m above the ground, agreeing with the lowest vertical level in WRF-Chem. The three sites, AMS1, AMS4, and AMS17, are within 45 km of each other and surrounded by many in-situ surface mining and oil sands operations facilities. AMS18 is over 150 km further from the major oil sands operation facilities. It represents the background condition of the AOSR because it is far away from the major oil sands industry and surrounded by several thermal in-situ bitumen extraction facilities.

The modeled meteorological conditions (air temperature, precipitation, wind speed, and wind direction) at the lowest model level (around 3 m) are validated through the comparison of modeled meteorology at the closest grid to AMS4 and observed weather conditions at the Mildred Lake weather station (57.0333° N, -111.5667° W) (Fig. 2.3c). The hourly meteorological measurement data at Mildred Lake are provided by Agriculture and Irrigation, Alberta Climate Information Service (ACIS) (https://acis.alberta.ca). The distance between AMS4 and Mildred Lake is only 4 km. The elevations of AMS4 and Mildred Lake are 320 m and 310 m, respectively (found at https://natural-

resources.canada.ca/science-and-data/science-and-research/earth-sciences/geography/topographic-information/web-services/elevation-api/17328).

2.7 Sensitivity test designs

Two sets of sensitivity experiments, an emission sensitivity test and a deposition sensitivity test, are designed to examine the sensitivity of simulated element concentration and deposition to emission seasonal variation and deposition schemes. Both the emission test and the deposition test are simulated by WRF-Chem in one-year period of 2017. The one-year period of 2016 is not selected because of a big forest fire occurring near the AOSR in May-June of 2016. This forest fire causes some impacts to the observed element concentrations (mainly K). To reduce the effect of the forest fire, the observed element concentrations during the forest fire period should be ignored and there will be less observed element concentrations data available in 2016. In the base case of simulation described above, the annual element emissions are equally split into each month. However, dust is a significant source for the elements in the AOSR (Mamun et al., 2021), and many observations indicate that the snow coverage during winter seasons suppresses the re-suspension of dust (Kyllönen et al., 2009; Phillips-Smith et al., 2017; Landis et al., 2019). It subsequently reduces the element emission from the surface. In the emission sensitivity test, 40% of element emissions in the cold season are relocated to the warm season. It leads to 30% and 70% annual emissions in the cold and warm seasons, respectively. Because of the high latitude of the AOSR, the definitions of warm season (May to October) and cold season (November to April) are used in this study following Cheng et al. (2018). This definition also agrees with meteorological conditions in the AOSR (Fig. 3.1-3.2). The monthly average surface temperature is above 0 °C from May to October. The snowfall mostly happens from November to April.

In the deposition sensitivity test, the default aerosol dry deposition scheme by Binkowski and Shankar (1995) is changed to aerosol dry deposition algorithm described in Zhang et al. (2001). The reason for this selection is that the latter one is the most widely used size-resolved particle dry deposition scheme and is

considered to provide reasonable dry deposition velocity (V_d) for $PM_{2.5}$. Binkowski and Shankar (1995) considered gravitational settling, Brownian diffusion, interception, and impaction processes for aerosol dry deposition velocity (Eq. 2.2). Zhang et al. (2001) estimated aerosol dry deposition velocity as

$$V_d = V_g + \frac{1}{R_a + R_s} \tag{2.6}$$

where V_g is the gravitational settling velocity, R_a is the aerodynamic resistance, and R_s is the surface resistance. In the surface resistance, Zhang et al. (2001) also considered Brownian diffusion, impaction, and interception processes, but the formulas of these processes are different from that in Binkowski and Shankar (1995). When particles move along with air flow and touch obstacles (such as trees) near surface, they will be collected by these obstacles through Brownian diffusion, impaction, and interception, and then deposit to the surface. The default below-cloud scavenging scheme by Slinn (1984) is replaced by a semi-empirical parameterization in Wang et al. (2014). The reason for the selection is that this semi-empirical formula is developed based on five existing theoretical below-cloud scavenging frameworks, including the theoretical formula by Slinn (1984) (Eq. 2.3). Wang et al. (2014) calculated scavenging coefficient (Λ) for rain as

$$\Lambda(d, R) = A(d) R^{B(d)} \tag{2.7}$$

$$\log_{10}(A(d)) = \begin{cases} a_0 + a_1(\log_{10} d) + a_2(\log_{10} d)^2 + a_3(\log_{10} d)^3 & d \le 2.0\mu m \\ b_0 + b_1(\log_{10} d) + b_2(\log_{10} d)^2 + b_3(\log_{10} d)^3 & \\ \quad + b_4(\log_{10} d)^4 + b_5(\log_{10} d)^5 + b_6(\log_{10} d)^6 & d > 2.0\mu m \end{cases} \tag{2.8}$$

$$B(d) = \begin{cases} c_0 + c_1(\log_{10} d) & d \le 2.0\mu m \\ e_0 + e_1(\log_{10} d) + e_2(\log_{10} d)^2 + e_3(\log_{10} d)^3 & \\ \quad + e_4(\log_{10} d)^4 + e_5(\log_{10} d)^5 + e_6(\log_{10} d)^6 & d > 2.0\mu m \end{cases} \tag{2.9}$$

where d is the diameter of aerosol, R is the precipitation intensity, and $a_{0\text{-}3}$, $b_{0\text{-}6}$, $c_{0\text{-}1}$, and $e_{0\text{-}6}$ are empirical constants. This scavenging coefficient only depends on the dimeter of particles and precipitation rate.

3. Validation of Modeling Results

In this chapter, the modeled meteorological conditions, including air temperature, precipitation, wind speed, and wind direction, at the AMS4 location are evaluated by comparing with hourly observed meteorological data at Mildred Lake weather station (because observed meteorological data are unavailable at the AMS4 location). The discrepancies of modeled meteorological conditions among the four air monitoring stations are discussed. The model performance on the modeled element concentrations is validated against the field measurement of element concentrations at three air monitoring stations (AMS1, AMS17, and AMS18) in the AOSR. The errors in our modeled annual element concentrations are compared with errors from a dispersion model. The modeled results at the nearest grid point for each AMS site in domain 2 are used for AMS sites.

3.1 Temperature and precipitation

Fig. 3.1 shows the measurement of monthly accumulated precipitation and monthly averaged air temperature at Mildred Lake weather station. The observed and modeled hourly 2m air temperature from January 1, 2016 to December 31, 2017 are averaged monthly. The hourly precipitation data are accumulated monthly. During 2016-2017, the air temperature varies in the range of −16.9 °C to 19.5 °C with an average of 2.8 °C, and peaks in July of both years. The monthly trend of air temperature is generally the same in the two years. At Mildred Lake weather station, the snow water equivalent (SWE) and rain are measured as the precipitation amount. The annual precipitation amount is 451 mm and 357 mm in 2016 and 2017, respectively. Most of precipitation occurs in the warm season (May-October) with an average of 73% of total annual precipitation.

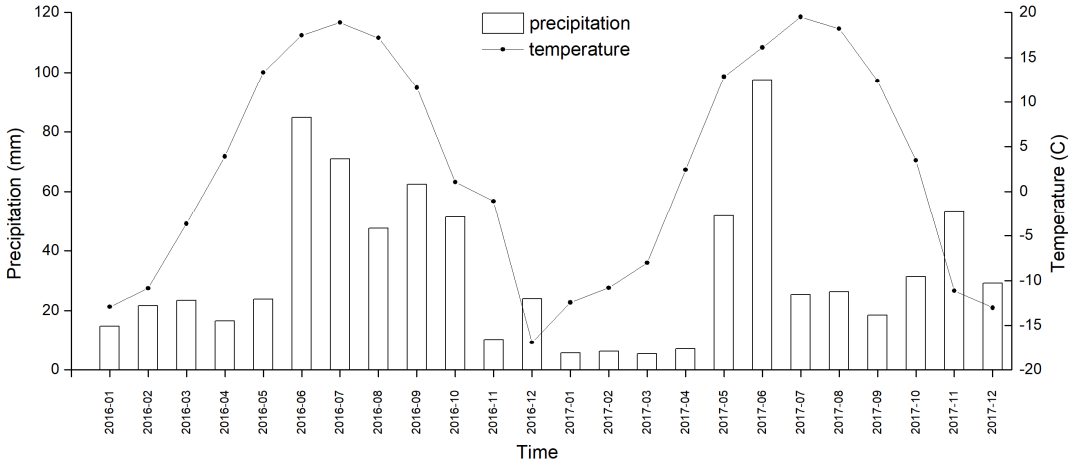

Figure 3.1 Observed monthly accumulated precipitation (mm) and monthly averaged 2m air temperature (°C) at Mildred Lake weather station during 2016-2017.

The modeled monthly accumulated precipitation (rain and SWE) and monthly averaged air temperature at the four AMS sites are showed in Fig 3.2. At AMS4, the air temperature ranges between −17.5 °C and 18.3 °C with an average of 1.9 °C in 2016-2017 (Fig. 3b). There are small differences between observed air temperature at Mildred Lake and modeled air temperature at AMS4. The absolute percentage difference is in the range of 0.4-87% with an average of 16%, and the root-mean-square error is 13 °C. The model performance on the simulation of air temperature is acceptable. In addition, the monthly trend of modeled air temperature at AMS4 is almost the same as that of observed air temperature at Mildred Lake. The predicted annual precipitation amount at AMS4 is 627 mm (603 mm for rain & 24 mm for SWE) and 555 mm (535 mm for rain & 20 mm for SWE) in 2016 and 2017, respectively. Similar to the observation at Mildred Lake, most of simulated rain (73% on average) and total precipitation (71% on average) are in the warm season. The snow amount in the cold season accounts for 95% on average of total snow amount in the whole year. The absolute monthly percentage difference between observed precipitation at Mildred Lake and predicted precipitation at AMS4 varies from 1.2% to 158% with an average of 55%, and the root-mean-square error is 30 mm. The model performance on the precipitation is acceptable because of the large uncertainties in WRF on the simulation of cloud microphysics (Rajeevan

et al., 2010; Morrison et al., 2020; Köcher et al., 2023). Microphysics is the scale of cloud droplets and rain droplets (micrometer to centimeter). These processes, including the nucleation, diffusion growth, collision, freezing, melting, and evaporation, determine the characteristics of cloud droplets and affect the formation of precipitation. In addition, it was found that the uncertainty in simulated precipitation by WRF was associated with the uncertainty in the dynamics (e.g., convection in the cloud) and thermodynamics (e.g., potential temperature & moisture) (Ajilesh et al., 2020; Jeworrek et al., 2021; Maddah and Mostamandi, 2024). Such uncertainties in the precipitation by WRF can induce the uncertainties in the predicted wet deposition of elements.

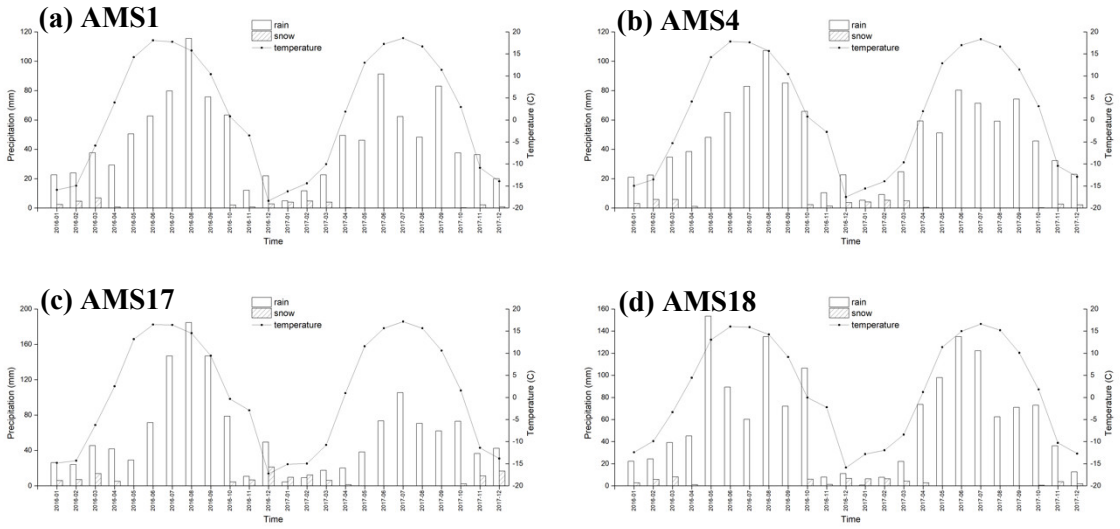

Figure 3.2 Modeled monthly accumulated precipitation (rain or snow, mm) and monthly averaged temperature (°C) at four AMS stations, (a) AMS1, (b) AMS4, (c) AMS17, and (d) AMS18.

The modeled air temperatures at AMS1, AMS17, and AMS18 are similar to that at AMS1 (Table 3.1). They have a similar monthly pattern with a peak in June or July during 2016-2017 (Fig. 3.2). Additionally, the monthly distribution of precipitations at AMS1 and AMS17 is similar to that at AMS4, because these three sites are within 45 km of each other and they are in a similar wind field (Fig. 3.3). On the contrary, the monthly distribution of the precipitation at AMS18 (peak in May-June) is different from those at the other three sites (peak in July-September), because of the over 150 km distance of AMS18 to other three

sites and the different wind field around AMS18 (Fig. 3.3). The modeled annual accumulated precipitation amounts are higher at AMS17 and AMS18, and smaller at AMS1 and AMS4 (Table 3.1).

Table 3.1 Modeled annual average temperature and accumulated precipitation at the four AMS sites during 2016-2017.

Stations	Temperature (°C)			Precipitation (mm)	
	max	min	average	rain	melted snow
AMS1	18.6	-18.4	1.6	554	18
AMS4	18.3	-17.5	1.9	570	21
AMS17	17.1	-17.2	1	704	62
AMS18	16.6	-15.9	1.8	740	29

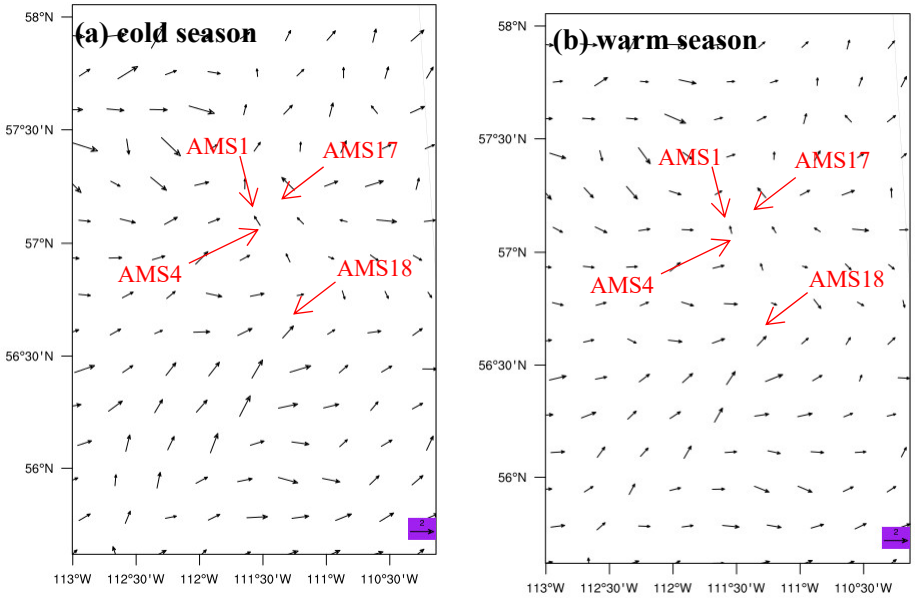

Figure 3.3 Modeled seasonal wind field for domain 2 (in Fig. 2.3b) in the (a) cold season and (b) warm season during 2016-2017.

3.2 Wind speed and wind direction

The observed surface wind speed and direction at Mildred Lake weather station during 2016-2017 are shown in Fig. 3.4. In both seasons, the prevailing winds are northerly and southerly, and winds are occasionally westerly. The AOSR is located in the Birch Mountains with elevations of 200 m to 800 m (red box in Fig. 3.5a). In the AOSR, Mildred Lake weather station is in a valley surrounded by elevated regions (yellow line in Fig. 3.5b). The Athabasca River flows through the major oil sands industry region from the southwest to the north with a stream going to the east (Fig. 3.5c). The prevailing wind blows along with the direction of the river and stream due to terrain channeling effects. In addition, the observed winds are stronger in the warm season than the cold season (Fig. 3.4). In both seasons, most of the winds are in the range of 1-5 m/s (Table 3.2).

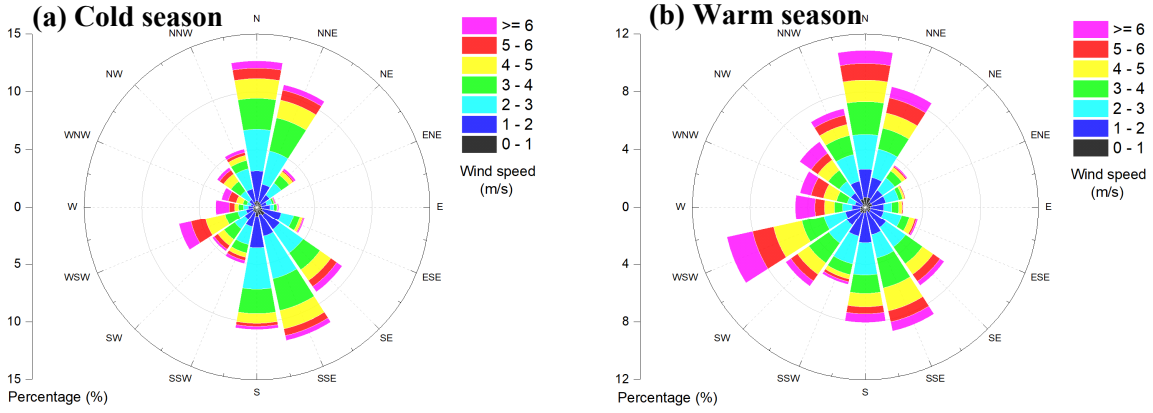

Figure 3.4 Observed wind roses at Mildred Lake weather station in the (a) cold season and (b) warm season during 2016-2017.

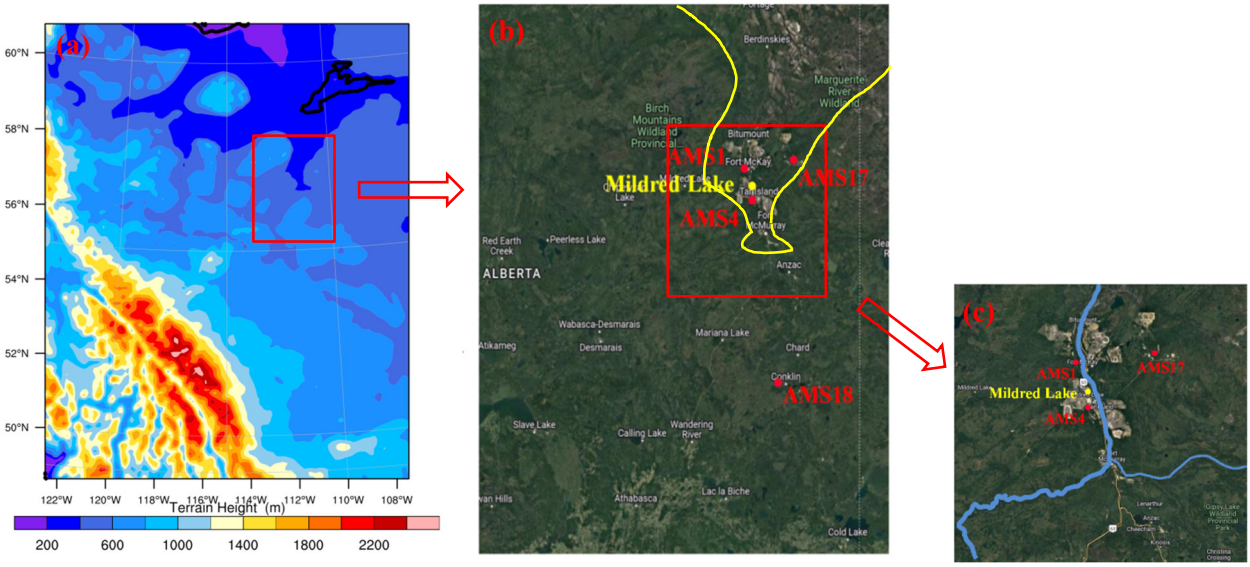

Figure 3.5 Terrain height (m) in Alberta, Canada (a) and geography in the AOSR (b-c) (red boxes for zoom-in regions shown in the next pannel, outside yellow line for elevated areas, and blue lines for river and stream) (from Google Maps).

Table 3.2 Percentages of modeled and observed wind speed at the five sites during 2016-2017.

Wind speed (m/s)	Percentage (%)									
	AMS1 (modeled)		AMS4 (modeled)		AMS17 (modeled)		AMS18 (modeled)		Mildred Lake (observed)	
	cold	warm	cold	warm	cold	warm	cold	warm	cold	warm
≥ 6	0.7	3.7	1.6	5.7	6.5	8.6	8.3	6.7	6.7	9.5
5-6	1.3	5.1	4.2	6.8	11.6	10.8	12.2	9.6	7.3	9.4
4-5	8.9	9	15.1	12.7	29.2	21.8	23.2	22.1	12.6	13.7
3-4	21	21.6	28.2	26.0	24	26.2	24.8	26.9	19.6	18.1
2-3	29.3	28.7	26.1	23.8	16.9	19.3	18.5	18.7	26.5	22.9
1-2	26.8	22.2	18.6	18.3	9	10.8	9.9	12.3	19.5	19.6
0-1	12	9.7	6.2	6.7	2.8	2.5	3.1	3.7	7.8	6.8

The modeled wind speed and direction during 2016-2017 at the four AMS sites are showed in Fig 3.6 & Fig. 3.7. At AMS4, the modeled prevailing winds are northerly and southerly in the cold season (Fig. 3.6b), while they are mostly northerly and southerly and partially westerly in the warm season (Fig. 3.7b). The modeled wind speeds at AMS4 during the warm season are larger than those during the cold season (Table 3.2). But the modeled winds at AMS4 are generally weaker than the observed winds at Mildred Lake station (Table 3.2). The similarity between modeled wind speed & direction at AMS4 and observed wind speed & direction at Mildred Lake confirms the acceptable model performance on the simulation of winds. Moreover, modeled wind directions at AMS1, AMS4, and AMS17 are similar, regardless of season (Fig. 3.6 & Fig. 3.7). Their dominant winds are from the north and the south, because AMS1 and AMS4 are within the valley and AMS17 is close to the valley (Fig. 3.5b). The modeled wind speeds at AMS1 and AMS4 are also similar, but those at AMS17 are different and larger than that at AMS1 and AMS4 (Table 3.2). The modeled wind directions at AMS18 are different from those at other three sites, and they were mostly westerly in both seasons (Fig. 3.6d & Fig. 3.7d). These agree with the synoptic wind pattern (Fig. 3.3) where AMS18 is in the southwesterly wind region while the other three sites are located in the southeasterly wind area. The modeled wind speeds at AMS18 are larger than those at AMS1 and AMS4, whereas they are similar to those at AMS17 (Table 3.2). Overall, the differences in modeled wind direction and speed among the four AMS sites indicates that the local terrain in the AOSR has a significant impact on wind conditions at AMS sites.

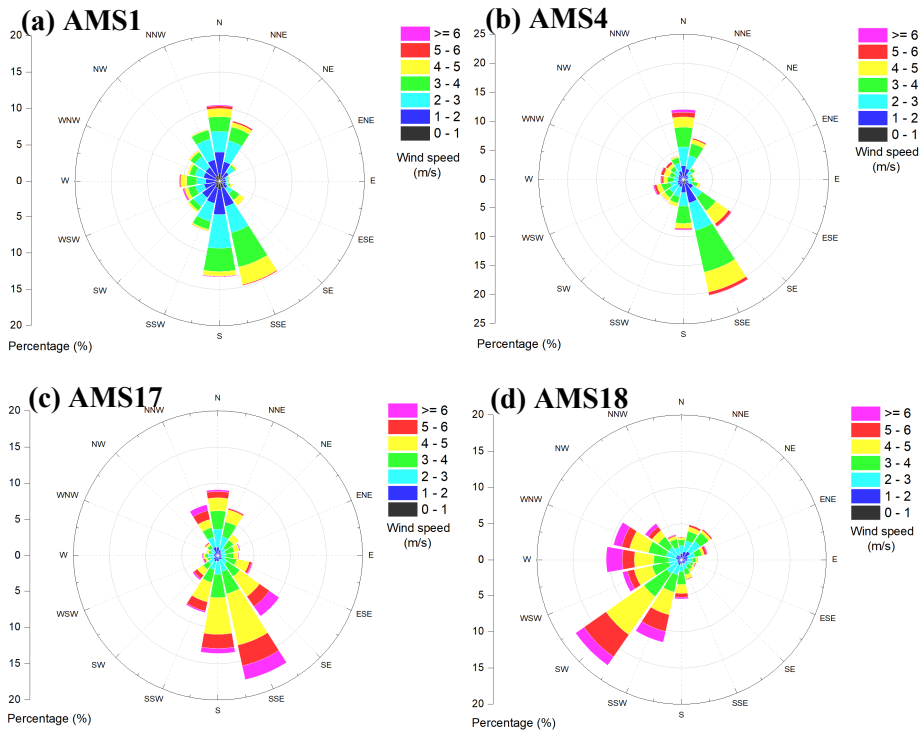

Figure 3.6 Modeled wind roses at the four AMS sites in the cold season during 2016-2017.

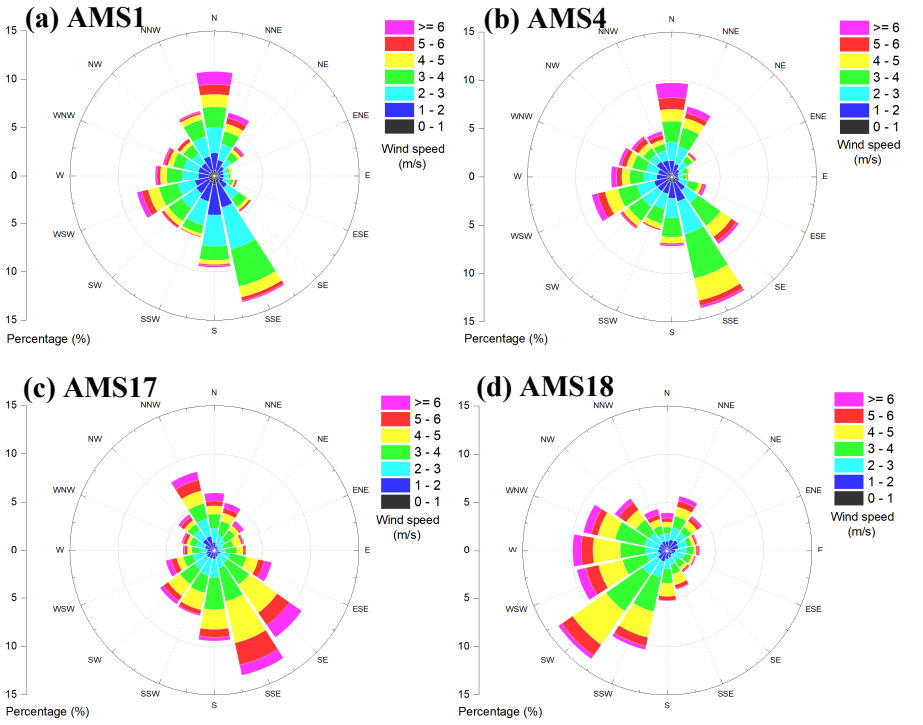

Figure 3.7 Modeled wind roses at the four AMS sites in the warm season during 2016-2017.

3.3 Element concentrations

3.3.1 Annual concentrations

The percentage differences between annual modeled and measured element concentrations in PM_{10} ($PM_{2.5}$ + $PM_{2.5-10}$) during 2016-2017 are shown in Fig. 3.8. The differences in modeled annual concentrations for all eight elements at the three monitoring sites are within a factor of two, suggesting good model performance on the element concentrations in a yearly basis. Yang et al. (2023) predicted the element concentrations in the AOSR by using a dispersion model, and their simulated element concentrations show a bias within a factor of two against the observations. Hutzell and Luecken (2008) modified the Community Multiscale Air Quality (CMAQ) model to include five elements, and simulated these elements over the continental United States. They found that the most of simulated element concentrations had a bias within a factor of two. Appel et al. (2013) used CMAQ to simulate elements in the dust for the continental United States, and they found biases were up to a factor of four in the modeled element concentrations.

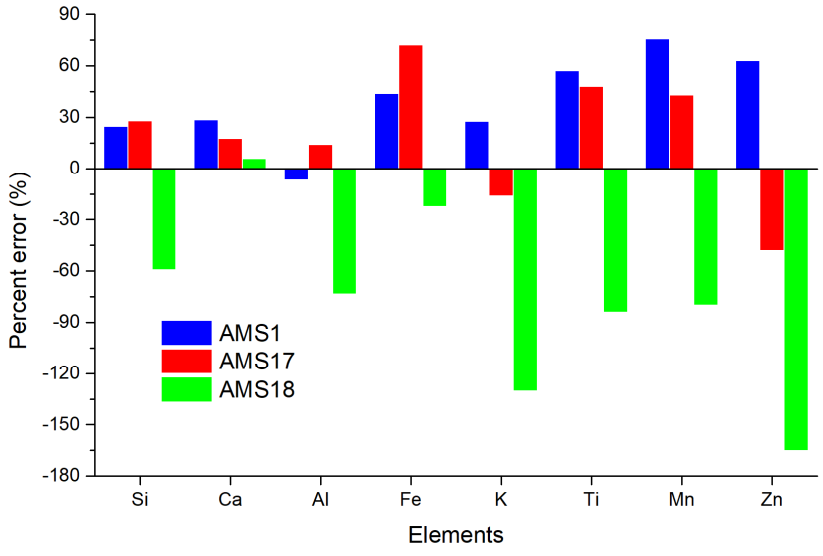

Figure 3.8 The percentage differences (%) between annual modeled and observed element concentrations in PM_{10} during 2016-2017.

The model-measurement differences in annual concentrations of the eight elements are in the range of -6.9% to 76%, -48% to 72%, and -165% to 5.8% at AMS1, AMS17, and AMS18, respectively. The model has a better performance on the annual element concentrations for the eight elements at AMS1 and AMS17. The percentage differences averaged over the eight elements are 23% and 25% for AMS1 and AMS17, respectively. The percentage difference in annual concentrations averaged over the eight elements is -56% at AMS18. In addition, the annual concentrations of all elements except Al are overpredicted by 29-122% at AMS1, and all elements except K and Zn are overestimated by 15-113% at AMS17, possibly due to their closest position to the major oil sands industry facilities and the uncertainty in the industry element emissions. On the contrary, it is found that the annual concentrations of all elements except Ca are underpredicted by 20-90% at AMS18. This is probably because AMS18 is over 150 km away from the hotspot of oil sands industry and element emissions are underrated near AMS18. These underpredictions may also be attributable to the simulated winds. The model produces weaker winds against the observations (Table 3.2). As a result, the regional transport of elements from the major oil sands industry facilities to AMS18 is weaker leading to lower element concentrations at AMS18. Yang et al. (2023) used a dispersion model to estimate element concentrations over the AOSR during 2016-2017 with the same element emission database as this study. Their comparison of modeling results with observations showed that modeled annual concentrations of the eight elements (Si, Ca, Al, Fe, K, Ti, Mn, and Zn) had averaged errors of 19%, 51%, and 51% at AMS1, AMS17, and AMS18, respectively. Compared with modeling results from Yang et al. (2023), WRF-Chem has a better performance at AMS17 and has a similar performance on the modeled annual concentrations of all eight elements. Similar to our results, Yang et al. (2023) reported that modeled annual concentrations for most of the eight elements were overestimated by 6-37% at AMS1 and 22-92% at AMS17, whereas they were underestimated by 25-80% at AMS18. They attributed these differences to the uncertainty of particulate matters emissions in the inventory and uncertainty of element emissions profiles in the speciation process.

Among all eight elements, the model performance for Ca is the best with averaged percentage

difference of 17% for the three monitoring stations. The averaged percentage difference for Si, Al, Fe, K, Ti, Mn, and Zn at the three stations are 37%, 31%, 46%, 58%, 63%, 66%, and 92%, respectively. It is obvious that the percentage difference for Zn is the largest (92%) and the percentage differences for other six elements are close to 40-60%, indicating that Zn emission has the largest relative uncertainties. Note that the total emission for Zn is the smallest among the eight elements (Fig. 2.1). Any small difference can lead to a large relative error. Yang et al. (2023) stated that the averaged percentage errors for Si, Ca, Al, Fe, K, Ti, Mn, and Zn at the three sites were 44%, 51%, 33%, 47%, 32%, 50%, 17%, and 30%, respectively. Their modeled biases are on the same order of magnitude as our modeling results.

3.3.2 Monthly concentrations

As shown in Fig. 3.9, the monthly modeled and observed concentrations of eight elements at AMS1 are compared. It is obvious that, except Zn, all elements have different seasonal trends between the observation and the simulation. The observed concentrations in PM_{10} are higher during the warm season than those during the cold season, whereas the higher modeled concentrations in PM_{10} occur during the cold season. This is likely because the annual element emissions are equally split into each month (discussed in Section 2.5), and thus the seasonal variation of element emissions is not considered. Dust is a major natural source of elements in the AOSR, however low temperature and snow cover during the cold season inhibit the dust from being eroded and re-suspending. Kyllönen et al. (2009) conducted research on element deposition in Finland. They found that snow cover had an impact on the re-suspension of crustal elements, such as Al, Fe, and Mn. In addition, Phillips-Smith et al. (2017) identified the source of elements in the AOSR, and they stated that there were fewer emissions of elements from soil and haul road dust in winter due to the freezing of the ground and the snow cover.

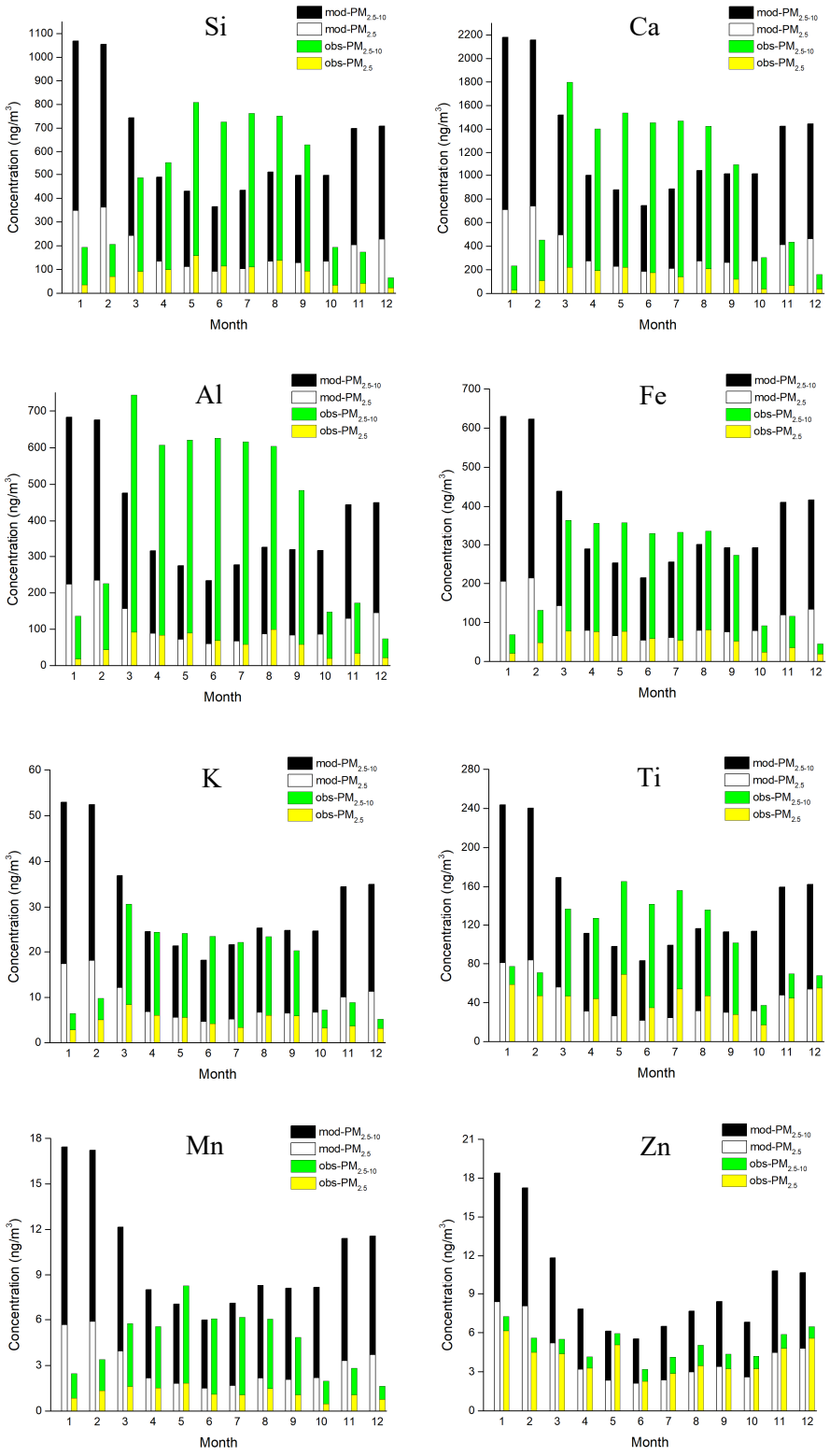

Figure 3.9 Monthly modeled and observed element concentrations at AMS1 during 2016-2017.

The modeled concentrations of five elements, Si, Ca, Al, Fe, and K, in PM_{10} are overpredicted during the cold season, while those during the warm season are underpredicted (Fig. 3.9). Among these five elements, Si, Ca, Al, and Fe are typical crustal elements, and K is enriched in the soil dust probably because of the cumulative amount from the deposition in decades when the oil sands industry developed. Without considering the seasonal variation of element emissions from dust, the model overestimated (underestimated) element concentrations in the cold (warm) season. The modeled concentrations for Si, Ca, Al, Fe, and K in PM_{10} during the cold season are overestimated by 117%, 184%, 55%, 159%, and 98%, respectively, whereas those values during the warm season are underestimated by 24%, 30%, 44%, 7%, and 16%. There is a big forest fire occurring near the AOSR in May-June of 2016. It potentially leads to a higher observed K concentration at the AMS sites. However, the modeled concentration for K is still underestimated by 9% during the warm season in 2017. The forest fire in 2016 causes some impacts to the discrepancy between the modeling and observation. This impact of forest fire is also found at AMS17 and AMS18.

The modeled concentrations of other three elements, Ti, Mn, and Zn in PM_{10} show less errors in the warm season, but an overprediction in the cold season (Fig. 3.9). These three elements are anthropogenic elements and there are probably lower anthropogenic emissions in the emission inventory and a lack of suitable element emission profile in the speciation (Yang et. al, 2023). The biases of modeled concentrations for Ti, Mn, and Zn in PM_{10} to the observations during the cold season are 177%, 260%, and 120%, respectively, and their biases during the warm season are 12%, 34%, and 53%. The overprediction of these three elements concentrations by the model is more evident during the cold season than warm season.

Similar to AMS1, discrepancies in monthly element concentration between simulations and measurements are found at AMS17 (Fig. 3.10). The model generates higher monthly element concentrations in PM_{10} during the cold season, while the measurement shows higher monthly element concentrations in PM_{10} during the warm season. This is because of the lack of the seasonal variation of

element emissions. The modeled concentrations for Si, Ca, Al, K, and Mn in PM_{10} during the cold season are overpredicted by 136%, 133%, 104%, 28%, and 151%, respectively, whereas their concentrations during the warm season are underpredicted by 18%, 30%, 30%, 46%, and 17%. The modeled concentrations for Fe and Ti in PM_{10} are mostly overpredicted in the whole year. Their biases are 284% and 125% during the cold season, and 31% and 13% during the warm season. Their overpredictions are more obvious in the cold season. At AMS17, only Zn is mostly underpredicted by the model in the whole year with the bias of 33% during the cold season and 48% during the warm season. These suggest the industry emissions for Fe and Ti are overrated, but are underrated for Zn. It is also possible that the element emission profile of Fe, Ti and Zn is unsuitable in the speciation.

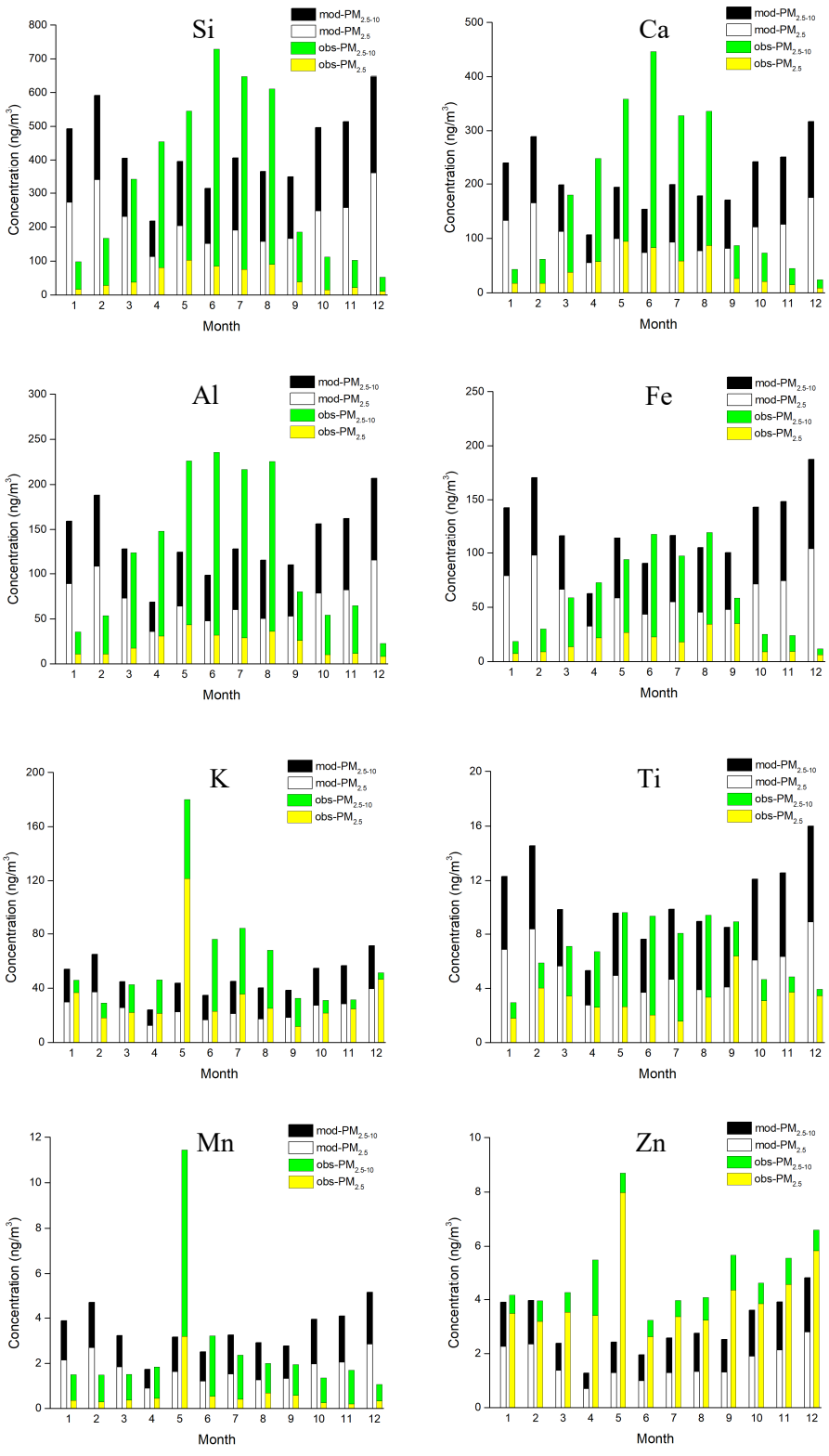

Figure 3.10 Monthly modeled and observed element concentrations at AMS17 during 2016-2017.

The difference in the seasonal trend of element concentrations between the observations and the simulations at AMS18 is similar to that at AMS1 and AMS17. At AMS18, the higher modeled monthly element concentrations in PM_{10} happen in the cold season, and the higher measured monthly element concentrations in PM_{10} occur in the warm season (Fig. 3.11). However, the model underestimates more elements at AMS18 than AMS1 and AMS17. The modeled concentrations for Al, K, Ti, Mn, and Zn in PM_{10} are mostly underpredicted throughout the whole year, and their biases were 24%, 70%, 41%, 39%, and 86% during the cold season and 72%, 87%, 73%, 69%, and 93% during the warm season, respectively. The modeled concentrations for Si, Ca, and Fe are overestimated by 2%, 65%, and 32% during the cold season, and underestimated by 71%, 37%, and 54% during the warm season, respectively. The fact that more elements are underestimated at AMS18 than AMS1 and AMS17 may be due to the weaker winds predicted by WRF-Chem against the observations. The weaker winds reduce the regional transport of elements from major oil sands industry to AMS18. It is also probably owing to the lower industry emissions near AMS18 in the element inventory.

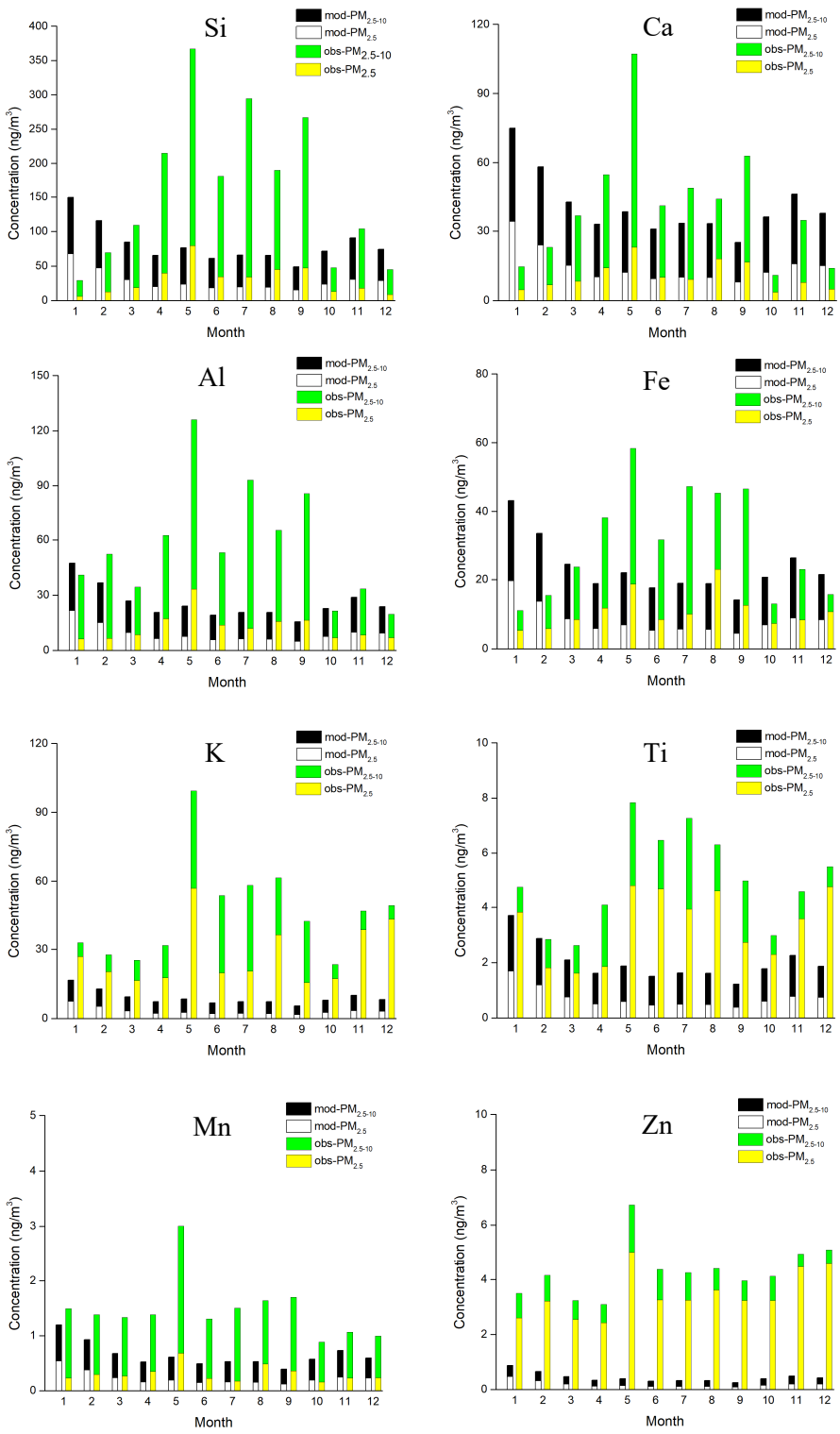

Figure 3.11 Monthly modeled and observed element concentrations at AMS18 during 2016-2017.

Daily modeled and observed element concentrations in PM_{10} at AMS1 are compared during the cold season (January as an example) and the warm season (July as an example), as shown in Fig. 3.12. The predicted element concentrations are higher than the observed concentrations in January, but they are lower than the observed concentrations in July. This agrees with discrepancies in the seasonal concentrations (Figs. 3.9-3.11). However, the model produces a similar trend in January and July. On an hourly basis, the model predicts lower element concentrations during the daytime (8:00-19:00) and higher element concentrations during the nighttime (19:00-8:00) (Fig. 3.13). This agrees with the atmospheric stability. During the daytime, the higher temperatures and less stable atmosphere support the vertical mixing of elements and lead to a lower element concentration near the surface. On the contrary, the lower temperature and stable atmosphere prevent the vertical mixing during the nighttime.

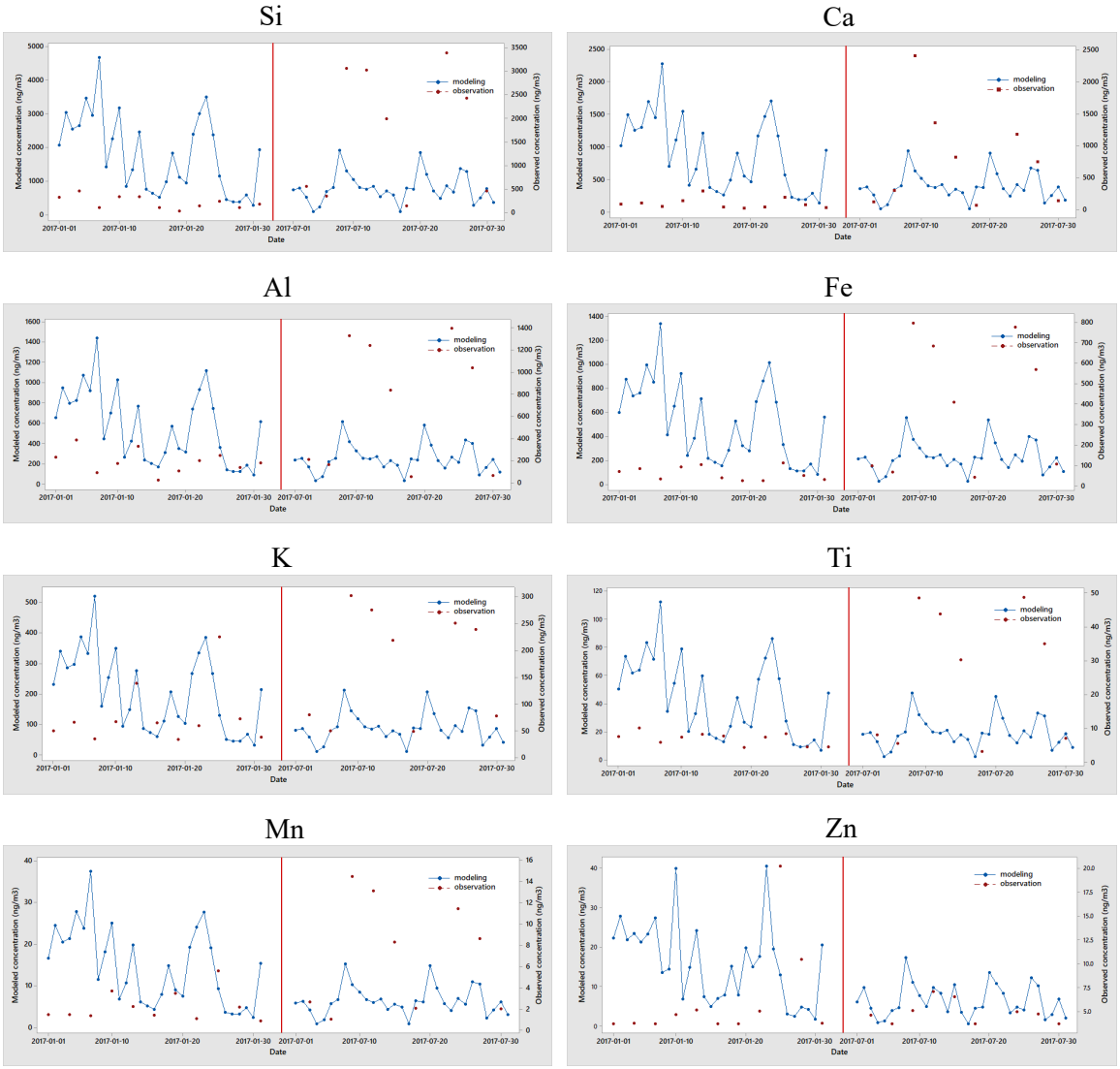

Figure 3.12 Daily modeled and observed element concentrations in PM_{10} at AMS1 during January 1-31 and July 1-31 in 2017.

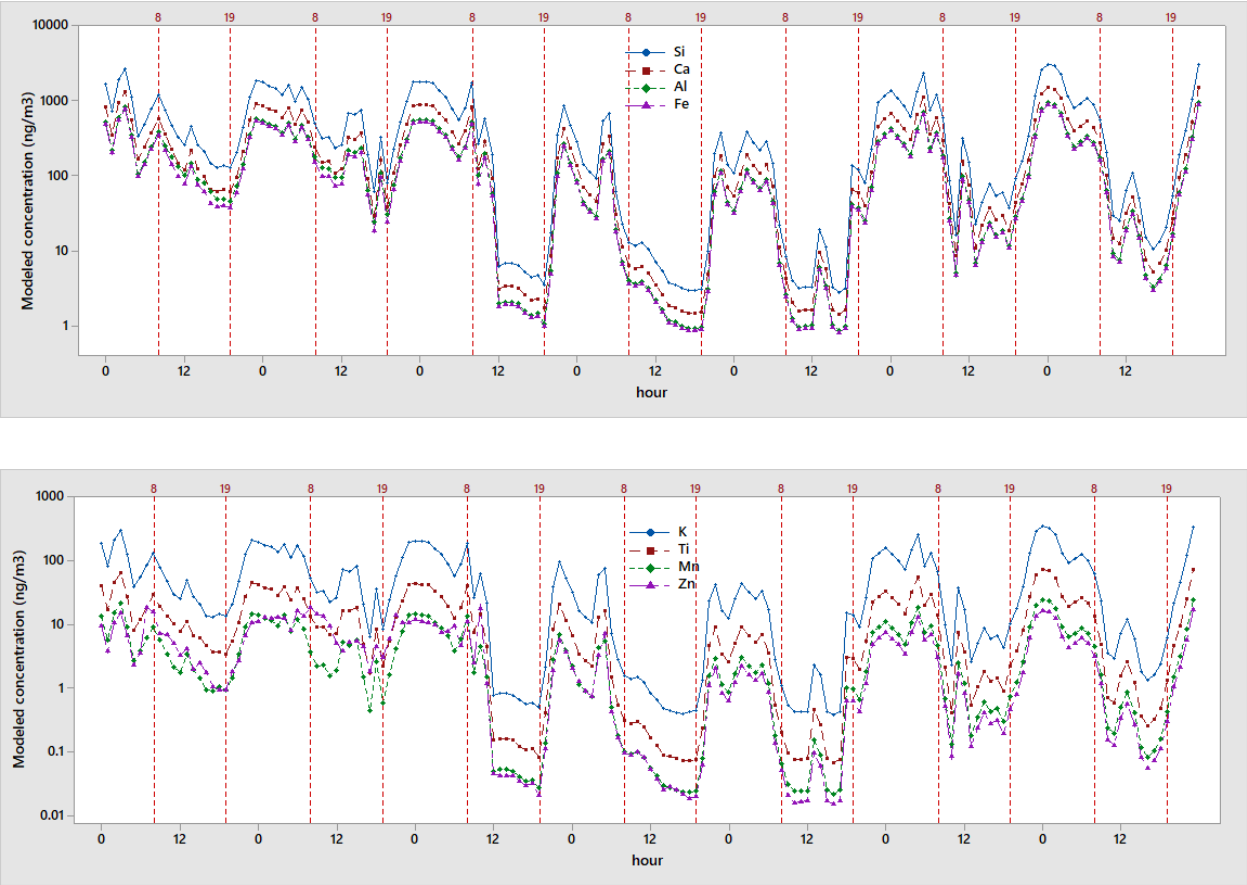

Figure 3.13 Hourly modeled element concentrations in PM_{10} at AMS1 during January 1-7, 2017.

Overall, the seasonal trend of element concentrations from the simulation is different to that from the measurement at the three monitoring stations. The modeling results show higher element concentrations during the cold season than warm season, whereas observed element concentrations are higher during the warm season than cold season. The low temperature and snow cover during the cold season prevent element emissions from the dust, however the model simulation lacks the consideration of seasonally varied element emissions. In addition, at the three AMS sites together, the modeled total concentrations of the eight elements are overestimated by 82% during the cold season and underestimated by 38% during the warm season in 2016-2017. This model performance on the monthly element concentration is worse than that on the annual element concentration, because of the lack of the seasonal variation in element

emissions.

4. Temporal and Spatial Distributions

In this chapter, the modeled annual and seasonal element concentrations and deposition are analyzed to reveal possible relations among the element concentration, deposition, and weather conditions. The simulated element concentrations and deposition in this study are compared with modeling results in the AOSR from a dispersion model. The spatial distributions of modeled element concentrations and dry & wet deposition in the AOSR are investigated. The environmental impacts by the oil sands industry to the local and remote communities are discussed.

4.1 Annual element concentrations

The modeled annual total concentrations of the eight elements in $PM_{2.5}$, $PM_{2.5-10}$, and PM_{10}, are listed in Table 4.1. The fine mode particles ($PM_{2.5}$) are mainly originated from anthropogenic sources while the coarse mode particles ($PM_{2.5-10}$) are from natural sources. There are 30%, 23%, 52%, and 36% of the annual total element concentrations contributed by the fine mode particles at AMS1, AMS4, AMS17, and AMS18, respectively. This suggests that ambient elements at AMS1, AMS4, and AMS18 are mostly from natural sources, such as the dust, whereas around the half of ambient elements at AMS17 come from anthropogenic productions, such as oil sands industry. In addition, the modeled total concentrations of eight elements are the highest at AMS1 and AMS4, followed by AMS17 and AMS18. This is because AMS1 and AMS4 are located at the hotspot of oil sands industry and they are close to each other (around 20 km in distance). The lowest modeled total concentration at AMS18 is due to few oil sands industry facilities near AMS18. AMS18 is 150 km away from to the hotspot of oil sands industry.

Table 4.1 The modeled annual concentrations (ng m^{-3}) of the eight elements in $PM_{2.5}$, $PM_{2.5-10}$ and PM_{10} at the four stations during 2016-2017.

Particles	Stations	Elements								Total
		Si	Ca	Al	Fe	K	Ti	Mn	Zn	
$PM_{2.5}$	AMS1	377	185.3	119.4	109.4	43.3	9.3	3	4.2	851
	AMS4	320.7	158.6	104.6	94.1	35.6	8.1	2.5	4.7	729
	AMS17	224.1	109.3	71.3	64.6	24.7	5.5	1.8	1.6	503
	AMS18	28.7	14.7	9.2	8.3	3.2	0.7	0.2	0.2	65
	average	237.6	117	76.1	69.1	26.7	5.9	1.9	2.7	537
$PM_{2.5-10}$	AMS1	897.7	439.3	279.6	258.6	99.2	21.7	7.2	5.7	2009
	AMS4	1122.5	546.5	353.4	323.9	123.3	27.3	8.9	8.2	2514
	AMS17	208.5	102.2	65.6	60.2	23	5.1	1.7	1.4	468
	AMS18	52.2	26.1	16.4	15	5.8	1.3	0.4	0.3	118
	average	570.2	278.5	178.8	164.4	62.8	13.9	4.6	3.9	1277.1
PM_{10}	AMS1	1274.7	624.5	399	368	142.5	31	10.2	9.8	2860
	AMS4	1443.2	705	457.9	417.9	158.9	35.4	11.5	12.9	3243
	AMS17	432.6	211.5	136.9	124.8	47.7	10.6	3.4	3	971
	AMS18	80.9	40.8	25.6	23.4	9	2	0.6	0.4	183
	average	807.9	395.5	254.9	233.5	89.5	19.8	6.4	6.5	1813.9
PM_{10} (Yang et al., 2023)	AMS1	1166	528	435	321	119	25	8.1	5.4	2607.5
	AMS17	642	324	221	123	71	1.2	4.3	4.4	1390.9
	AMS18	120	63	37	39	15	3.3	0.98	0.7	278.98

Table 4.1 lists the modeled annual concentrations of the eight elements in $PM_{2.5}$, $PM_{2.5-10}$ and PM_{10} at the four stations during 2016-2017. Regardless of particle size and AMS site, Si has the highest modeled

annual concentration, generally followed by Ca, Al, Fe, K, Ti, Mn, and Zn, agreeing with the order of their magnitudes of emission rates (Fig. 2.1). For $PM_{2.5}$, the modeled annual element concentrations are the highest at AMS1, followed by AMS4, AMS17, and AMS18. These indicate that there are more oil sands industry productions near AMS1. In $PM_{2.5-10}$, the modeled annual element concentrations are the highest at AMS4, followed by AMS1, AMS17, and AMS18. These suggest that AMS4 is surrounded by more natural emissions (dust). Similar to $PM_{2.5-10}$, the modeled annual element concentrations in PM_{10} are the highest at AMS4 and the lowest at AMS18. This is because elements in $PM_{2.5-10}$ dominate that in PM_{10}. Regardless of the particle size, the total annual concentrations of Si, Ca, Al, and Fe account for 93% of the total annual concentrations of the eight elements. This is because Si, Ca, Al, and Fe are crustal elements and the dust is the significant emission source for elements in the AOSR.

Yang et al. (2023) predicted annual concentrations of the eight elements over the AOSR during 2016-2017. They found that the simulated annual element concentrations were highest at AMS1 followed by AMS17 and AMS18, agreeing with our modeling results. Their modeled annual element concentrations for Si, Ca, Al, Fe, K, Ti, Mn, and Zn can be found in Table 4.1. Generally, their modeled annual element concentrations at the three monitoring stations were in the same order of magnitude as ours. However, their results showed lower annual element concentrations at AMS1 and higher annual element concentrations at AMS17 and AMS18 than ours. Similar to our simulations, they also found the highest annual concentration for Si, followed by Ca, Al, Fe, K, Ti, Mn, and Zn.

4.2 Annual element deposition

The modeled annual total dry deposition of the eight elements are 264.7 mg $m^{-2}yr^{-1}$, 221.5 mg $m^{-2}yr^{-1}$, 207.8 mg $m^{-2}yr^{-1}$, and 26.8 mg $m^{-2}yr^{-1}$ at AMS1, AMS4, AMS17, and AMS18, respectively. The modeled annual total dry deposition is the highest at AMS1, followed by AMS4, AMS17, and AMS18. This order is similar to the order of modeled annual total element concentrations at the four AMS sites. The element dry deposition is proportional to the element concentration and dry deposition velocity. This

similar order indicates that the ambient element concentration is a significant factor determining the element dry deposition flux. The modeled annual total wet deposition of the eight elements at AMS1, AMS4, AMS17, and AMS18 are 113.9 mg $m^{-2}yr^{-1}$, 126.8 mg $m^{-2}yr^{-1}$, 124.1 mg $m^{-2}yr^{-1}$, and 9.5 mg $m^{-2}yr^{-1}$, respectively. The highest modeled annual total wet deposition is at AMS4 and AMS17. The removal of aerosols by below-cloud scavenging depends on aerosol concentration, precipitation rate, and scavenging coefficient. Although the modeled annual total concentrations in PM_{10} is much smaller at AMS17 than AMS1 (971 ng m^{-3} < 2860 ng m^{-3}), the modeled annual total wet deposition is higher at AMS17 than AMS1 (124.1 mg $m^{-2}yr^{-1}$ > 113.9 mg $m^{-2}yr^{-1}$). This is because AMS17 has higher modeled annual precipitation than AMS1 (766 mm > 572 mm). Therefore, the element wet deposition flux can be largely altered by both the ambient element concentration and the precipitation amount.

Table 4.2 shows the modeled annual dry and wet deposition of the eight elements at the four stations during 2016-2017. For both dry and wet deposition, Si has the largest value, generally followed by Ca, Al, Fe, K, Ti, Mn, and Zn, agreeing with the order of their magnitudes of ambient element concentrations. For both dry (and wet) deposition, Si, Ca, Al, and Fe account for 93% of total dry (wet) deposition at the four sites. Si, Ca, Al, and Fe are crustal elements, and they make up 93% of modeled total annual concentrations of the eight elements (Table 4.1). In addition, the modeled annual dry deposition of the eight elements are much larger at AMS1, AMS4, and AMS17 than AMS18. This is because of the lowest modeled annual concentrations of the eight elements at AMS18 (Table 4.1). Similarly, AMS1, AMS4, and AMS17 have much larger modeled annual wet deposition of the eight elements, while AMS18 has the smallest wet deposition due to over 150 km distance of AMS18 to the hotspot of oil sands industry.

Table 4.2 The modeled annual dry and wet deposition (mg $m^{-2}yr^{-1}$) of the eight elements at the four stations during 2016-2017.

Deposition	Stations	Elements							
		Si	Ca	Al	Fe	K	Ti	Mn	Zn
Dry	AMS1	117.6	57.2	38.0	34.1	12.8	2.9	0.9	1.2
	AMS4	98.1	47.0	32.9	28.6	10.4	2.5	0.8	1.2
	AMS17	92.6	45.2	29.4	26.8	10.2	2.3	0.7	0.6
	AMS18	11.9	5.9	3.8	3.4	1.3	0.3	0.09	0.06
	average	80.05	38.83	26.03	23.23	8.68	2	0.62	0.77
Wet	AMS1	50.5	24.4	16.7	14.7	5.4	1.3	0.4	0.5
	AMS4	55.1	25.9	20.9	16.4	5.5	1.6	0.4	1.0
	AMS17	55.5	27.1	17.4	16.0	6.1	1.3	0.4	0.3
	AMS18	4.2	2.1	1.3	1.2	0.5	0.1	0.03	0.03
	average	41.33	19.88	14.08	12.08	4.38	1.08	0.31	0.46

Table 4.2 The modeled annual dry and wet deposition (mg $m^{-2}yr^{-1}$) of the eight elements at the four stations during 2016-2017 (continued).

Deposition	Stations	Elements							
		Si	Ca	Al	Fe	K	Ti	Mn	Zn
Total (dry+wet)	AMS1	168.1	81.6	54.7	48.8	18.2	4.2	1.3	1.7
	AMS4	153.2	72.9	53.8	45	15.9	4.1	1.2	2.2
	AMS17	148.1	72.3	46.8	42.8	16.3	3.6	1.1	0.9
	AMS18	16.1	8	5.1	4.6	1.8	0.4	0.12	0.09
	average	121.38	58.7	40.1	35.3	13.05	3.08	0.93	1.22
Total (dry+wet) (Mamun et al., 2022)	AMS1	172	118	71.7	35	19.7	2.7	0.83	1.6
	AMS4	167	66.9	74	30.1	18.7	3.1	0.86	2.3
	AMS17	78.4	64.9	27.8	11.3	14.3	2	0.66	2.2
	AMS18	101	31.7	35.5	11.7	28	2.1	0.64	2

Fig. 4.1 shows modeled annual dry and wet deposition of the eight elements at the four AMS sites. It is obvious that, although the modeled annual dry and wet deposition are in the same order of magnitude, the modeled annual dry deposition is always larger than the modeled annual wet deposition, regardless of element and AMS station. The modeled annual dry deposition of the eight elements contribute 69-71%, 55-67%, 63-67%, and 67-75% of the modeled annual total deposition at AMS1, AMS4, AMS17, and AMS18, respectively. This is because the predominance of removal processes being dry or wet deposition is determined by the precipitation amount, and the modeled annual precipitation is in the range of 572-769 mm at the four monitoring sites. Some studies on the measurement of element dry and wet deposition have revealed the relationship between element deposition and precipitation amount. Al-Momani et al. (2002) measured the element deposition near an industrial area in Jordan where the annual rainfall amount was less than 200 mm. They reported that annual dry deposition was

larger than wet deposition. On the contrary, Wu et al. (2018) observed the element deposition near an industrialized region in China with over 1900 mm annual precipitation. They found that annual dry deposition was smaller than wet deposition. Thus, in this study, it is reasonable that the modeled annual dry deposition is within a factor of three of the modeled annual wet deposition for all eight elements at four AMS sites.

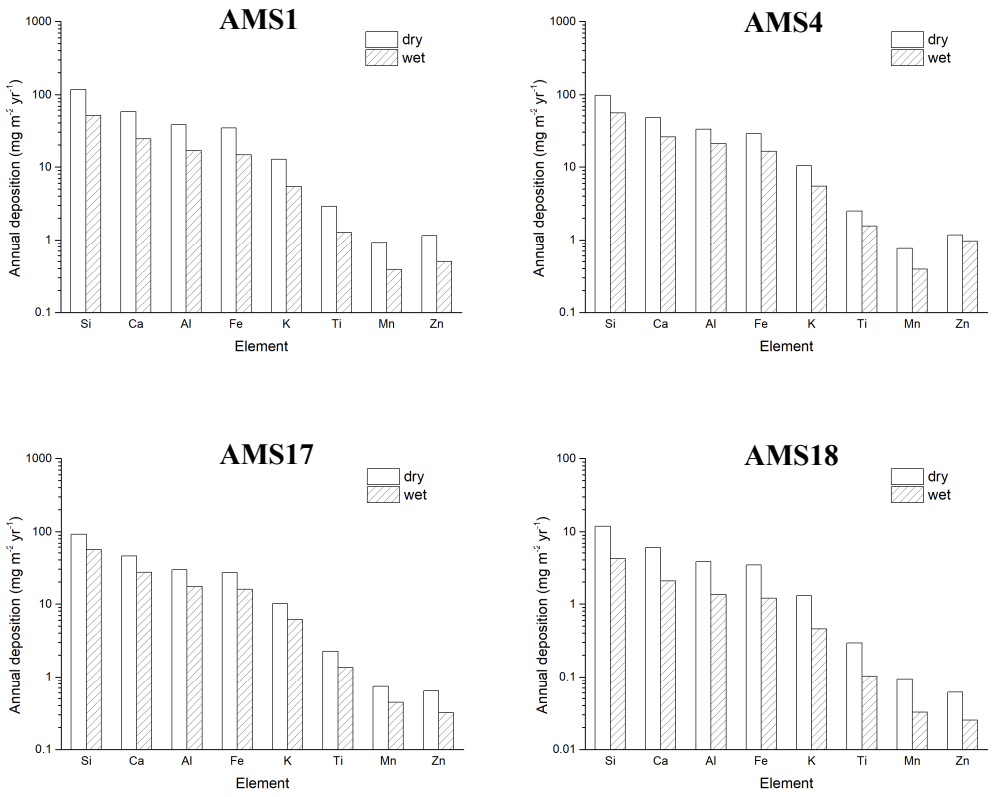

Figure 4.1 The modeled annual dry and wet deposition of the eight elements at the four AMS sites.

Mamun et al. (2022) developed a framework to estimate element dry and wet deposition. They calculated the dry and wet deposition of 35 particulate elements at the four AMS sites in 2016-2017 by combining this deposition framework and observed element concentrations at AMS sites (Table 4.2). Their annual total deposition fluxes of the eight elements are similar to our modeled annual total

deposition fluxes at AMS1, AMS4, and AMS17 (Table 4.2). However, our predicted annual total deposition at AMS18 are much smaller than their calculations. They used observed element concentrations for the calculation of element deposition, while our model underestimated the element concentrations of all elements, except Ca, at AMS18 (Fig. 3.8). They also reported that the calculated annual dry and wet deposition of the eight elements were in the same order of magnitude, but the annual wet deposition was larger than annual dry deposition, although their annual precipitation at AMS sites (488-603 mm) was smaller than ours (572-769 mm). This is because the framework for calculating element deposition that they developed was different from the deposition schemes in WRF-Chem that we chose. They chose an empirical dry deposition formula for fine and coarse particles developed by Zhang and He (2014) while we use a theoretical dry deposition scheme (Eq. 2.2). In the wet deposition, they determined a regression formula from literature (Cheng et al., 2021), whereas we select a theoretical scheme (Eq. 2.3).

4.3 Seasonal element concentrations

The modeled total concentrations of the eight elements in $PM_{2.5}$ at AMS1 during the cold season and the warm season are 1162 ng/m^3 and 539 ng/m^3, respectively. The modeled total concentrations in $PM_{2.5}$ are 2.15 times higher during the cold season than the warm season. The modeled total concentrations of the eight elements in $PM_{2.5\text{-}10}$ at AMS1 during the cold season and the warm season are 2475 ng/m^3 and 1545 ng/m^3, respectively. The modeled total concentrations in $PM_{2.5\text{-}10}$ are higher during the cold season than the warm season by a factor of 1.6. In addition, regardless of season, modeled total concentrations are higher in $PM_{2.5\text{-}10}$ than $PM_{2.5}$. This indicates that the dust is a major element natural emission source in the AOSR. In both $PM_{2.5}$ and $PM_{2.5\text{-}10}$, modeled total concentrations are higher during the cold season than the warm season. This is because of a constant element emission rate used in the simulation and the modeled meteorological conditions. The strong stability in the atmosphere, resulting from the low surface temperature, and the shallow boundary layer in the cold season trapping more elements in the planetary

boundary layer (PBL). As a consequence, elements concentrate near the surface. Fig. 4.2 shows the modeled seasonal concentrations of the eight elements in $PM_{2.5}$ and $PM_{2.5-10}$ at AMS1. The modeled concentrations of the eight elements in $PM_{2.5}$ and $PM_{2.5-10}$ during the cold season are around 2.1 and 1.6 times higher than that during the warm season, respectively (Table 4.3). Under the constant element emission rates throughout the year, the shallow PBL and stable atmosphere in the cold season suppress the vertical diffusion of elements, leading to higher element concentrations near the surface in the cold season.

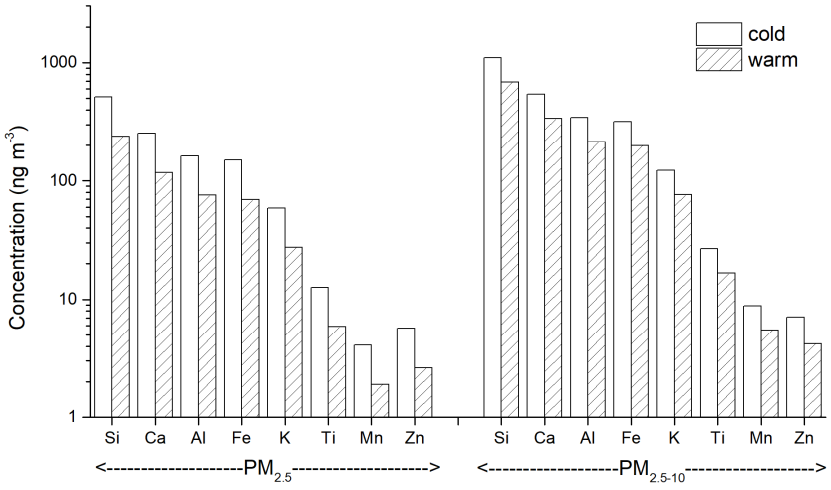

Figure 4.2 Modeled seasonal concentrations (ng/m^3) of the eight elements in $PM_{2.5}$ and $PM_{2.5-10}$ at AMS1.

Table 4.3 The modeled seasonal concentrations (ng m^{-3}) of the eight elements in $PM_{2.5}$ and $PM_{2.5-10}$ at the four stations during 2016-2017.

Stations	Sizes	Seasons	Elements							
			Si	Ca	Al	Fe	K	Ti	Mn	Zn
AMS1	$PM_{2.5}$	cold	515	253	163	149	59	13	4.1	5.7
		warm	239	117	76	69	28	5.9	1.9	2.6
	$PM_{2.5-10}$	cold	1106	541	344	319	122	27	8.8	7.1
		warm	690	338	215	199	76	17	5.5	4.2
AMS4	$PM_{2.5}$	cold	360	178	118	106	40	9.1	2.9	5.4
		warm	281	139	92	82	31	7.1	2.2	4
	$PM_{2.5-10}$	cold	1040	506	329	300	114	25	8.3	8.4
		warm	1205	587	378	347	133	29	9.6	8
AMS17	$PM_{2.5}$	cold	262	128	84	76	29	6.5	2.1	1.9
		warm	186	91	59	54	21	4.6	1.5	1.4
	$PM_{2.5-10}$	cold	216	106	68	62	24	5.3	1.7	1.4
		warm	201	99	63	58	22	4.9	1.6	1.3
AMS18	$PM_{2.5}$	cold	37	19	12	11	4.2	0.94	0.3	0.25
		warm	20	10	6.4	5.8	2.2	0.5	0.16	0.12
	$PM_{2.5-10}$	cold	59	30	19	17	6.6	1.5	0.48	0.29
		warm	45	23	14	13	5	1.1	0.36	0.22

The modeled total concentrations of the eight elements in $PM_{2.5}$ at AMS4 are 819 ng/m^3 and 638 ng/m^3 during the cold season and the warm season, respectively. The modeled total concentrations in $PM_{2.5}$ are higher during the cold season than the warm season by a factor of 1.28. This ratio is much smaller than that at AMS1 (1.28 < 2.15). The modeled total concentrations of the eight elements in $PM_{2.5-10}$ at AMS4

during the cold season and the warm season are 2330 ng/m^3 and 2696 ng/m^3, respectively. Contrary to AMS1, the modeled total concentrations in $PM_{2.5-10}$ are higher during the warm season than the cold season by a factor of 1.2, although the stable atmosphere and the shallow boundary layer in the cold season strengthened the element concentration near the surface. This is because AMS4 is located to the east (downstream) of a major emission source (Fig. 2.4). During the warm season, there are more westerly winds blowing from this major emission source (Fig 3.6b & 3.7b). As a result, more elements are transported from this major emission source to AMS4. Therefore, the ratio of modeled total concentrations in $PM_{2.5}$ during the cold season to that during the warm season at AMS4 is much smaller than AMS1 (1.28 < 2.15). The modeled total concentrations in $PM_{2.5-10}$ at AMS4 are higher during the warm season than the cold season.

Fig. 4.3 shows the modeled seasonal concentrations of the eight elements in $PM_{2.5}$ and $PM_{2.5-10}$ at AMS4. The modeled concentrations in $PM_{2.5}$ during the cold season are higher than that during the warm season by around a factor of 1.3 (Table 4.3). This difference in modeled concentrations between the cold season and the warm season is smaller than that at AMS1 (1.3 < 2.1). Similar to the discrepancy in the modeled total concentrations in $PM_{2.5-10}$ at AMS4, the modeled concentrations of the eight elements in $PM_{2.5-10}$, except Zn, are higher during the warm season than the cold season by around a factor of 1.2 (Table 4.3). This is because AMS4 is located downstream of a major emission source (Fig. 2.4). During the warm season, there are more westerly winds bringing more elements from this major emission source to AMS4 (Fig 3.6b & 3.7b). Thus the modeled element concentrations at AMS4 increase in the warm season.

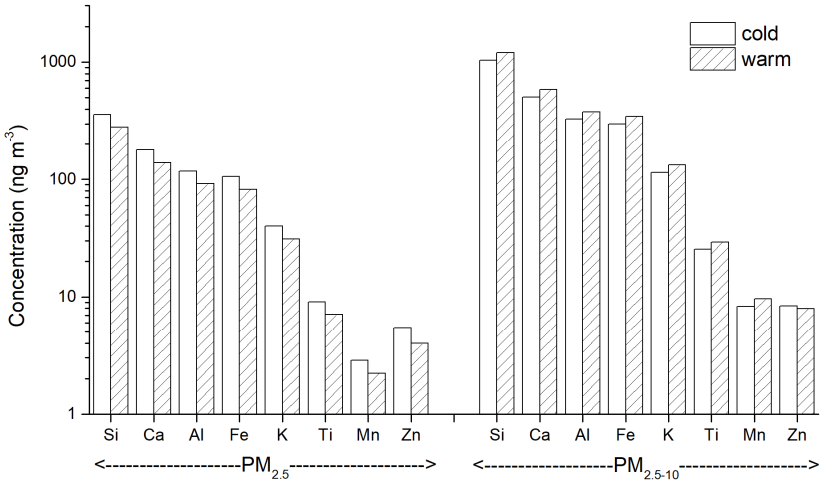

Figure 4.3 Modeled seasonal concentrations (ng/m^3) of the eight elements in $PM_{2.5}$ and $PM_{2.5-10}$ at AMS4.

The modeled total concentrations of the eight elements in $PM_{2.5}$ at AMS17 are 588 ng/m^3 and 417 ng/m^3 during the cold season and the warm season, respectively. The modeled total concentrations in $PM_{2.5}$ are 41% higher during the cold season than the warm season. The modeled total concentrations of the eight elements in $PM_{2.5-10}$ during the cold season and the warm season are 484 ng/m^3 and 450 ng/m^3, respectively. The modeled total concentrations in $PM_{2.5-10}$ are 8% higher during the cold season than the warm season. Fig. 4.4 shows the modeled concentrations of the eight elements in $PM_{2.5}$ and $PM_{2.5-10}$ during the cold and warm seasons at AMS17. The modeled concentrations of the eight elements in $PM_{2.5}$ and $PM_{2.5-10}$ during the cold season are around 40% and 10% higher than that during the warm season, respectively (Table 4.3). These seasonal differences are much smaller than those at AMS1 (40% < 110% for $PM_{2.5}$; 10% < 60% for $PM_{2.5-10}$). This is because AMS17 is located downstream of major emission sources (Fig. 2.4). During the warm season, there are more westerly winds coming from these major emission sources (Fig 3.6c & 3.7c) and more elements disperse from the emission sources to AMS17. But the modeled element concentrations are still higher in the cold season than the warm season, because the shallow PBL and stable atmosphere in the cold season prevent the vertical diffusion of elements and enhance the element concentrations near

the surface.

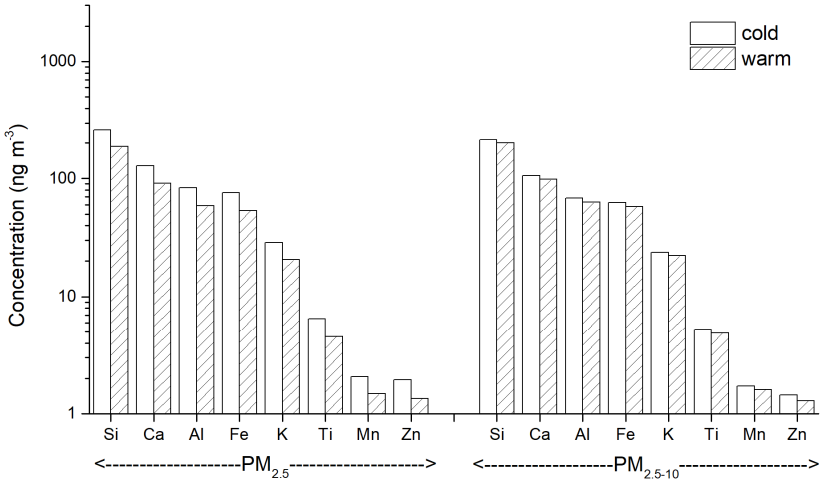

Figure 4.4 Modeled seasonal concentrations (ng/m^3) of the eight elements in $PM_{2.5}$ and $PM_{2.5\text{-}10}$ at AMS17.

The modeled total concentrations of the eight elements in $PM_{2.5}$ at AMS18 are 85 ng/m^3 and 46 ng/m^3 during the cold season and the warm season, respectively. The modeled total concentrations in $PM_{2.5}$ are 87% higher during the cold season than the warm season. The modeled total concentrations of the eight elements in $PM_{2.5\text{-}10}$ during the cold season and the warm season are 134 ng/m^3 and 101 ng/m^3, respectively. The modeled total concentrations in $PM_{2.5\text{-}10}$ are 32% higher during the warm season than the cold season. Regardless of $PM_{2.5}$ and $PM_{2.5\text{-}10}$, the seasonal difference in the modeled total concentrations at AMS18 is smaller than that at AMS1, but larger than that at AMS17. The modeled concentrations of the eight elements in $PM_{2.5}$ and $PM_{2.5\text{-}10}$ during the cold season are around 1.9 and 1.3 times higher than that during the warm season, respectively (Fig. 4.5 & Table 4.3). This is because the constant element emission rates are used in the whole year. The shallow PBL and stable atmosphere in the cold season strengthen the element concentrations near the surface.

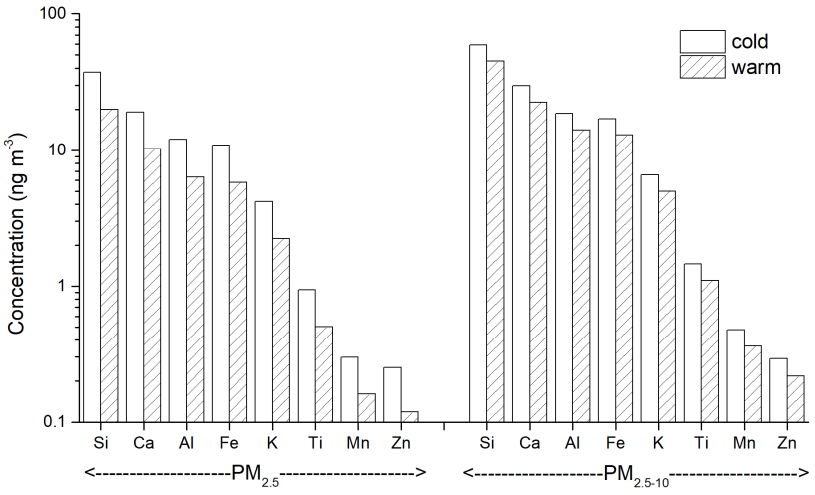

Figure 4.5 Modeled seasonal concentrations (ng/m^3) of the eight elements in $PM_{2.5}$ and $PM_{2.5\text{-}10}$ at AMS18.

Overall, the modeled concentrations of the eight elements at AMS1, AMS17, and AMS18 are higher in the cold season than the warm season. The low surface temperature in the cold season produces a stable atmosphere. The shallow PBL and stable atmosphere prevent elements from the vertical mixing and enhance the elements near the surface. The seasonal difference in the modeled concentrations of the eight elements is largest at AMS1, followed by AMS18 and AMS17. On the contrary, the modeled concentrations of seven elements (Si, Ca, Al, Fe, K, Ti, and Mn) in $PM_{2.5\text{-}10}$ at AMS4 are higher during the warm season than the cold season. This is because AMS4 is located downstream of a major emission source. During the warm season, there are more westerly winds blowing from this major emission source to AMS4. Thus, more elements spread from this emission source to AMS4, leading to the higher modeled element concentrations at AMS4.

4.4 Seasonal element deposition

At AMS1, the modeled total dry deposition of the eight elements during the cold season and the warm season are 140 mg m^{-2}yr^{-1} and 125 mg m^{-2}yr^{-1}, respectively. The modeled total wet deposition of the eight

elements are 65 mg $m^{-2}yr^{-1}$ and 49 mg $m^{-2}yr^{-1}$ during the cold season and the warm season, respectively. For both dry and wet deposition, the total deposition are higher during the cold season than the warm season, because of the higher modeled element concentrations during the cold season (Fig. 4.2). The total dry deposition are higher than the total wet deposition by a factor of 2.2 and 2.6 in the cold season and the warm season, respectively. Regardless of element and dry or wet deposition, the modeled deposition of the eight elements is 1.2 times higher in the cold season than that in the warm season on average (Table 4.4 & Fig. 4.6). This is because both dry and wet element deposition depend on the modeled element concentrations. In the cold season, higher modeled element concentrations at AMS1 are predicted by the model under the shallow PBL and stable atmosphere near the surface (Fig. 4.2). The modeled dry deposition of individual elements are higher than the modeled wet deposition by around a factor of 2.1 during the cold season and by around a factor of 2.5 during the warm season (Fig. 4.6), indicating the removal of elements in the atmosphere is dominated by the dry deposition although the modeled dry and wet deposition are in the same order of magnitude.

Table 4.4 The modeled seasonal dry and wet deposition (mg $m^{-2}yr^{-1}$) of the eight elements at the four stations during 2016-2017.

Stations	Deposition	Seasons	Elements							
			Si	Ca	Al	Fe	K	Ti	Mn	Zn
AMS1	Dry	cold	62	30	20	18	6.8	1.5	0.49	0.58
		warm	55	27	18	16	6	1.4	0.43	0.57
	Wet	cold	29	14	9.5	8.4	3.1	0.73	0.22	0.27
		warm	22	10	7.3	6.3	2.3	0.55	0.17	0.23
AMS4	Dry	cold	42	20	14	12	4.6	1.1	0.33	0.45
		warm	56	27	19	16	5.9	1.4	0.43	0.73
	Wet	cold	29	14	11	8.5	2.9	0.79	0.21	0.43
		warm	27	12	10	8	2.6	0.77	0.18	0.54
AMS17	Dry	cold	46	22	14	13	5	1.1	0.36	0.31
		warm	47	23	15	14	5.2	1.2	0.37	0.32
	Wet	cold	28	14	8.8	8	3.1	0.68	0.22	0.16
		warm	28	13	8.7	7.9	3	0.67	0.22	0.16
AMS18	Dry	cold	6.5	3.2	2.1	1.9	0.72	0.16	0.052	0.034
		warm	5.3	2.6	1.7	1.5	0.58	0.13	0.042	0.027
	Wet	cold	2	1	0.65	0.59	0.22	0.05	0.016	0.013
		warm	2.1	1.1	0.68	0.62	0.24	0.053	0.017	0.012

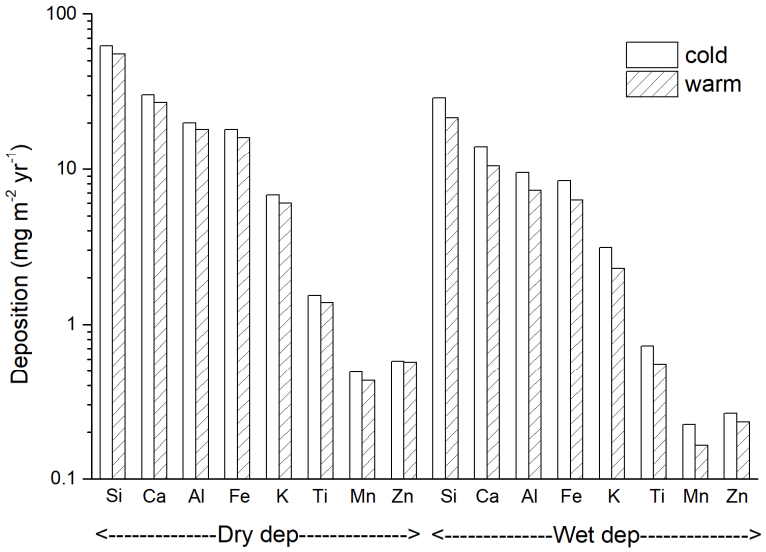

Figure 4.6 Modeled seasonal dry and wet deposition (mg $m^{-2}yr^{-1}$) of the eight elements at AMS1.

The modeled total dry deposition of the eight elements at AMS4 during the cold season and the warm season are 95 mg $m^{-2}yr^{-1}$ and 126 mg $m^{-2}yr^{-1}$, respectively, whereas the modeled total wet deposition are 66 mg $m^{-2}yr^{-1}$ and 61 mg $m^{-2}yr^{-1}$ during the cold season and the warm season, respectively. Similar to AMS1, the total dry deposition are 1.46 and 2.06 times higher than the total wet deposition in the cold season and the warm season, respectively. However, contrary to AMS1, the total dry deposition is 33% higher during the warm season than the cold season, due to the higher modeled element concentrations in $PM_{2.5-10}$ during the warm season at AMS4 (Fig. 4.3). Although the modeled element concentrations in the fine mode ($PM_{2.5}$) during the warm season are lower (Fig. 4.3), the removal of elements through dry deposition is dominated by the coarse mode ($PM_{2.5-10}$) with a larger particle size. Thus, the higher modeled element concentrations in $PM_{2.5-10}$ during the warm season lead to the higher dry deposition during the warm season. Contrary to AMS1, the total wet deposition in the cold season is close to that in the warm season. The higher modeled element concentrations in $PM_{2.5-10}$ and more precipitations during the warm season produce a similar wet deposition in both seasons, indicating that the coarse modes cannot control

the wet deposition.

Similar to AMS1, the dry deposition of individual elements at AMS4 are higher than their wet deposition by around a factor of 1.6 and a factor of 2 during the cold season and the warm season, respectively (Fig. 4.7 & Table 4.4). However, contrary to AMS1, although the wet deposition of individual elements (except Zn) are around 10% higher in the cold season, the dry deposition of individual elements are around 1.6 times higher in the warm season than the cold season (Fig. 4.7) due to the higher modeled element concentrations in $PM_{2.5-10}$ during the warm season (Fig. 4.3) and the dominance of $PM_{2.5-10}$ in the dry deposition.

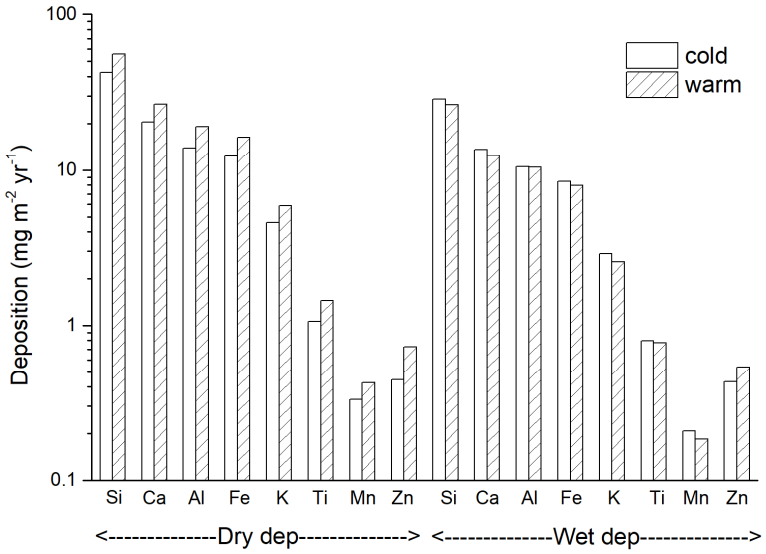

Figure 4.7 Modeled seasonal dry and wet deposition (mg $m^{-2}yr^{-1}$) of the eight elements at AMS4.

At AMS17, the modeled total dry deposition of the eight elements are 102 mg $m^{-2}yr^{-1}$ and 106 mg $m^{-2}yr^{-1}$ during the cold season and the warm season, respectively, whereas the modeled total wet deposition are 63 mg $m^{-2}yr^{-1}$ and 62 mg $m^{-2}yr^{-1}$ during the cold season and the warm season, respectively. Contrary to AMS1, both total dry and wet deposition during the cold season are close to that during the warm season. Similarly, both dry and wet deposition of individual elements in the cold season are close to that in the

warm season at AMS17 (Fig. 4.8). Although the modeled concentrations of the eight elements are higher in the cold season than the warm season at both AMS1 and AMS17 (Fig. 4.2 & 4.4), the seasonal differences are smaller at AMS17 than AMS1 (40% < 110% for $PM_{2.5}$; 10% < 60% for $PM_{2.5\text{-}10}$). The modeled precipitation during the warm season at AMS17 is more than that at AMS1 (Fig. 3.2). As a result, the modeled wet deposition at AMS17 is similar in both seasons, while that at AMS1 is higher in the cold season. The modeled dry deposition velocity is higher in the warm season at AMS1 and AMS17 (Fig. 4.9), but the seasonal differences are smaller at AMS17 than AMS1 (averaged for 4 size bins, 23% < 81%). As a production of the modeled element concentration and the modeled dry deposition velocity, the modeled dry deposition at AMS17 are similar in both seasons, whereas that at AMS1 is higher in the cold season. In addition, similar to AMS1, the dry deposition of individual elements at AMS17 are around 1.6 times and 2 times higher than that wet deposition during the cold season and the warm season, respectively (Fig. 4.8).

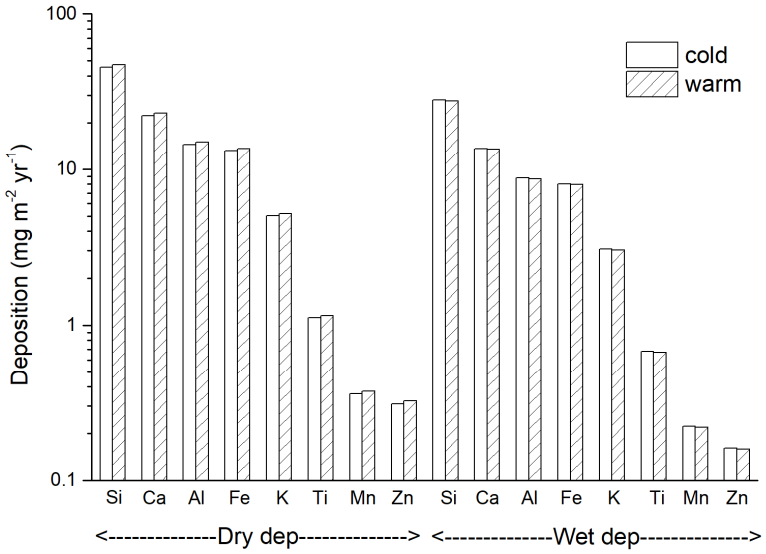

Figure 4.8 Modeled seasonal dry and wet deposition (mg $m^{-2}yr^{-1}$) of the eight elements at AMS17.

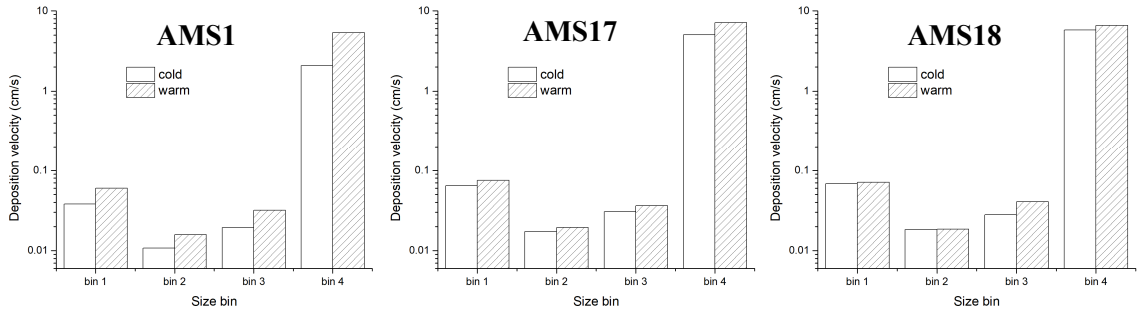

Figure 4.9 Seasonal dry deposition velocity (cm/s) for the four size bins at AMS1, AMS17, and AMS18.

The modeled total dry deposition of the eight elements at AMS18 are 15 mg $m^{-2}yr^{-1}$ and 12 mg $m^{-2}yr^{-1}$ during the cold season and the warm season, respectively. The modeled total wet deposition are 4.6 mg $m^{-2}yr^{-1}$ and 4.8 mg $m^{-2}yr^{-1}$ during the cold season and the warm season, respectively. Similar to other three sites, the total dry deposition are 3.2 and 2.5 times higher than that total wet deposition during the cold and warms seasons, respectively. Similar to AMS17, the total dry and wet deposition during the warm season are similar to that in the cold season. Similar to other three sites, the dry deposition of individual elements are higher than their wet deposition by around a factor of 3 and 2.2 during the cold season and the warm season, respectively (Fig. 4.10). Similar to AMS1, the modeled dry deposition of individual elements are around 1.23 times higher during the cold season than the warm season (Fig. 4.10) because of the higher modeled element concentrations during the cold season (Fig. 4.5). Similar to AMS17, the modeled wet deposition of individual elements are similar in both seasons (Fig. 4.10) as a result of more precipitations during the warm season (Fig. 3.2), despite the lower modeled element concentrations during the warm season (Fig. 4.5).

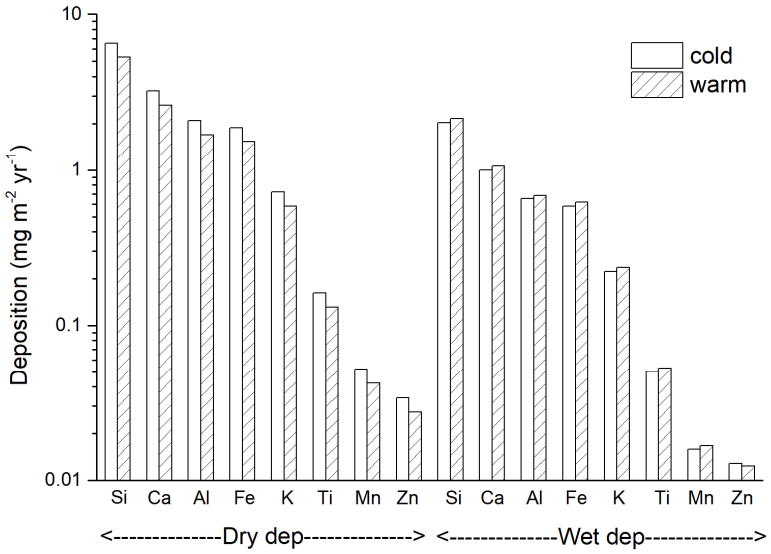

Figure 4.10 Modeled seasonal dry and wet deposition (mg $m^{-2}yr^{-1}$) of the eight elements at AMS18.

Overall, regardless of AMS site and season, the modeled dry deposition of individual elements (or the eight elements together) are always larger than their modeled wet deposition, suggesting that the dry deposition process dominates the removal of elements in the AOSR. This is because the precipitation amount determines the predominance of removal processes being dry or wet deposition. The modeled annual precipitation (SWE + rain) is around 700 mm in the AOSR during 2016-2017. In the in-situ observations of element dry and wet deposition near industrial areas, it was reported that the predominance of element removal was different at measurement locations with different precipitation amount (Al-Momani et al., 2002; Wu et al., 2018). In addition, on the seasonal basis, the modeled element dry deposition is determined by the modeled element concentration and the modeled element dry deposition velocity. The higher dry deposition during the cold season at AMS1 and AMS18 and the higher dry deposition during the warm season at AMS4 are because of their higher modeled element concentrations in the corresponding season. The higher dry deposition during the warm season at AMS17 is due to the larger dry deposition velocities. However, the modeled element wet deposition is determined by the

modeled element concentration and the modeled precipitation, as discussed in Eq. 2.3 & 2.4. The higher wet deposition during the cold season at AMS1 and AMS4 were owing to their higher modeled element concentrations during the cold season. The wet deposition during the cold season are close to that during the warm season at AMS17 and AMS18, due to more precipitations during the warm season.

Mamun et al. (2022) estimated the seasonal dry and wet deposition for elements at three AMS sites during 2016-2017 by developing a deposition framework. Contrary to our modeling results, they reported that the calculated wet deposition of elements was larger than that dry deposition, and they concluded that wet deposition was the dominant process for the removal of elements in the AOSR. Similar to our findings, they found that the wet deposition of almost all elements were higher in winter at AMS1 and AMS17, whereas the wet deposition was higher in summer at AMS18. However, they stated that the dry deposition of the seven elements (Si, Ca, Al, Fe, K, Ti, and Mn) were higher in summer than in winter at AMS1, AMS17, and AMS18 because of the higher estimated deposition velocities in summer.

4.5 Spatial distribution for element concentrations

Figure 4.11 are longitude-height and latitude-height cross sections of modeled seasonal averaged potential temperature, wind, and total concentration of the eight elements centered at AMS1. Along with altitude and latitude, the modeled wind speed is always smaller near the surface in the warm season than in the cold season. The modeled potential temperature increases from 266 K to 282 K with 2 km height in the cold season. In the warm season, the potential temperature varies from 290 K to 304 K in 4 km height. The atmosphere is more stable in the cold season when the potential temperature increases more rapidly with height. The stable atmosphere in the cold season prevents the vertical diffusion of elements, and thus the modeled total concentrations of the eight elements decline dramatically from the surface to the upper air. The total concentration is low under 0.001 μg m^{-3} (1 ng m^{-3}) at around 2 km, and it is up to 3 μg m^{-3} in the surface. However, during the warm season, the total concentrations decrease from 2 μg m^{-3} to 0.001 μg m^{-3} (1 ng m^{-3}) between the surface and a height of 3 km.

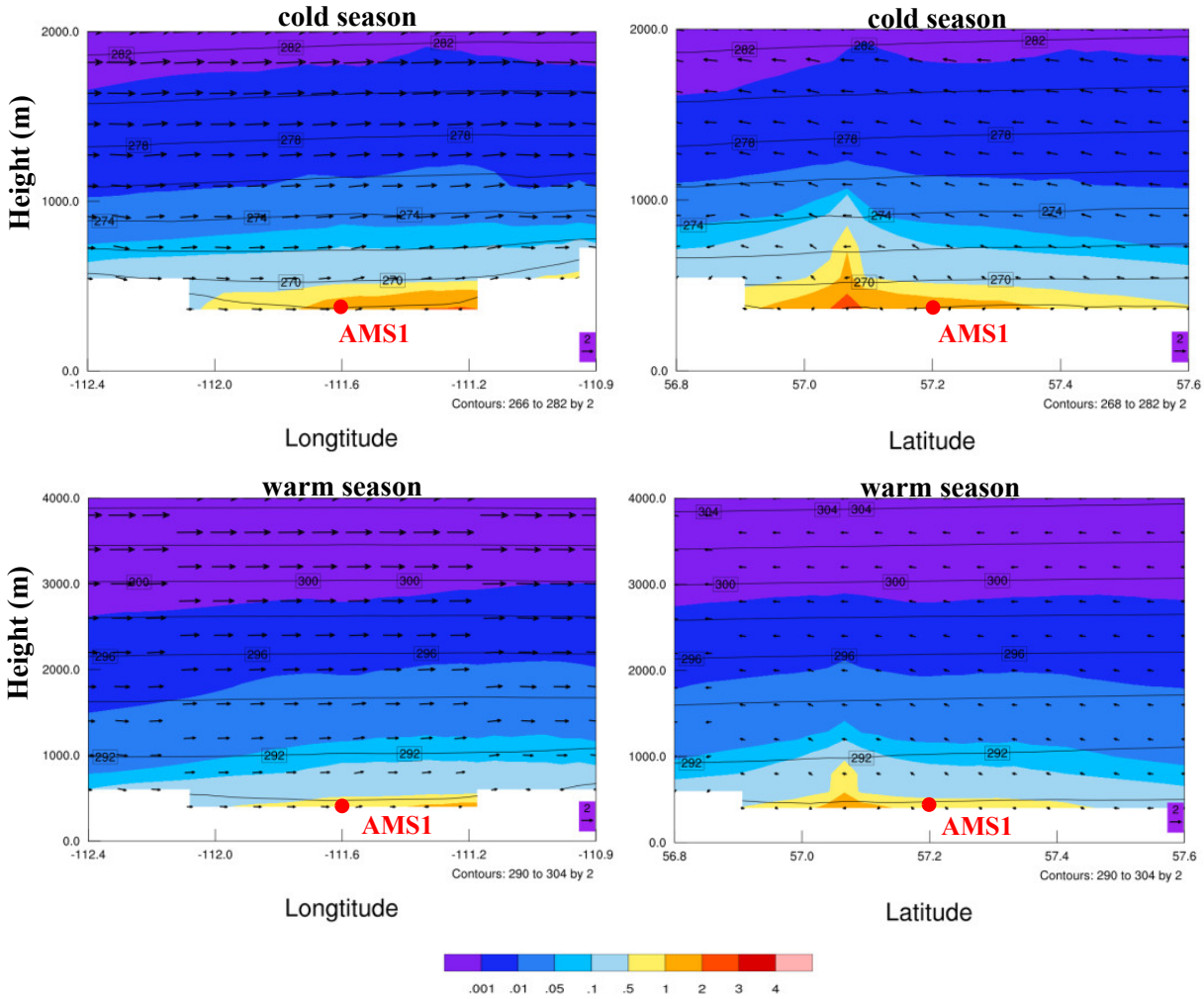

Figure 4.11 Longitude-height and latitude-height cross sections of seasonal modeled potential temperature (K, contour lines), wind (m/s, wind arrows), and total concentration of the eight elements (μg m^{-3}, shaded contours) with AMS1 as the center point (w-component of wind is multiplied by 10).

The modeled seasonal meteorological conditions (potential temperature and wind) with the height at AMS4, AMS17, and AMS18 (Fig. 4.12-4.14) are similar to those at AMS1 (Fig. 4.11). During the cold season, the modeled wind speed is larger and the modeled potential temperature increases more rapidly with increased height. At all three sites, the modeled total concentrations of the eight elements are higher near the surface and decrease significantly to 0.001 μg m^{-3} (1 ng m^{-3}) at around 2 km in the cold season when the atmosphere is more stable. The vertical dispersion of elements is suppressed and elements are forced to move horizontally near the surface, potentially leading to serious local environmental impacts.

On the contrary, the warm and less stable atmosphere in the warm season supports the vertical diffusion of elements and weakens the horizontal transport of elements. As a result, the modeled total concentrations are lower near the surface and are 0.001 μg m^{-3} (1 ng m^{-3}) at around 3 km.

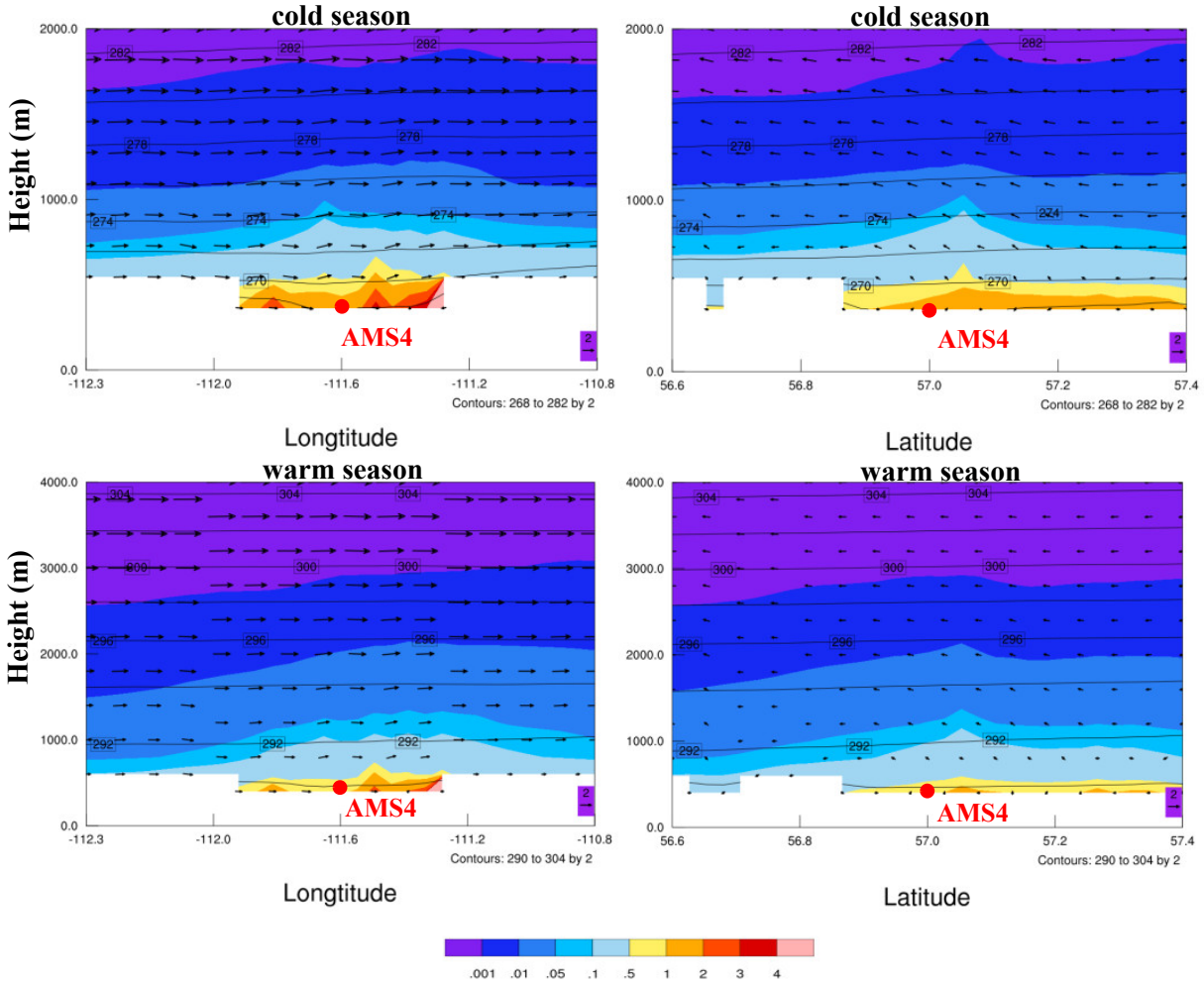

Figure 4.12 Same as Fig. 4.11 but with AMS4 as the center point.

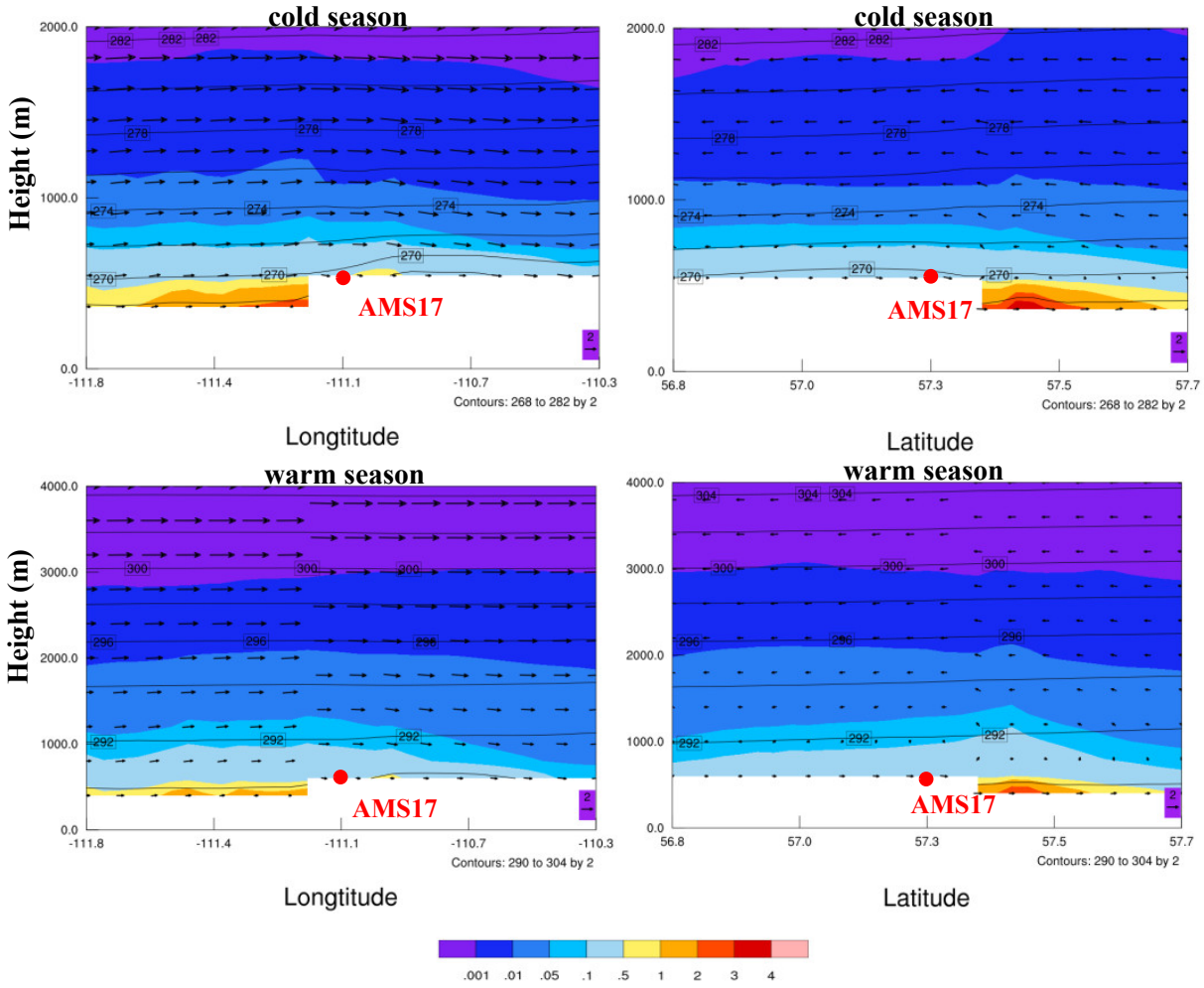

Figure 4.13 Same as Fig. 4.11 but with AMS17 as the center point.

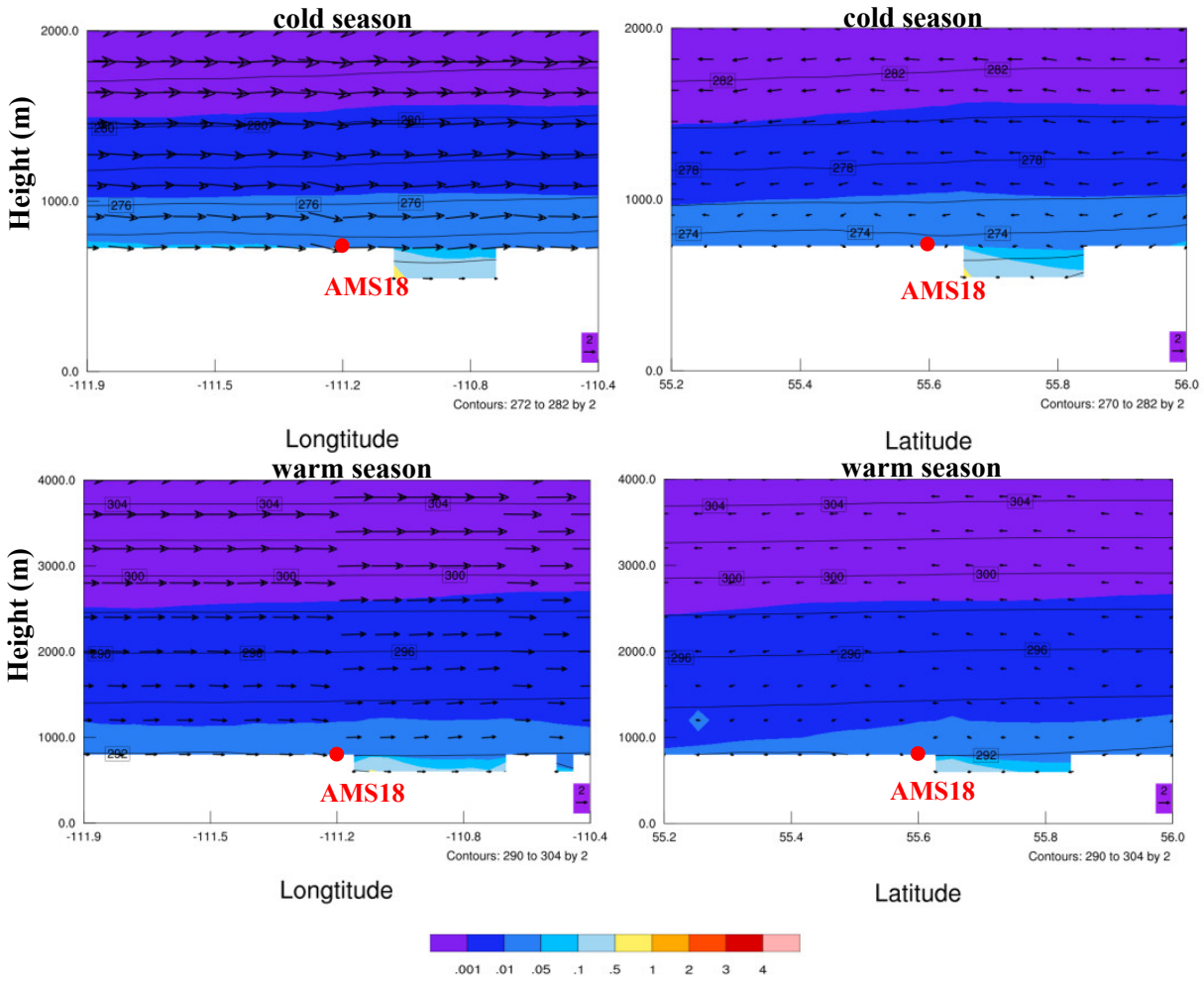

Figure 4.14 Same as Fig. 4.11 but with AMS18 as the center point.

The spatial distributions of modeled seasonal concentrations of the eight elements in PM_{10} are shown as Fig. 4.15 and Fig. 4.16. The spatial distribution covers the AOSR (Fig. 4.17b). During the cold season, all elements have a similar spatial pattern with a major spread in the north and south direction (Fig. 4.15), agreeing with the prevailing winds blowing from north and south at the four AMS sites (Fig. 3.5). Si has the highest modeled concentration, followed by Ca, Al, Fe, K, Ti, Mn, and Zn, agreeing with the order of their magnitudes of emission rates (Fig. 2.1). Similar to the cold season, all elements mostly disperse in the north and south direction during the warm season (Fig. 4.16). For different elements, the discrepancies in the emission mostly affect their spatial distributions. Their different emission sources firstly have an impact on the spatial distribution. Even at the same emission source location, their different emission rates

and their different speciation between fine and coarse modes also have an influence on the spatial distribution. The emission speciation determines the mass in the fine and coarse modes, and subsequently determines the removal of elements by deposition.

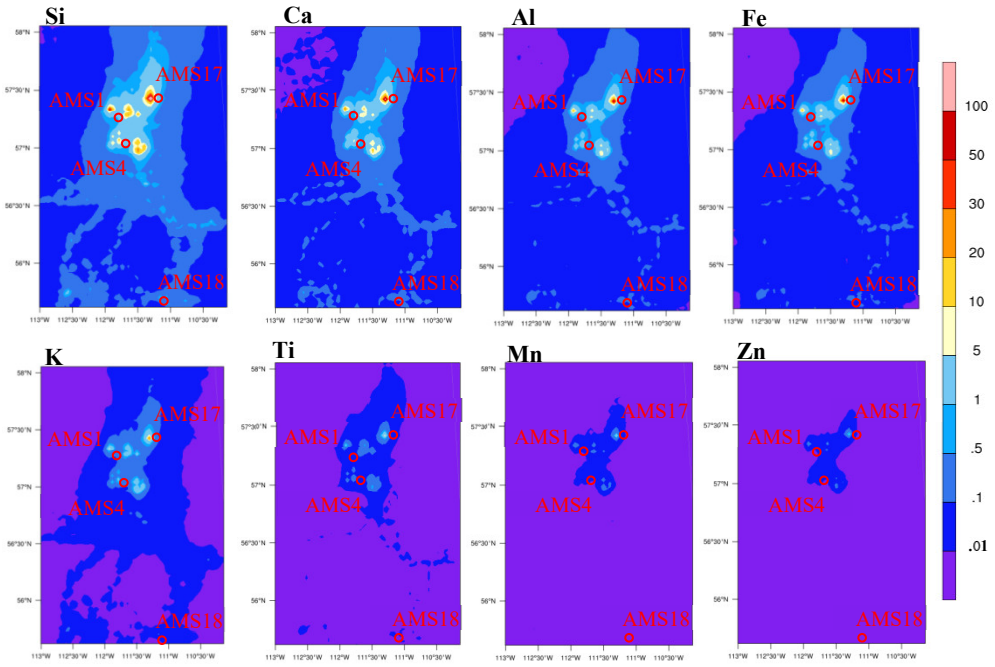

Figure 4.15 Spatial distribution for modeled concentrations (μg/m^3) of the eight elements in PM_{10} during the cold season at the lowest model level about 3 m above the ground.

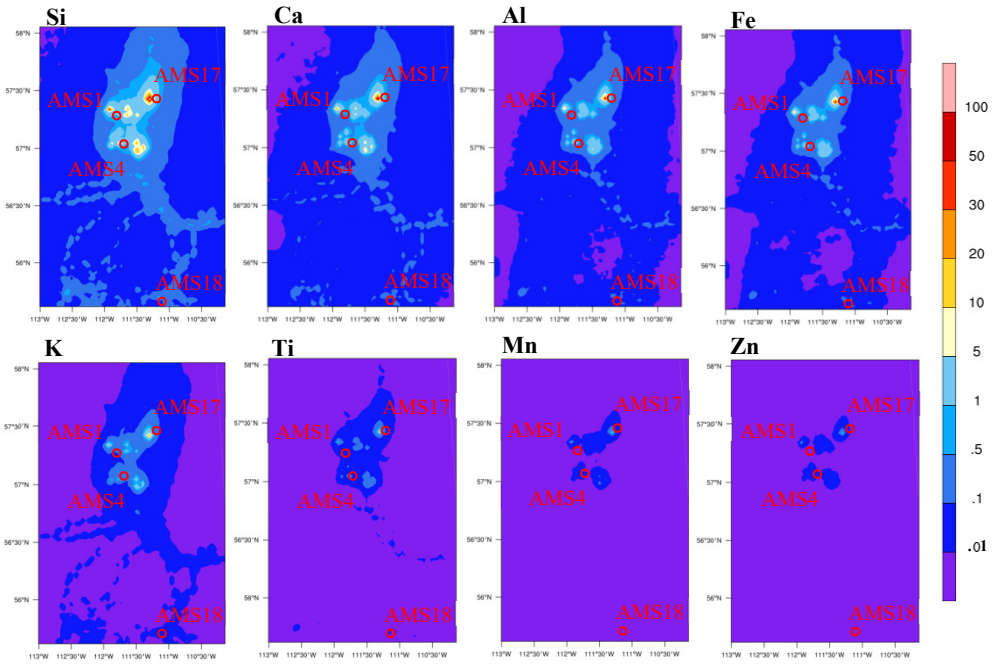

Figure 4.16 Spatial distribution for modeled concentrations (μg/m^3) of the eight elements in PM_{10} during the warm season at the lowest model level about 3 m above the ground.

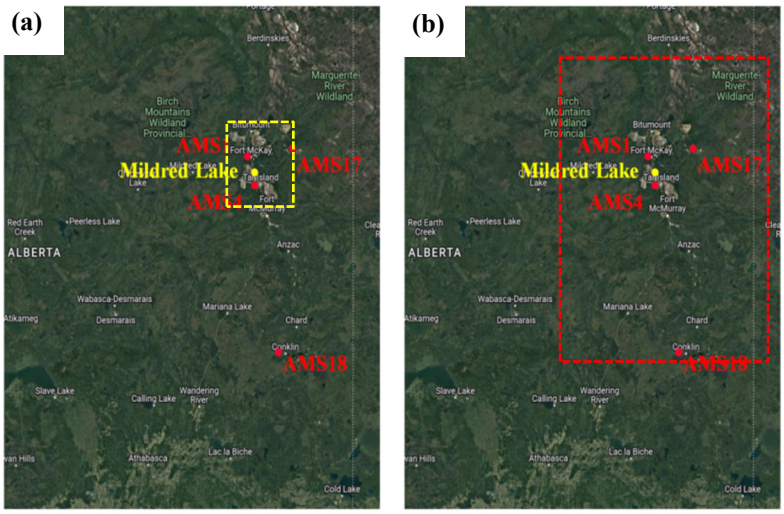

Figure 4.17 The (a) central region (yellow box, 45 km×54 km) and (b) spatial distribution mapping region (red box) in the AOSR (from Google Maps).

Additionally, in both seasons, most of the elements are concentrated in the central region (45km×54km, Fig. 4.17a) with the major oil sands industry facilities in the AOSR. The three monitoring sites,

namely AMS1, AMS4, and AMS17, are also located within this central region for the measurement of elements in the ambient air. The domain averaged concentrations of the elements are computed by averaging all the grid point values in this central region (yellow box in Fig. 4.17a). In the central region, the modeled concentrations of the eight elements are in the range of 0.02-3.25 μg m^{-3} and 0.013-2.1 μg m^{-3} in the cold and warm seasons, respectively (Table 4.5). Kelly et al. (2010) investigated the concentrations of 13 USEPA priority toxic elements in water of the AOSR. These elements may enter water from the atmosphere through dry or wet deposition. They found that some elements increased significantly near oil sands development. Additionally, in our study, the modeled concentrations of the eight elements are larger during the cold season because the constant element emission rate is used throughout the whole year and the stable atmosphere elevates the element concentrations near the surface in the cold season (Fig. 4.12-4.14). The element concentrations decline by three orders of magnitude in the distance of around 150 km from the hotspot of oil sands industry to the remote area. Gueguen et al. (2016) reported that some element concentrations (e.g. Al, Fe, Ti, and Zn) had a high level within a 60-80 km radius before they exponentially decreased to a relatively constant value in the AOSR. Huang et al. (2016) also stated that some element concentrations (e.g. Al and Fe) had an exponential decrease with distance from the mining sites.

Table 4.5 The modeled element concentrations (μg m^{-3}) and deposition (mg $m^{-2}yr^{-1}$) on average of grids in the center region.

Variables	Seasons	Elements							
		Si	Ca	Al	Fe	K	Ti	Mn	Zn
Concentration	cold	3.25	1.59	1.01	0.94	0.36	0.078	0.026	0.02
	warm	2.1	1.02	0.65	0.6	0.23	0.05	0.017	0.013
	annual	2.67	1.31	0.83	0.77	0.3	0.065	0.021	0.016
Deposition (dry+wet)	cold	194	94	61	56	21	4.73	1.54	1.29
	warm	191	93	61	55	21	4.68	1.51	1.34
	annual	385	187	122	111	42	9.4	3.05	2.62

As shown in the spatial distribution of modeled total concentrations of the eight elements in PM_{10} during the cold season and the warm season (Fig. 4.18), the distribution of total concentrations is similar to that of concentrations for individual elements (Fig. 4.15 and 4.16) with the dispersion in the direction of north and south. The modeled total concentrations of the eight elements are slightly higher during the cold season when the stable atmosphere and shallow PBL enhances the element concentrations near the surface. In both seasons, the maximum total concentrations are located around 15 km west of AMS17. The modeled annual concentrations of the eight elements in the central region of oil sands industry are listed in Table 4.5 and their modeled annual total concentration is 5.98 μg m^{-3}. The modeled total concentration declines by around three orders of magnitude in the distance of around 150 km from the central region of oil sands industry to the remote area, indicating the substantial contribution by oil sands facilities to ambient element concentrations at nearby communities and the small impact on the remote environment. Yang et al. (2023) plotted spatial distributions of element concentrations in PM_{10} predicted by a dispersion model over the AOSR during 2016-2017. Their spatial pattern of elements is similar to ours. They also found that the location of maximum element concentrations was to the northwest of AMS17, and the

elevated element concentrations were restrained within the region with oil sands industry activities. However, their magnitude of simulated Mn is smaller than our predictions by approximately a factor of five. This discrepancy is expected because the dispersion model and WRF-Chem produce different modeled meteorological conditions, dispersion, and deposition.

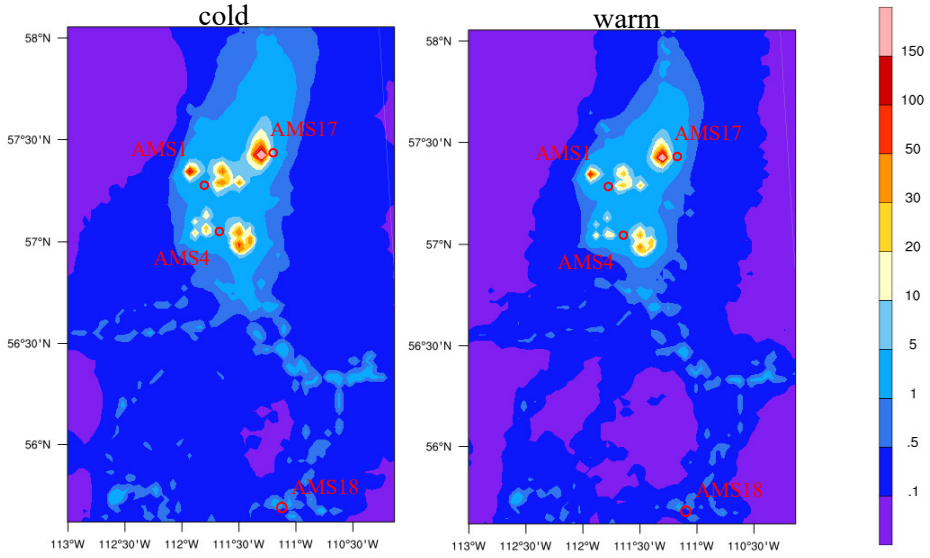

Figure 4.18 Spatial distribution for modeled total concentrations (μg/m^3) of the eight elements in PM_{10} during the cold and warm seasons at the lowest model level about 3 m above the ground.

4.6 Spatial distribution for element deposition

The spatial mapping of modeled dry deposition of the eight elements in PM_{10} during the cold season and the warm season are shown in Fig. 4.19 and Fig. 4.20, respectively. For all the eight elements, the patterns during the cold season are similar to those during the warm season. During the warm season, the dry deposition spreads more in the direction of east and west. There are more easterly & westerly winds during the warm season (Fig. 3.5-3.6). These winds carry the elements further away from the emission sources, allowing more deposition along the path. Si has the highest modeled dry deposition, followed by Ca, Al, Fe, K, Ti, Mn, and Zn, agreeing with their modeled concentrations (Fig. 4.15 & 4.16). Similar to dry deposition, the modeled wet deposition of the eight elements in PM_{10} during the cold season mainly

have a distribution in the north-south direction (Fig. 4.21), whereas they have a more round pattern in all directions during the warm season (Fig. 4.22) due to winds (Fig. 3.5-3.6) and precipitation distributions (Fig. 4.23). The largest modeled wet deposition is from Si, followed by Ca, Al, Fe, K, Ti, Mn, and Zn. For both dry and wet deposition, the large values of individual elements occur in the central region of the AOSR where the major oil sands industry is located. Around 150 km distance from the hotspot of the oil sands region to the remote region, there is a decrease in the deposition by three orders of magnitude. In the central region, the modeled total deposition (dry + wet) of the eight elements range from 1.29 mg $m^{-2}yr^{-1}$ to 194 mg $m^{-2}yr^{-1}$ and from 1.34 mg $m^{-2}yr^{-1}$ to 191 mg $m^{-2}yr^{-1}$ in the cold and warm seasons, respectively (Table 4.5). Contrary to the seasonal modeled element concentrations, the modeled total deposition of individual elements in the central region during the cold season are close to that during the warm season (Table 4.5), although the modeled concentration of each element in the hotspot region is lower during the warm season (Fig. 4.15-4.16 & Table 4.5). This is because more precipitations in the warm season strengthens the removal of elements through wet deposition. At the same time, rougher surfaces with growing plants in the warm season weaken the surface resistance and enhance the removal of elements by dry deposition (Eq. 2.2).

Mamun et al. (2023) calculated seasonal element deposition in the central region of the AOSR, and they found that dry deposition of the eight elements (Si, Ca, Al, Fe, K, Ti, Mn, and Zn) were higher in the warm season due to the higher simulated element concentrations during the warm season. They also reported that wet deposition of the eight elements were larger in the cold season than that in the warm season or close to each other in both seasons owing to the larger removal efficiency by snow than rain. They produced higher total deposition (dry + wet) of two elements (Ca & Mn) and lower total deposition of five elements (Si, Al, Fe, K, and Zn) during the cold season, and similar total deposition of Ti in both seasons. However, their seasonal total deposition of the eight elements have the same order of magnitude as ours. This is because they used the modeled element concentrations from a dispersion model. The dispersion model and WRF-Chem produce different meteorological conditions, different atmospheric

dispersions, and different element concentrations. In addition, they used a different deposition scheme than ours.

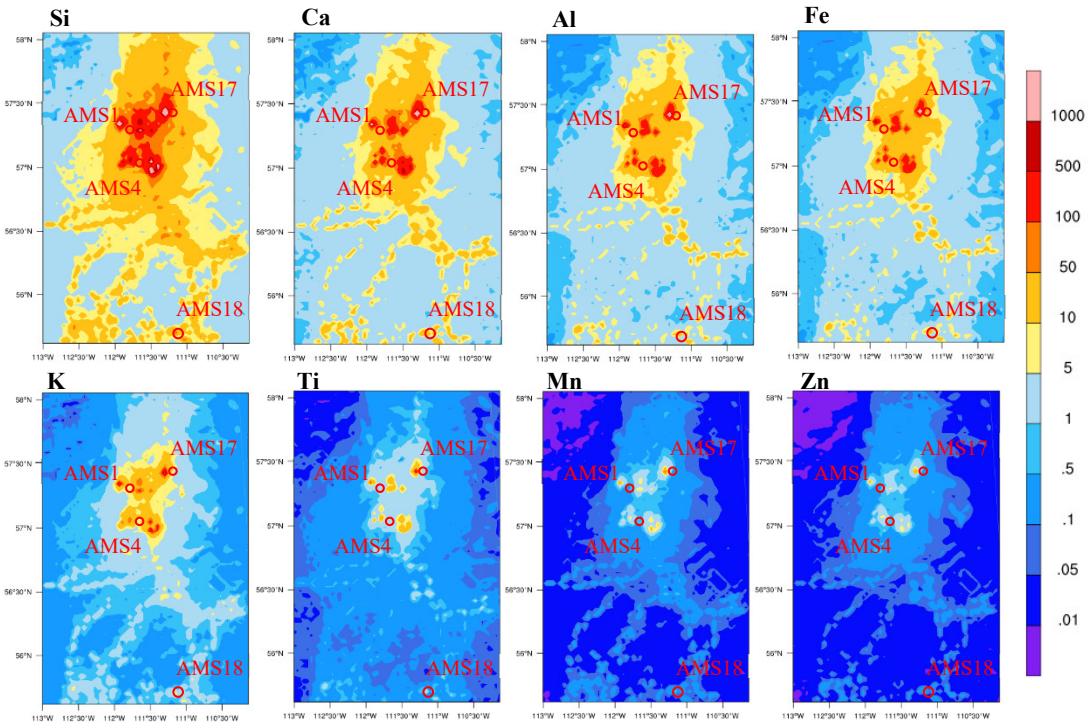

Figure 4.19 Spatial distribution for modeled dry deposition (mg $m^{-2}yr^{-1}$) of the eight elements in PM_{10} during the cold season.

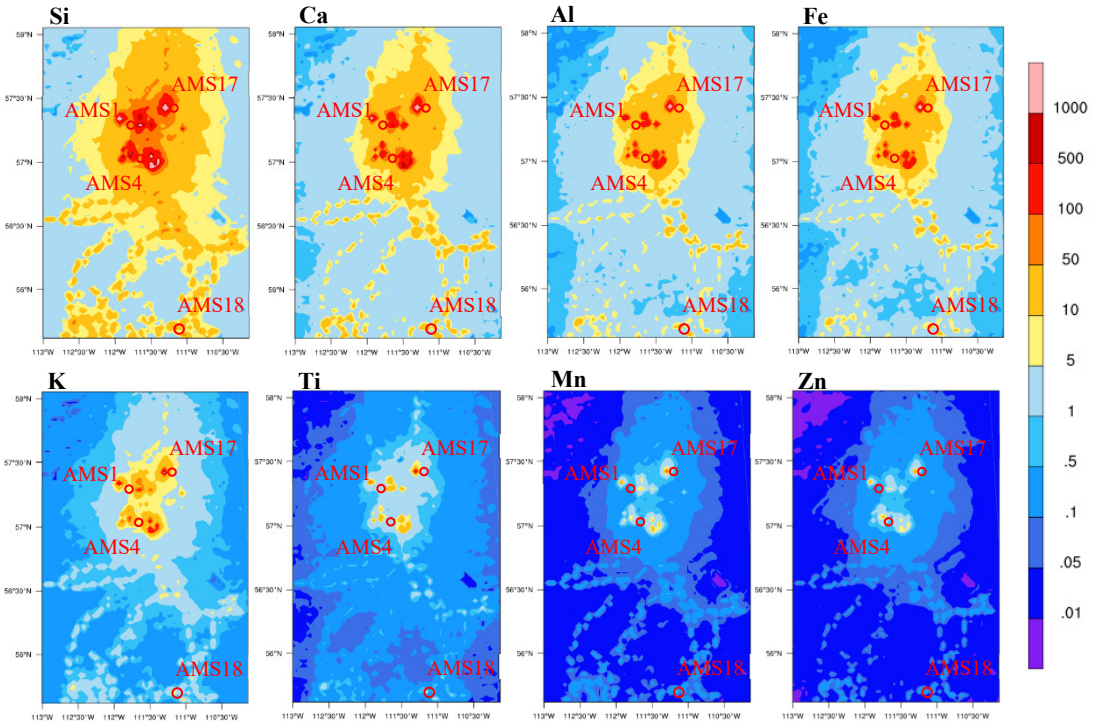

Figure 4.20 Spatial distribution for modeled dry deposition (mg $m^{-2}yr^{-1}$) of the eight elements in PM_{10} during the warm season.

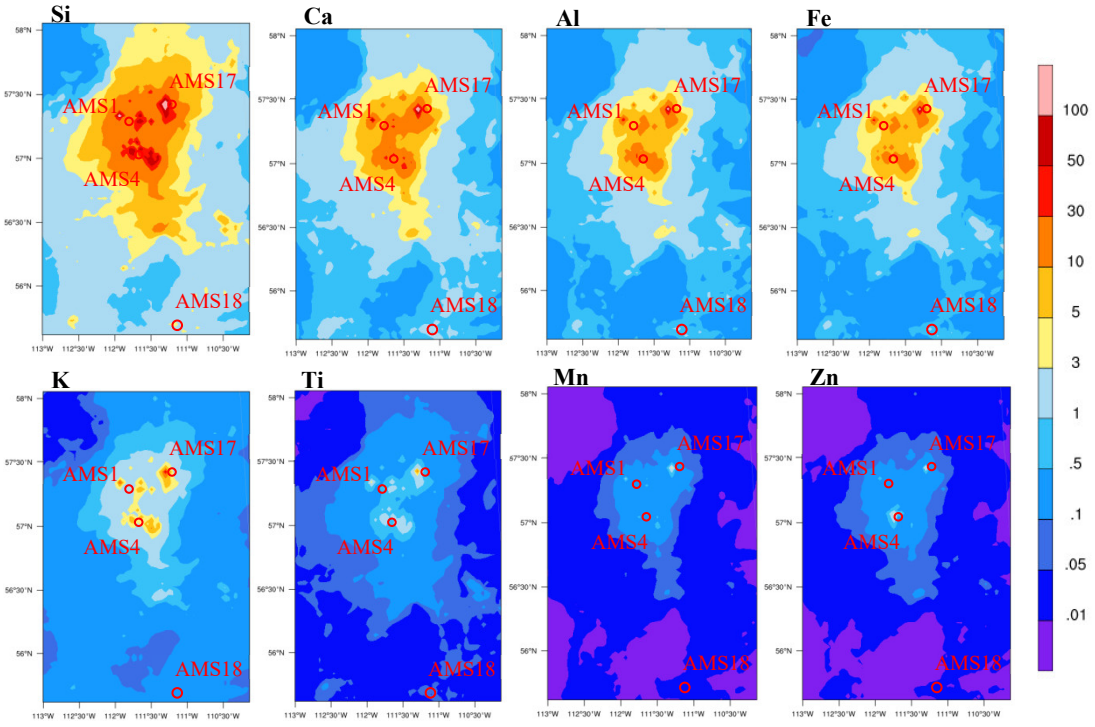

Figure 4.21 Spatial distribution for modeled wet deposition (mg $m^{-2}yr^{-1}$) of the eight elements in PM_{10} during the cold season.

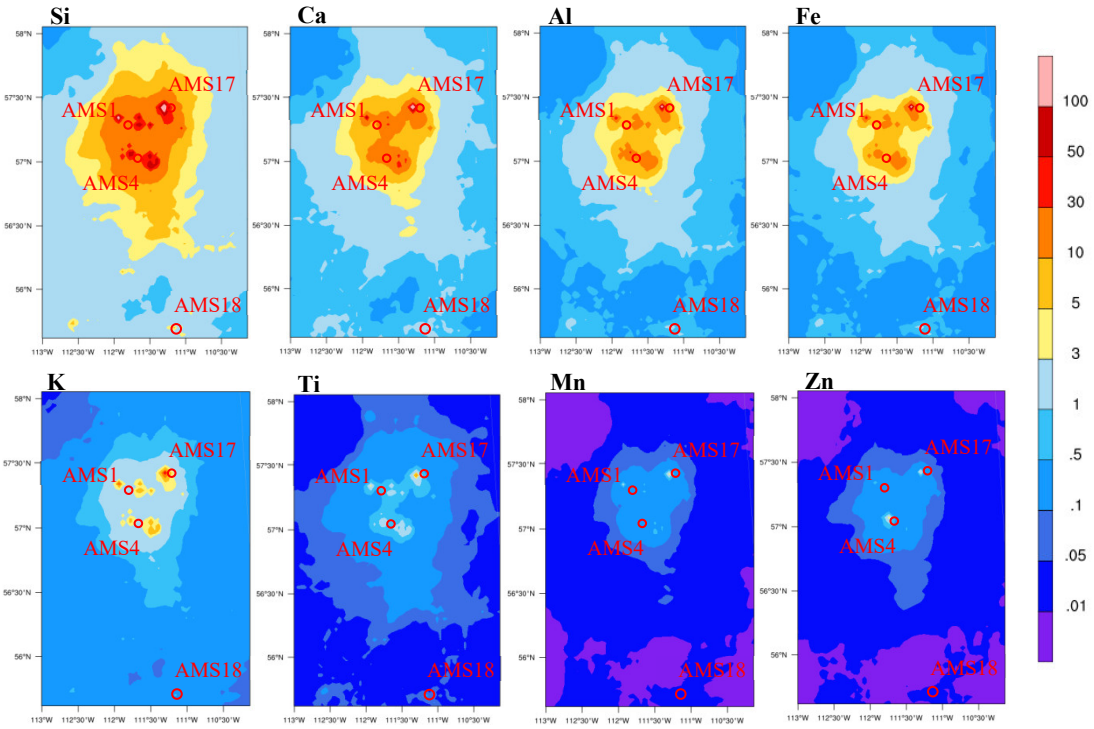

Figure 4.22 Spatial distribution for modeled wet deposition (mg $m^{-2}yr^{-1}$) of the eight elements in PM_{10} during the warm season.

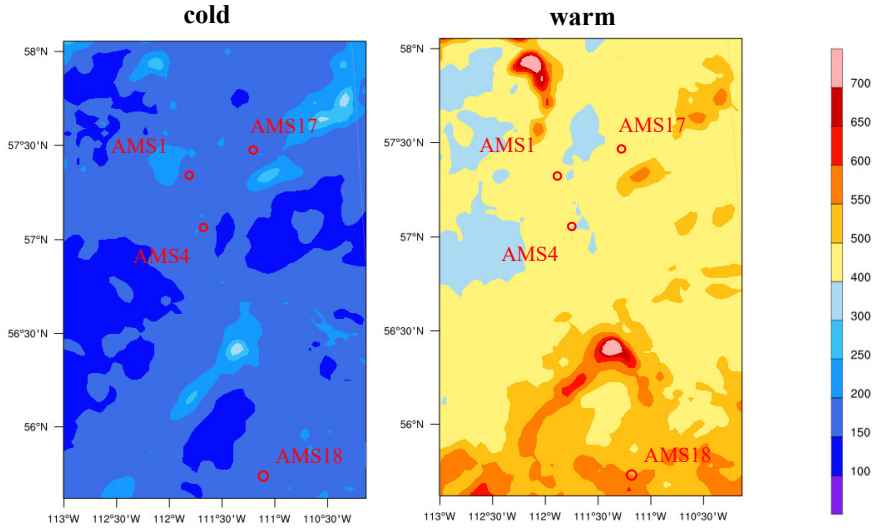

Figure 4.23 Modeled precipitation (mm) during the cold and warm seasons.

Similar to the seasonal spatial distribution of modeled dry and wet deposition of the eight elements, the spatial pattern of modeled annual total dry and wet deposition of the eight elements mainly spreads in

the north-south direction (Fig. 4.24). Gueguen et al. (2016) reported that the maximum element deposition were along river stations in the AOSR because north-south prevailing winds of the oil sands region in winter caused effects on element deposition. On the yearly basis, around 20% of elements from the emission sources are removed from the atmosphere to the surfaces within the hotspot region of the AOSR by dry and wet deposition. Around 80% is finally removed by atmospheric deposition in domain 2 (Fig. 2.3), and the other 20% is suspended in the atmosphere and removed outside domain 2. In the central region, the modeled annual total deposition (dry + wet) of the eight elements are listed in Table 4.5. Both total dry and wet deposition of all eight elements decline by around three orders of magnitude from the central region to the remote region, suggesting the substantial contribution to the local environment by the oil sands industry development.

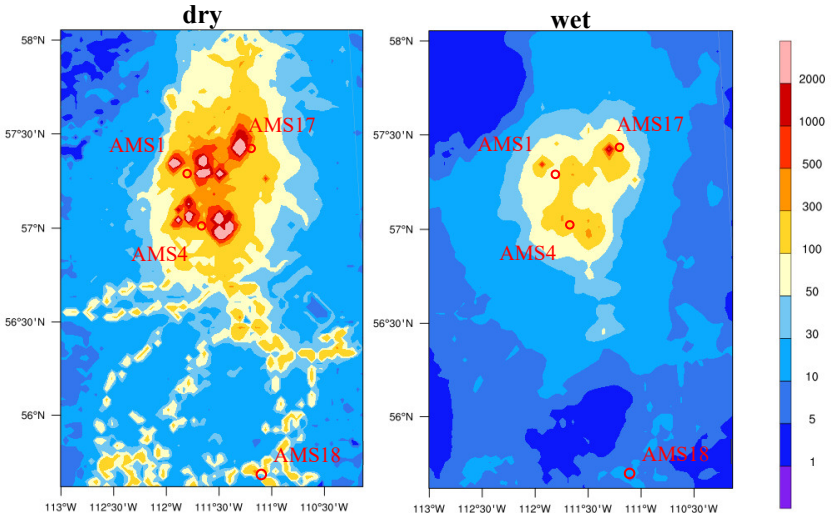

Figure 4.24 Spatial distribution for modeled annual total dry and wet deposition (mg $m^{-2}yr^{-1}$) of all eight elements in PM_{10}.

Mamun et al. (2023) also plotted a similar spatial distribution of annual total dry and wet deposition of all elements in the AOSR as in Fig. 4.24. Their calculation of the annual total dry and wet deposition of elements in the central region of the AOSR is in a similar order of magnitude as ours. They stated that the element deposition peaked around the center of AOSR and varied by three orders of magnitude from the

industry area to the remote area, agreeing with our predictions. In our study, the advantage of the use of WRF-Chem, a more sophisticated model than dispersion models, is that more physical processes are involved in the simulation on the dispersion of elements in the atmosphere. In addition, we can generate cross sections for element concentrations and meteorological conditions predicted by WRF-Chem, analyzing how meteorological condition affects the vertical mixing of elements in different seasons. There are also some uncertainties in the dry and wet deposition schemes. WRF-Chem provides alternative options for deposition schemes or these schemes can be added. WRF-Chem can help reveal the uncertainties caused by using different deposition schemes, as discussed in the chapter 5.

5. Sensitivity of Element Concentrations and Deposition

In chapter 3, the model-measurement comparison indicates that the modeled total concentrations of the eight elements are overestimated in the cold season and underestimated in the warm season due to the lack of considering seasonally varied element emissions in the base case. In this chapter, in order to test the model performance on the element concentrations and deposition, one full year of 2017 is selected for the simulation of two sensitivity tests. Three monitoring sites (AMS1, AMS17, and AMS18) are considered for the model-measurement comparison in this chapter and AMS4 is not considered because of its limited observed element concentrations. The annual and seasonal modeled element concentrations and deposition in the emission and deposition sensitivity tests are compared with those in the base case, as shown in previous chapters, with the aim to reveal the sensitivity of modeling results to the seasonally varied element emission database and dry&wet deposition schemes.

5.1 Emission sensitivity test

Yang et al. (2023) found a nearly linearity between the emissions and concentrations in the dispersion modeling results. Under this linearity, we try different adjustments to the element emissions in the cold and warm seasons. Finally, annual total element emission is reallocated as 30% in the cold season and 70% in the warm season (meaning a 40% decrease in the cold season and a 40% increase in the warm season compared to the base discussed above), which results in the smallest model-measurement difference in the annual element concentrations. All the other model configurations are the same as that in the simulation of base case. When comparing the emission sensitivity test to the base case, the modeling results in 2017 for base case are considered.

5.1.1 Element concentrations

The modeled annual total concentrations of the eight elements in $PM_{2.5}$, $PM_{2.5\text{-}10}$, and PM_{10} at the

three sites are listed in Table 5.1. Similar to the base case, for any particle size, the modeled annual total concentration is the highest at AMS1, followed by AMS17 and AMS18. This agrees with the location of the three AMS sites, namely the closest position of AMS1 and the furthest position of AMS18 to the major oil sands industry. Compared with the base case, for all particle sizes and sites, the modeled annual total concentration of the eight elements is smaller in the emission sensitivity test with seasonally varied element emissions. Compared with the base case, the annual total concentrations at $PM_{2.5}$, $PM_{2.5-10}$, and PM_{10} decrease by only 7-13%, 2-8%, and 4-9%, respectively. This indicates that the consideration of seasonally variable element emissions has some impacts on the modeled annual total concentrations of the eight elements. Same as the base case, Si has the highest modeled annual concentration, generally followed by Ca, Al, Fe, K, Ti, Mn, and Zn, regardless of particle size and site. For the eight elements, compared with the base case, the change in the modeled annual concentrations at the three sites is shown in Table 5.2. These deductions suggest the small effect of the seasonally variable element emissions on the modeled annual concentrations of the eight elements.

Table 5.1 The modeled annual concentrations (ng m^{-3}) of the eight elements in $PM_{2.5}$, $PM_{2.5-10}$ and PM_{10} at the three AMS sties for the emission sensitivity test.

Particles	Stations	Elements								Total
		Si	Ca	Al	Fe	K	Ti	Mn	Zn	
$PM_{2.5}$	AMS1	293.6	144.4	93.3	85.3	33.8	7.2	2.3	3.4	663.3
	AMS17	199.2	97.2	63.4	57.5	22	4.9	1.6	1.5	447.3
	AMS18	23.6	12.1	7.5	6.8	2.6	0.6	0.2	0.2	53.6
	average	172.1	84.6	54.7	49.9	19.5	4.2	1.4	1.7	388.1
$PM_{2.5-10}$	AMS1	760.6	372.3	237	219.1	84.1	18.4	6.1	4.8	1702.4
	AMS17	201.2	98.6	63.3	58.1	22.2	4.9	1.6	1.3	451.2
	AMS18	45.8	23	14.4	13.2	5.1	1.1	0.4	0.2	103.2
	average	335.9	164.6	104.9	96.8	37.1	8.1	2.7	2.1	752.3
PM_{10}	AMS1	1054.2	516.7	330.3	304.4	117.9	25.6	8.4	8.2	2365.7
	AMS17	400.4	195.8	126.7	115.5	44.2	9.8	3.2	2.9	898.5
	AMS18	69.4	35.1	21.9	20	7.7	1.7	0.6	0.4	156.8
	average	508	249.2	159.6	146.6	56.6	12.4	4.1	3.8	1140.3

Table 5.2 The change of modeled annual element concentrations in sensitivities tests compared with the base case at the three AMS sties (positive for increase and negative for decrease).

Cases	Particles	Stations		
		AMS1	AMS17	AMS18
Emission sensitivity test	$PM_{2.5}$	-13%	-7%	-12%
	$PM_{2.5-10}$	-8%	-3%	-7%
	PM_{10}	-10%	-5%	-9%
Deposition sensitivity test	$PM_{2.5}$	-20.9%	-16.1%	-19.6%
	$PM_{2.5-10}$	19.3%	57.4%	39%
	PM_{10}	6.8%	19.6%	17.7%

The percentage differences of the model & measurement for the annual concentrations of the eight elements in PM_{10} are shown as Fig. 5.1. It is obvious that considering the seasonally variable element emissions causes a small effect on the model-measurement percentage differences in the annual concentrations of the eight elements. With the consideration of seasonally varied element emissions, the model-measurement percentage differences in the annual concentrations of the eight elements change from -30%~60% to -40%~51% at AMS1 (from 3% to -7% for the eight elements together), from -42%~55% to -45%~51% at AMS17 (from 9% to 5% for the eight elements together), and from -167%~4% to -170%~-5% at AMS18 (from -66% to -74% for the eight elements together). This is because the modeled annual concentrations of the eight elements are smaller in the emission sensitivity test than that in the base case. The underprediction of element concentrations in the base case is enhanced in the emission sensitivity test. On the other hand, the overprediction of element concentrations in the base case is weakened in the emission sensitivity test. As a result, in the model-measurement comparison, the negative percentage differences (underprediction) are increased while the positive percentage differences (overprediction) are decreased.

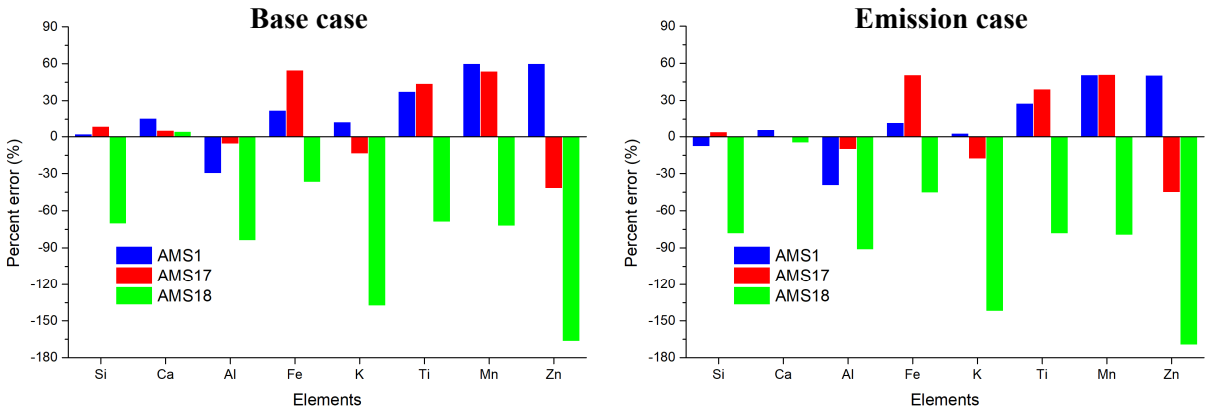

Figure 5.1 The percentage differences (%) between annual modeled and observed element concentrations in PM_{10} at the three sites for the base case and the emission sensitivity test.

Figure 5.2 shows the modeled seasonal concentrations of the eight elements in PM_{10} at AMS1 for the base and emission cases. For the base case, the modeled concentrations of the eight elements during the cold season are higher than that during the warm season by around a factor of 1.6, because the constant element emission rates are used in the whole year and the stable atmosphere in the cold season enhances the element concentrations near the surface. However, for the emission sensitivity test, the modeled concentrations of the eight elements during the warm season are higher than that during the cold season by around 47%. This is due to the seasonal variation of element emissions in the emission sensitivity test. The annual element emission is allocated as 30% during the cold season and 70% during the warm season. As a result of more element emissions occurring in the warm season, the modeled concentrations of the eight elements are higher during the warm season. In addition, compared the emission sensitivity test with the base case, the modeled concentrations of the eight elements during the cold season decrease by around 40.5% and those during the warm season increase by around 40.7% in the emission sensitivity test. These changes agree with the modification to the element emissions, namely, 40% reduction in the cold season and 40% increase in the warm season.

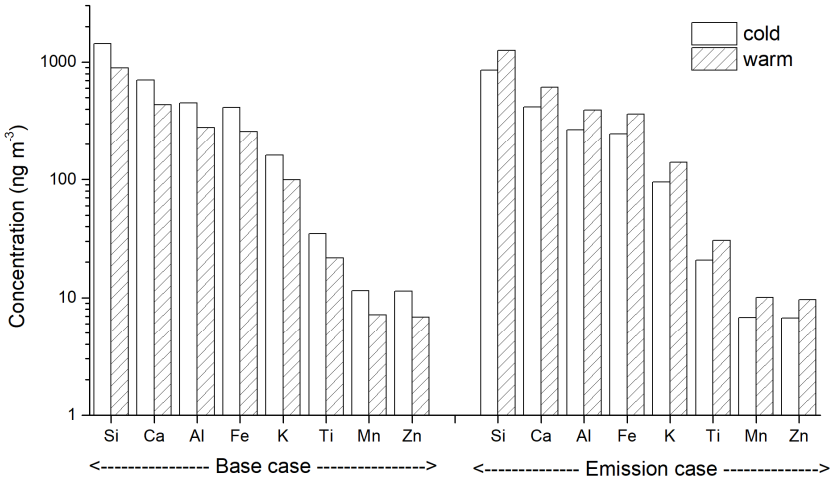

Figure 5.2 Modeled seasonal concentrations (ng/m^3) of the eight elements in PM_{10} at AMS1 for the base case and the emission sensitivity test.

Similar to AMS1, for the base case, the modeled concentrations of the eight elements at AMS17 are around 1.2 times higher during the cold season than the warm season (Fig. 5.3), owing to the weak vertical diffusion under the stable atmosphere during the cold season. On the contrary, for the emission sensitivity test, the modeled concentrations of the eight elements during the warm season are higher than that during the cold season by around a factor of 1.9 (Fig. 5.3), due to more element emissions during the warm season than the cold season. Comparing the emission sensitivity test with the base case, the modeled concentrations of the eight elements during the cold season reduce by around 39.5% and those during the warm season increase by around 38.4% in the emission sensitivity test, agreeing with the 40% reduction of element emissions in the cold season and 40% increase of element emissions in the warm season.

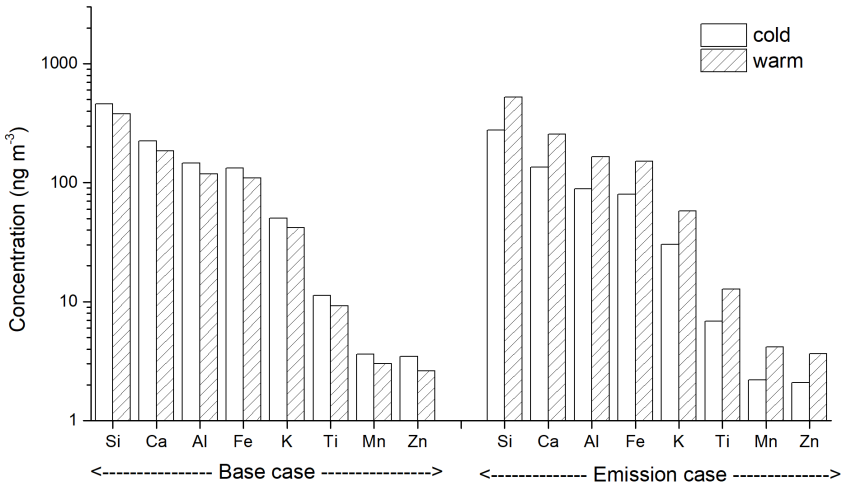

Figure 5.3 Modeled seasonal concentrations (ng/m^3) of the eight elements in PM_{10} at AMS17 for the base case and the emission sensitivity test.

Similar to AMS1 and AMS17, at AMS18, the modeled concentrations of the eight elements are around 1.6 times higher during the cold season than the warm season for the base case, whereas they are around 1.5 times higher during the warm season than the cold season for the emission sensitivity test (Fig. 5.4). Compared the emission sensitivity test with the base case, the modeled concentrations of the eight elements during the cold season decrease by around 40.2% and those during the warm season increase by around 39.6% in the emission sensitivity test.

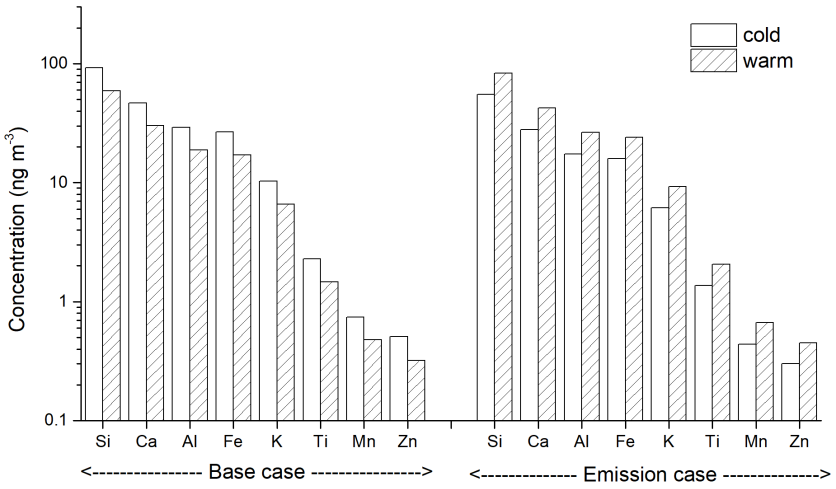

Figure 5.4 Modeled seasonal concentrations (ng/m^3) of the eight elements in PM_{10} at AMS18 for the base case and the emission sensitivity test.

The ratios of modeled total concentration to averaged observed total concentration averaged for the three sites are shown in Fig. 5.5. In the base case, the ratios are 2.71, 1.3, 1.08, and 0.52 for $PM_{2.5}$ in the cold season, $PM_{2.5-10}$ in the cold season, $PM_{2.5}$ in the warm season, and $PM_{2.5-10}$ in the warm season, respectively. The modeled total concentrations of the eight elements are always overestimated, except around 50% underestimation for $PM_{2.5-10}$ in the warm season. With the consideration of seasonally varied element emissions in the emission sensitivity test, the ratios for $PM_{2.5}$ in the cold season, $PM_{2.5-10}$ in the cold season, $PM_{2.5}$ in the warm season, and $PM_{2.5-10}$ in the warm season are 1.63, 0.77, 1.5, and 0.74, respectively. Compared with base case, the averaged biases in the modeled total concentrations of the eight elements against the observations reduce from 45% to 13% in the cold season and from 45% to 24% in the warm season. The model performance on the modeled element concentrations becomes better in the emission sensitivity test than in the base case. However, even though seasonal variation of element emissions is considered, total concentrations of the eight elements in $PM_{2.5}$ are still overpredicted by 63% during the cold season and 50% during the warm season, whereas those in $PM_{2.5-10}$ are still underpredicted by 23% during the cold season and 26% during the warm season (Fig. 5.5), suggesting that there are still

some uncertainties in the speciation of element emissions. These discrepancies are also possibly caused by the uncertainties in modeled meteorological conditions and atmospheric deposition processes.

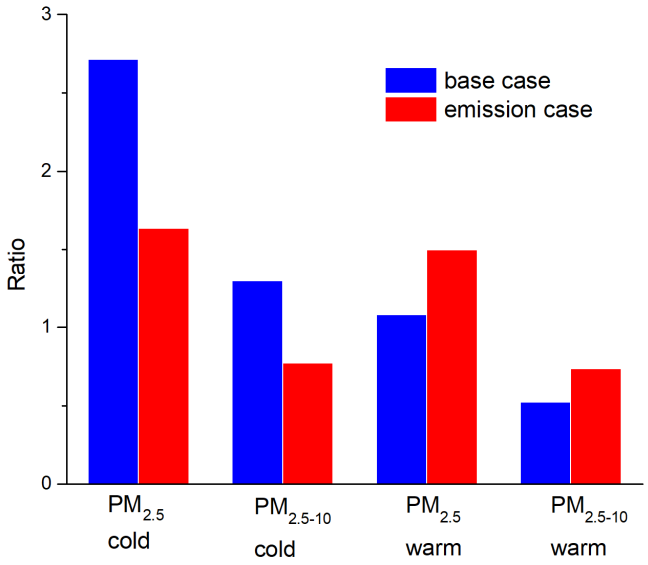

Figure 5.5 Ratios of modeled total concentration to observed total concentration on average of the three sites in the base case and the emission sensitivity test.

Overall, compared with the base case, the seasonal variations in element emissions lead to some influences on the modeled annual concentration of the eight elements (or the eight elements together). The modeled annual concentrations of the eight elements in PM_{10} reduce by 9.5%, 4.4%, and 8.8% on average at AMS1, AMS17, and AMS18, respectively, and the corresponding reductions for the eight elements together are 9.4%, 4.3%, and 8.7%. The model-measurement percentage differences for the annual concentration of the eight elements (or the eight elements together) in PM_{10} is similar between the base case and the emission sensitivity test. However, as expected, on the seasonal basis, the seasonal variations of element emissions cause a significant impact on the modeled concentration of the eight elements (or the eight elements together). Regardless of site and element, the higher modeled concentrations in PM_{10} occur in the cold season for the base case, while they happen in the warm season for the emission sensitivity test. Compared with the base case, the modeled concentrations of the eight elements increase by around 40% during the warm season and decrease by around 40% during the cold season, because of 40% increase of

element emissions in the warm season and 40% reduction of element emissions in the cold season. The modeled element concentrations are mainly determined by the element emissions. Compared with base case, the averaged biases in the modeled total concentrations of the eight elements in PM_{10} against the observations reduce from 45% to 13% in the cold season and from 45% to 24% in the warm season. The model performance on the modeled element concentration becomes better in the emission sensitivity test than the base case. However, despite the consideration of seasonal variation of element emissions, elements in $PM_{2.5}$ are overestimated by 55% and those in $PM_{2.5-10}$ are underestimated by 25% in the whole year, indicating that there are still some uncertainties in the speciation of element emissions. The model biases in the element concentration are mainly caused by the uncertainties in the emission database, such as the lack of considering seasonal variation and the emission speciation. After considering the seasonal varied element emissions, the model biases in the element concentration are possibly due to the uncertainties in the dispersion and deposition processes.

5.1.2 Element deposition

The modeled annual total dry and wet deposition of the eight elements at AMS1, AMS17, and AMS18 are shown in Table 5.3. The annual total deposition (dry + wet) of the eight elements is the largest at AMS1, followed by AMS17 and AMS18, agreeing with the modeled annual element concentrations at three sites. Compared with the base case, the percentage errors in the annual total dry, total wet, and total dry+wet deposition for three sites are -6.3% to 0.4%, -8.9% to 1.8%, and -4.5% to 0.8%, respectively. These small differences indicate the small impact of seasonally varied element emissions on the annual total deposition of the eight elements. Similar to the base case, for all deposition and sites, Si has the highest annual deposition, followed by Ca, Al, Fe, K, Ti, Mn, and Zn. Regardless of deposition and site, the modeled annual deposition in the emission sensitivity test is similar to that in the base case. Compared the emission sensitivity test to the base case, the percentage errors in the annual deposition of the eight elements are shown in Table 5.4. These small discrepancies indicate the small

effect of seasonally variable element emissions on the modeled annual deposition of the eight elements. In addition, similar to the base case, the removal of the eight elements from the atmosphere to the surface is dominated by dry deposition at all three sites in the emission sensitivity test (Fig. 5.6). The annual dry deposition of the eight elements are larger than the annual wet deposition by around a factor of 3.2, 2.4, and 2.9 at AMS1, AMS17, and AMS18, respectively.

Table 5.3 The modeled annual dry and wet deposition (mg $m^{-2}yr^{-1}$) of the eight elements at three stations for the emission sensitivity test.

Deposition	Stations	Elements								Total
		Si	Ca	Al	Fe	K	Ti	Mn	Zn	
Dry	AMS1	107.8	52.3	35.4	31.4	11.6	2.7	0.84	1.2	243.2
	AMS17	93.8	45.8	29.8	27.1	10.3	2.3	0.74	0.67	210.5
	AMS18	11.4	5.6	3.6	3.3	1.3	0.28	0.091	0.06	25.6
	average	71	34.57	22.93	20.6	7.73	1.76	0.56	0.64	159.79
Wet	AMS1	35	16.9	11.6	10.2	3.8	0.89	0.27	0.36	79
	AMS17	42.4	20.3	13.4	12.2	4.7	1.03	0.34	0.25	94.6
	AMS18	3.8	1.9	1.2	1.09	0.41	0.093	0.029	0.022	8.5
	average	27.07	13.03	8.73	7.83	2.97	0.67	0.21	0.21	60.73
Total (dry+wet)	AMS1	142.8	69.2	47	41.6	15.4	3.59	1.11	1.56	322.3
	AMS17	136.2	66.1	43.2	39.3	15	3.33	1.08	0.92	305.1
	AMS18	15.2	7.5	4.8	4.39	1.71	0.373	0.12	0.082	34.2
	average	98.07	47.6	31.67	28.43	10.7	2.43	0.77	0.85	220.52

Table 5.4 The percentage errors in the annual deposition of the eight elements between sensitivities tests and the base case at the three AMS sties.

Cases	Deposition	Stations		
		AMS1	AMS17	AMS18
Emission sensitivity test	Dry	-3.6% to 0%	0% to 1.5%	-7.7% to 0%
	Wet	-10% to -2.7%	0.5% to 4.2%	0% to 2.7%
	Total	-5.1% to -0.6%	0.5% to 2.2%	-5.9% to 0%
Deposition sensitivity test	Dry	-59.4% to -44.6%	-68.2 to -67.1%	-58.3% to -56.6%
	Wet	12.7% to 26.5%	34.3% to 37.3%	71.1% to 79.9%
	Total	-42.4% to -26.5%	-40.1 to -35.5%	-26.9% to -24%

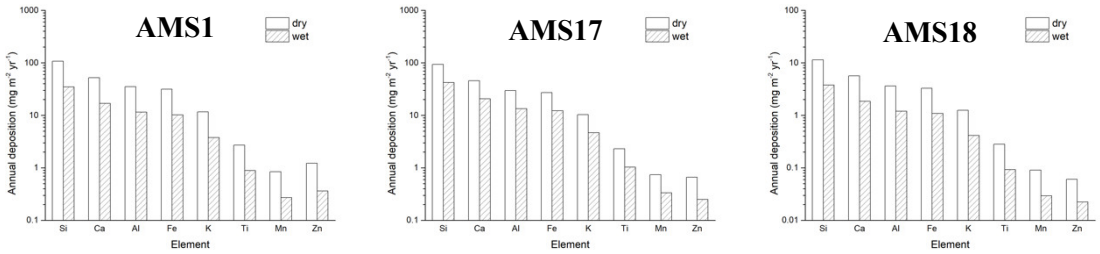

Figure 5.6 The modeled annual dry and wet deposition of the eight elements at three sites for the emission sensitivity test.

At AMS1, the modeled total dry deposition of the eight elements during the cold season and the warm season are 79 mg $m^{-2}yr^{-1}$ and 164 mg $m^{-2}yr^{-1}$, respectively. The modeled total wet deposition of the eight elements are 31 mg $m^{-2}yr^{-1}$ and 48 mg $m^{-2}yr^{-1}$ during the cold season and the warm season, respectively. In the base case, the total dry and wet deposition are higher during the cold season than the warm season. However, the total dry and wet deposition of the eight elements in the emission sensitivity test are higher during the warm season than the cold season by a factor of 2.08 and 1.57, respectively. This is because of the higher modeled element concentrations during the warm season in the emission sensitivity test (Fig. 5.2). Similar to the base case, the total dry deposition of the eight elements is higher than that total wet

deposition by a factor of 2.57 and 3.4 in the cold season and the warm season, respectively, though the total dry and wet deposition are in the same order of magnitude. The dry deposition plays a dominant role for the removal of elements. The modeled seasonal dry and wet deposition of individual elements at AMS1 are listed in Table 5.5. In the base case, the modeled dry and wet deposition of each element are 1.2 times higher in the cold season than that in the warm season on average. However, the modeled dry and wet deposition of the eight elements are on average 2.14 and 1.61 times higher during the warm season than the cold season (Fig. 5.7), respectively in the emission sensitivity test, owing to the higher modeled element concentrations during the warm season (Fig. 5.2). Similar to the base case, the modeled dry deposition of individual elements are higher than the modeled wet deposition by around a factor of 2.6 during the cold season and 3.4 during the warm season (Fig. 5.7), suggesting the predominance of dry deposition in the removal of elements. Additionally, compared to the base case, the modeled dry and wet deposition of the eight elements during the cold season decrease by around 40.3% and 39.8%, respectively, whereas those during the warm season increase by 41.1% and 35.9%, respectively. These variations are similar to the change to the element emissions in the two seasons, namely, 40% reduction in the cold season and 40% increase in the warm season.

Table 5.5 The modeled seasonal dry and wet deposition (mg $m^{-2}yr^{-1}$) of the eight elements at three stations for the emission sensitivity test.

Stations	Deposition	Seasons	Elements								Total
			Si	Ca	Al	Fe	K	Ti	Mn	Zn	
AMS1	Dry	cold	35	17	11	10	3.8	0.87	0.28	0.34	78
		warm	73	35	24	21	7.8	1.8	0.56	0.89	164
	Wet	cold	14	6.6	4.5	4	1.5	0.34	0.11	0.12	31
		warm	21	10	7.1	6.2	2.3	0.54	0.16	0.24	48
AMS17	Dry	cold	27	13	8.7	7.9	3	0.67	0.22	0.2	61
		warm	67	32	21	19	7.3	1.6	0.53	0.47	149
	Wet	cold	14	6.9	4.4	4.1	1.6	0.34	0.11	0.083	32
		warm	28	14	9	8.2	3.1	0.69	0.22	0.17	63
AMS18	Dry	cold	4.2	2.1	1.3	1.2	0.46	0.1	0.033	0.021	9.4
		warm	7.2	3.6	2.3	2.1	0.79	0.18	0.058	0.039	16
	Wet	cold	1	0.5	0.32	0.29	0.11	0.025	0.008	0.006	2.3
		warm	2.8	1.4	0.88	0.8	0.3	0.068	0.021	0.017	6.3

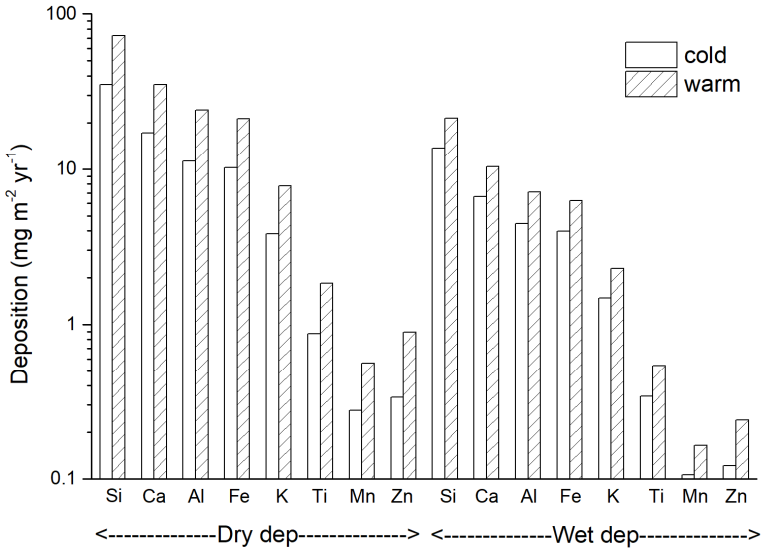

Figure 5.7 The modeled seasonal dry and wet deposition (mg $m^{-2}yr^{-1}$) of the eight elements at AMS1 for the emission sensitivity test.

The modeled total dry and wet deposition of the eight elements in the cold and warm seasons at AMS17 and AMS18 are listed in Table 5.5. Similar to AMS1, the total dry and wet deposition of the eight elements at AMS17 is 2.44-fold and 2.01-fold higher during the warm season than the cold season, respectively. At AMS18, the total dry and wet deposition is 174% and 275% higher during the warm season than the cold season. This is because of the higher modeled element concentrations during the warm season than that during the cold season in the emission sensitivity test (Fig. 5.3&5.4). In addition, similar to AMS1, the total dry deposition of the eight elements in the cold season and the warm season is 194% and 236% higher than the total wet deposition, respectively, at AMS17. At AMS18, the total dry deposition is 416% and 262% higher than the total wet deposition in the cold season and the warm season, respectively.

The modeled seasonal dry and wet deposition of individual elements at AMS17 and AMS18 are listed in Table 5.5. Similar to AMS1 but contrary to the base case, the modeled dry and wet deposition of each element at AMS17 are averaged 2.44-fold and 2.01-fold higher during the warm season than the cold season, respectively (Table 5.5 & Fig. 5.8). At AMS18, the modeled dry and wet deposition of individual

elements are 75% and 178% on average higher during the warm season than the cold season (Table 5.5 & Fig. 5.9). The higher dry and wet deposition of the eight elements during the warm season are a result of the higher modeled element concentrations during the warm season (Fig. 5.3&5.4). Similar to AMS1, the modeled dry deposition of the eight elements at AMS17 is around 2 and 2.4 times higher than the modeled wet deposition during the cold season and the warm season, respectively (Fig. 5.8). The modeled dry deposition of the eight elements at AMS18 are higher than that modeled wet deposition by around a factor of 4.1 and 2.5 in the cold season and the warm season, respectively (Fig. 5.9). Additionally, similar to AMS1, compared to the base case, the modeled dry deposition of the eight elements at AMS17 show a decrease of 39.6% during the cold season and an increase of 37.8% during the warm season. The modeled wet deposition of the eight elements at AMS17 show a decrease of 37.8% during the cold season and an increase of 50.4% during the warm season. At AMS18, there is a decrease of around 40.3% during the cold season and an increase of around 40.1% during the warm season for the modeled dry deposition. There is a decrease of around 39.5% during the cold season and an increase of around 32.6% during the warm season for the modeled wet deposition. These changes to the modeled dry and wet deposition of the eight elements at AMS17 and AMS18 in the two seasons are similar to the modification to the element emissions in the two seasons.

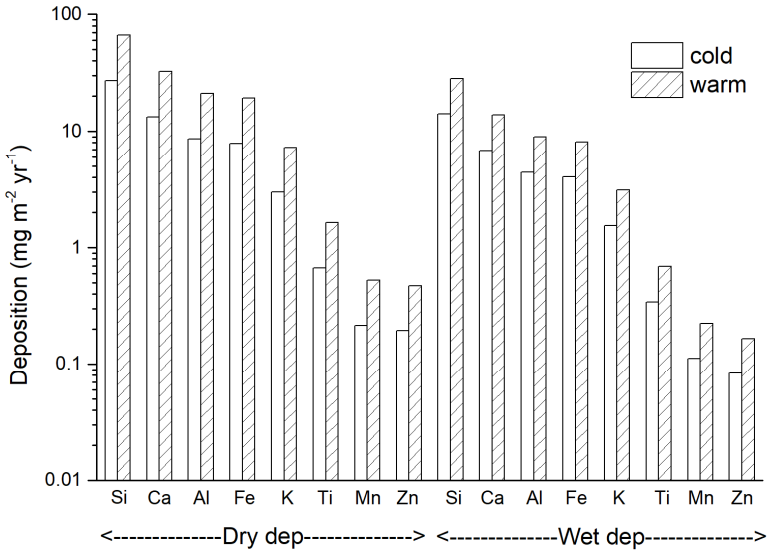

Figure 5.8 The modeled seasonal dry and wet deposition (mg $m^{-2}yr^{-1}$) of the eight elements at AMS17 for the emission sensitivity test.

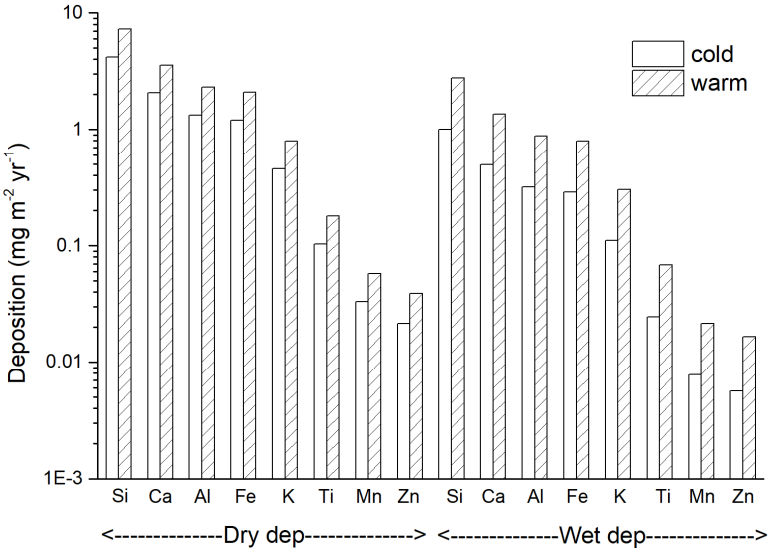

Figure 5.9 The modeled seasonal dry and wet deposition (mg $m^{-2}yr^{-1}$) of the eight elements at AMS18 for the emission sensitivity test.

Overall, compared with the base case, the seasonal variations of element emissions result in a small effect on the modeled annual dry, wet, and total (dry + wet) deposition of the eight elements (or the eight elements together). The differences in the modeled annual total deposition (dry + wet) of the eight elements are -3.9%, 1%, and -4.2% on average at AMS1, AMS17, and AMS18, respectively, and the corresponding differences for the eight elements together are -4.2%, 0.8%, and -4.5%. However, the seasonal variations of element emissions lead to a significant effect on the modeled dry and wet deposition of the eight elements (or the eight elements together) on the seasonal base. At all AMS sites, the dry and wet deposition of the eight elements (or the eight elements together) are always higher during the warm season than the cold season, because of the higher modeled element concentrations in the warm season when more elements are emitted. Similar to the base case, the dry deposition of the eight elements (or the eight elements together) are higher than the wet deposition. In addition, compared to the base case, a decrease by around 40% during the cold season and an increase by around 40% during the warm season are found for both dry and wet deposition of the eight elements at the three sites. These changes are due to 40% reduction of element emissions in the cold season and 40% increase of element emissions in the warm season.

5.2 Deposition sensitivity test

In the deposition sensitivity test, the default dry and wet deposition schemes in WRF-Chem are changed to below-cloud scavenging scheme of Wang et al. (2014) and dry deposition scheme of Zhang et al. (2001). These schemes have been evaluated in other studies and they estimate particle deposition reasonably well. All the other model configurations are the same as that in the simulation of base case. When comparing the deposition sensitivity test to the base case, the modeling results in 2017 for base case are considered.

5.2.1 Element concentrations

The modeled annual total concentrations of the eight elements in $PM_{2.5}$, $PM_{2.5-10}$, and PM_{10} at AMS1, AMS17, and AMS18 are shown in Table 5.6. Similar to the base case and the emission sensitivity test, AMS1 always has the highest modeled annual total concentration, followed by AMS17 and AMS18, regardless of particle size. Comparing with the base case, at all three sites, the modeled annual total concentrations of the eight elements in $PM_{2.5}$ are smaller while that in $PM_{2.5-10}$ and PM_{10} are higher in the deposition sensitivity test. In the deposition sensitivity test, there are a decrease by 16-21%, an increase by 19-57%, and an increase by 7-20% for the annual total concentrations in $PM_{2.5}$, $PM_{2.5-10}$, and PM_{10}, respectively. This suggests that the replaced dry & wet deposition schemes strengthen the element removal in $PM_{2.5}$, but they weaken the element removal in $PM_{2.5-10}$. Same as the base case and the emission sensitivity test, Si has the highest modeled annual concentration, generally followed by Ca, Al, Fe, K, Ti, Mn, and Zn, regardless of particle size and site. The modeled annual element concentrations ranged from the highest to the lowest are at AMS1, AMS17, and AMS18, for all particle sizes and elements. The modeled annual concentrations of individual elements are smaller in $PM_{2.5}$, but larger in $PM_{2.5-10}$ and PM_{10} at three sites (Table 5.6), compared with the base case. For the eight elements, compared with the base case, the change in the modeled annual concentrations at the three sites is shown in Table 5.2. These variations in the modeled annual concentration of the eight elements prove the impact by the selection of different dry & wet deposition schemes.

Table 5.6 The modeled annual concentrations (ng m^{-3}) of the eight elements in $PM_{2.5}$, $PM_{2.5-10}$ and PM_{10} at three stations for the deposition sensitivity test.

Particles	Stations	Elements								Total
		Si	Ca	Al	Fe	K	Ti	Mn	Zn	
$PM_{2.5}$	AMS1	266.6	131	84.8	77.5	30.8	6.6	2.1	3.2	602.6
	AMS17	178.5	87	57.1	51.5	19.6	4.4	1.4	1.4	400.9
	AMS18	21.6	11.1	6.9	6.3	2.4	0.5	0.2	0.1	49.1
	average	155.6	76.4	49.6	45.1	17.6	3.8	1.2	1.6	350.9
$PM_{2.5-10}$	AMS1	979.3	479.3	305.8	282.3	108.2	23.7	7.8	6.4	2192.8
	AMS17	322.5	158	101.8	93.1	35.5	7.9	2.6	2.2	723.6
	AMS18	68.2	33.9	21.5	19.6	7.5	1.7	0.5	0.3	153.2
	average	456.7	223.7	143	131.7	50.4	11.1	3.6	3	1023.2
PM_{10}	AMS1	1245.9	610.3	390.6	359.7	139	30.3	10	9.6	2795.4
	AMS17	501	245	158.9	144.6	55.1	12.3	4	3.6	1124.5
	AMS18	89.8	45	28.4	25.9	9.9	2.2	0.7	0.5	202.4
	average	612.2	300.1	192.6	176.7	68	14.9	4.9	4.6	1374.1

Fig. 5.10 shows the model-measurement percentage differences in the annual concentrations of the eight elements in PM_{10} for the base case and the deposition sensitivity test. It seems that using different dry & wet deposition schemes leads to some influences on the model-measurement percentage differences in the annual concentrations of the eight elements. With the replacement of dry & wet deposition schemes, these changes from -30%~60% to -23%~66% at AMS1 (from 3% to 10% for the eight elements together), from -42%~55% to -25%~71% at AMS17 (from 9% to 27% for the eight elements together), and from -167%~4% to -162%~20% at AMS18 (from -66% to -51% for the eight elements together) are found to the model-measurement differences in the annual concentrations of the eight elements. Compared the

deposition sensitivity test with the base case, the model performance on the modeled annual element concentrations is similar at AMS1, worse at AMS17, and better at AMS18. This is probably because the replaced dry and wet deposition schemes weaken the removal of elements. The weaker wind speeds simulated by WRF-Chem cause a weaker dispersion of elements in both base case and deposition sensitivity test. The modeled element concentrations at AMS1 and AMS17 near the major oil sands industry tend to be overestimated, while those at AMS18 away from the major oil sands industry tend to be underestimated. By using Wang et al. (2014) and Zhang et al. (2001) deposition schemes, the overestimation at AMS1 and AMS17 is larger, whereas the underestimation at AMS4 is smaller.

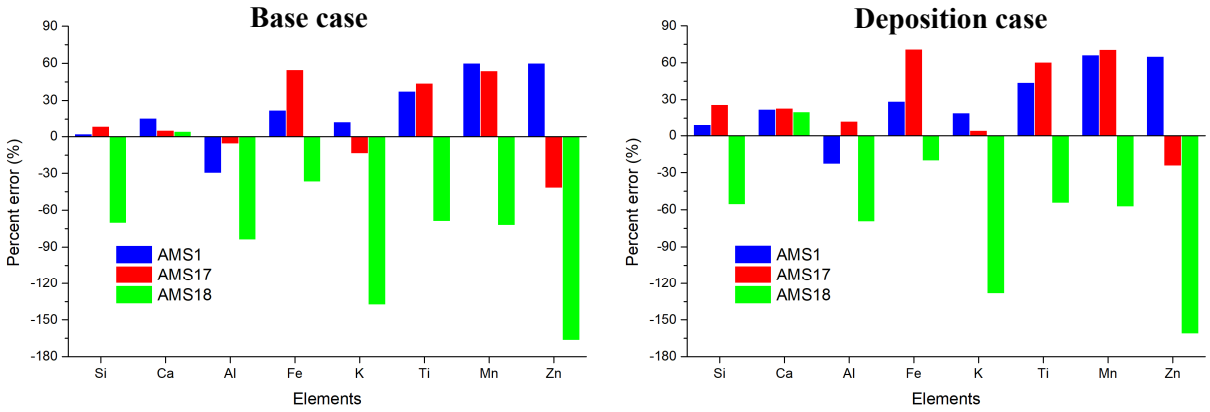

Figure 5.10 The percentage difference (%) between annual modeled and observed element concentrations in PM_{10} for the base case and the deposition sensitivity test.

Fig. 5.11 shows the modeled seasonal concentrations of the eight elements in PM_{10} at AMS1 for the base case and the deposition sensitivity test. In the deposition sensitivity test, the modeled concentrations of the eight elements during the cold season are 57% higher than that during the warm season, due to the constant element emissions in the whole year and the increase of element concentrations near the surface under the stable atmosphere in the cold season. This discrepancy in the modeled element concentrations between the cold season and the warm season is similar to that in the base case (60%). It indicates that the

replacement of dry & wet deposition schemes has almost no effect on the seasonal distribution of modeled element concentrations in PM_{10}. Additionally, compared the deposition sensitivity test to the base case, the modeled concentrations of the eight elements in PM_{10} increase by around 5.7% and 8.8% during the cold season and the warm season, respectively. These differences suggest that the replaced dry & wet deposition schemes weaken the removal of elements in PM_{10} in the both seasons.

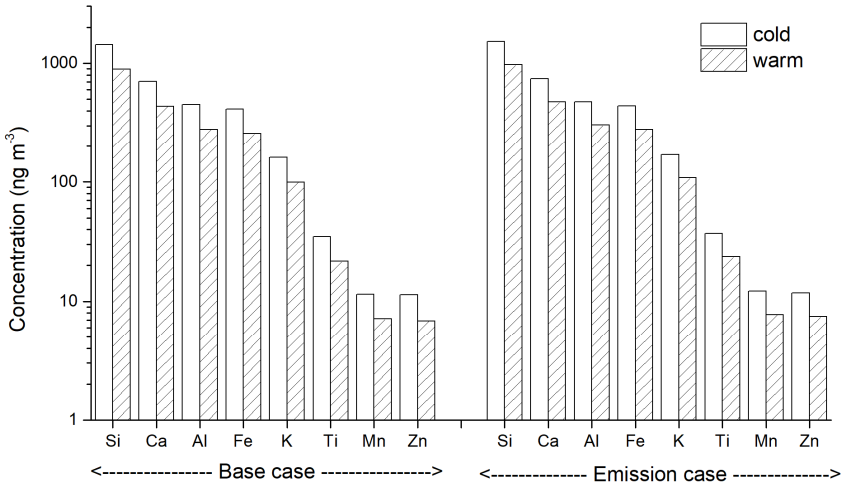

Figure 5.11 Modeled seasonal concentrations (ng/m^3) of the eight elements in PM_{10} at AMS1 for the base case and the deposition sensitivity test.

The modeled seasonal concentrations of the eight elements in PM_{10} at AMS17 for the base case and the deposition sensitivity test are shown in Fig. 5.12. The modeled concentrations of the eight elements during the cold season are higher than that during the warm season by a factor of 1.24 in the deposition sensitivity test, as a result of the constant element emissions and the stable atmosphere in the cold season. This difference in the modeled element concentrations between the cold season and the warm season is similar to that in the base case (a factor of 1.23). It implies that there is almost no impact on the seasonal distribution of modeled element concentrations in PM_{10} by using different dry & wet deposition schemes.

Compared with the base case, the modeled concentrations of the eight elements in PM_{10} during the cold season and the warm season in the deposition sensitivity test have around 20% and 19% increases, respectively.

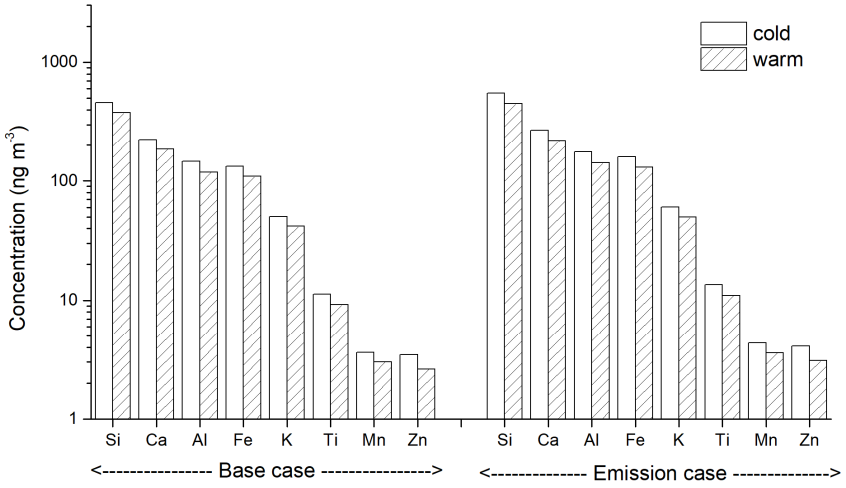

Figure 5.12 Modeled seasonal concentrations (ng/m^3) of the eight elements in PM_{10} at AMS17 for the base case and the deposition sensitivity test.

At AMS18, the modeled seasonal concentrations of the eight elements in PM_{10} for the base case and the deposition sensitivity test are shown as Fig. 5.13. The modeled concentrations of the eight elements during the cold season are 1.53-fold higher than that during the warm season in the deposition sensitivity test, owing to the constant element emissions throughout the whole year and the stable atmosphere in the cold season. This difference in the modeled element concentrations between the cold season and the warm season is similar to the base case (1.56-fold). It agrees with the findings at AMS1 and AMS17 that there is almost no impact on the seasonal distribution of modeled element concentrations by replaced dry & wet deposition schemes. Compared the deposition sensitivity test with the base case, increases by around 16.8% in the cold season and 18.9% in the warm season are found for the modeled concentrations of the eight elements in PM_{10}.

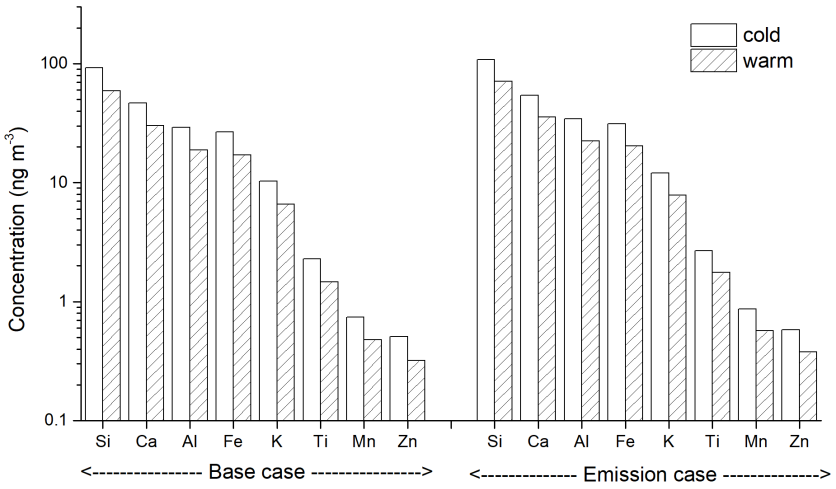

Figure 5.13 Modeled seasonal concentrations (ng/m^3) of the eight elements in PM_{10} at AMS18 for the base case and the deposition sensitivity test.

Fig. 5.14 shows ratios of modeled total concentration to observed total concentration on average of the three sites in the base case and the deposition sensitivity test. In the deposition sensitivity test, the ratios are 2.15, 1.66, 0.9, and 0.66 for $PM_{2.5}$ in the cold season, $PM_{2.5-10}$ in the cold season, $PM_{2.5}$ in the warm season, and $PM_{2.5-10}$ in the warm season, respectively. Compared with the base case, the ratio decreasing from 2.71 to 2.15 for $PM_{2.5}$ in the cold season and increasing from 0.52 to 0.66 for $PM_{2.5-10}$ in the warm season indicates the better model performance by using Wang et al. (2014) and Zhang et al. (2001) deposition schemes. There are an increase from 45% to 66% in the cold season and a decrease from 45% to 37% in the warm season for the averaged bias in the modeled total concentrations of the eight elements in PM_{10} against the observations. The model performance on the modeled element concentration in PM_{10} becomes better in the deposition sensitivity test than the base case during the warm season, but it becomes worse during the cold season. The model tends to overpredict the elements in the cold season and underpredict the elements in the warm season without considering seasonal variations of element emissions. The replaced dry and wet deposition schemes weaken the removal of elements. As a consequence, this overprediction in the cold season is larger and this underprediction in the warm season

is smaller. The model performance on the element concentration is worse during the cold season but is better during the warm season. In addition, in the deposition sensitivity test, total concentrations of the eight elements during the cold season are overestimated by 115% for $PM_{2.5}$ and 66% for $PM_{2.5-10}$, while those during the warm season are underestimated by 10% for $PM_{2.5}$ and 34% for $PM_{2.5-10}$ (Fig. 5.14). This is partially because the seasonally varied element emissions are not considered in the deposition sensitivity test. The element emissions during the cold season are overestimated while those during the warm season are underestimated. It is expected that the combination of emission and deposition sensitivity tests will further improve the model performance of the element concentrations, because the overestimation of modeled elements in $PM_{2.5}$ (ratio > 1 in Fig. 5.5) and the underestimation of modeled elements in $PM_{2.5-10}$ (ratio < 1 in Fig. 5.5) in the emission sensitivity test are expected to be reduced by Wang et al. (2014) and Zhang et al. (2001) deposition schemes.

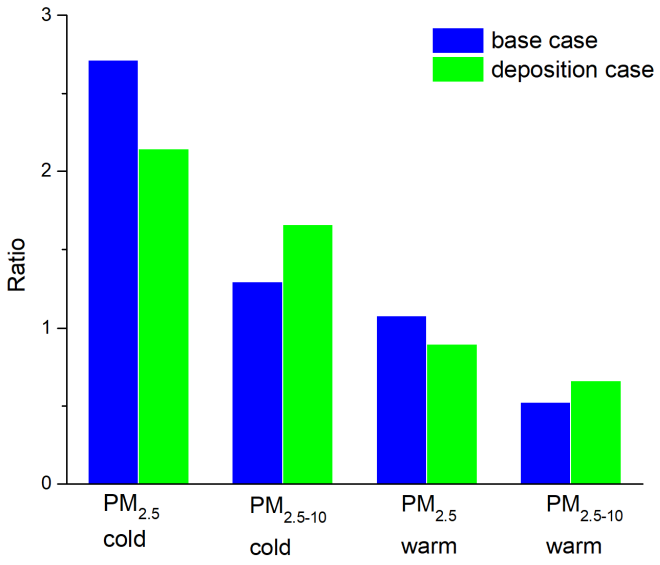

Figure 5.14 Ratios of modeled total concentration to observed total concentration on average of three sites in the base case and the deposition sensitivity test.

Overall, compared with the base case, the replacement of dry & wet deposition schemes leads to some impacts on the modeled annual concentration of the eight elements (or the eight elements together). The

modeled annual concentrations of the eight elements in PM_{10} increase by averaged 6.8%, 19.6%, and 17.7% at AMS1, AMS17, and AMS18, respectively, and the corresponding increases for the eight elements together are 7%, 19.8%, and 17.9%. The model-measurement percentage differences in the annual concentrations of the eight elements (or the eight elements together) suggest that the model performance on the modeled annual element concentrations is similar at AMS1 (from 3% to 10%), worse at AMS17 (from 9% to 27%), and better at AMS18 (from -66% to -51%). On the seasonal basis, there are some effects on the modeled concentration of the eight elements (or the eight elements together) by using different dry & wet deposition formulas. Compared with the base case, the modeled concentrations of the eight elements at three sites increase by 12-15% on average during the cold season and 15-16% during the warm season, and the corresponding increases in the modeled total concentrations of the eight elements are 14% and 16%. This suggests that the reduction in the removal of elements in PM_{10} by using different dry & wet deposition schemes occurs in both seasons. The averaged bias in the modeled total concentrations of the eight elements in PM_{10} against the observations increases from 45% to 66% in the cold season and decreases from 45% to 37% in the warm season, suggesting a better model performance during the warm season but a worse model performance during the cold season. Because of the lack of seasonally varied element emissions in the deposition sensitivity test, the modeled total element concentration is further overestimated during the cold season, while the underestimation during the warm season is reduced.

5.2.2 Element deposition

The modeled annual total dry and wet deposition of the eight elements are shown in Table 5.7. Similar to the base case and the emission sensitivity test, the annual total deposition (dry + wet) of the eight elements is the largest at AMS1, followed by AMS17 and AMS18. The biases between the deposition sensitivity test and base case in the annual total dry, total wet, and total dry+wet deposition of the eight elements for the three sites are -68.1% to -45.9%, 24.2% to 76.5%, and -35.9% to -26.2%, respectively. These differences suggest obvious impacts by different dry & wet deposition schemes on the annual total

deposition of the eight elements.

As with the base case and the emission sensitivity test, Si has the highest annual deposition, followed by Ca, Al, Fe, K, Ti, Mn, and Zn, at all three sites. Regardless of the site and element, compared with base case, there are decreases in the modeled annual dry deposition and annual total deposition, while there is an increase in the modeled annual wet deposition. The biases between deposition sensitivity test and base case in the annual deposition are shown in Table 5.4. These discrepancies indicate the significant impact on the modeled annual deposition of the eight elements by using different dry & wet deposition schemes. Additionally, contrary to the base case, the wet deposition dominates the removal of the eight elements at AMS17 and AMS18 (Fig. 5.15). Although the annual dry deposition is larger than annual wet deposition at AMS1, their differences are smaller than that in the base case (Fig. 5.15). In the deposition sensitivity test, the annual dry deposition of the eight elements are 17-28% higher than their annual wet deposition at AMS1, whereas the annual wet deposition are 48-92% and 28-36% higher than the annual dry deposition at AMS17 and AMS18, respectively. This is because Wang et al. (2014) below-cloud scavenging scheme enhances the wet deposition of elements while Zhang et al. (2001) dry deposition scheme weakens the dry deposition of elements.

Table 5.7 The modeled annual dry and wet deposition (mg $m^{-2}yr^{-1}$) of the eight elements at three stations for the deposition sensitivity test.

Deposition	Stations	Elements								Total
		Si	Ca	Al	Fe	K	Ti	Mn	Zn	
Dry	AMS1	60.2	29.5	19	17.4	6.64	1.5	0.48	0.49	135.2
	AMS17	29.8	14.5	9.46	8.6	3.27	0.73	0.24	0.22	66.8
	AMS18	5.12	2.55	1.63	1.48	0.56	0.13	0.041	0.028	11.5
	average	31.71	15.52	10.03	9.16	3.49	0.79	0.25	0.25	71.2
Wet	AMS1	47.9	23.2	15.6	13.9	5.19	1.2	0.37	0.42	107.8
	AMS17	56.9	27.7	17.8	16.4	6.27	1.38	0.45	0.32	127.2
	AMS18	6.62	3.27	2.1	1.91	0.73	0.16	0.052	0.038	14.9
	average	37.14	18.06	11.83	10.74	4.06	0.91	0.29	0.26	83.3
Total (dry+wet)	AMS1	108.1	52.7	34.5	31.3	11.8	2.67	0.85	0.9	242.8
	AMS17	86.6	42.3	27.3	25	9.54	2.11	0.69	0.54	194.1
	AMS18	11.7	5.81	3.73	3.39	1.29	0.29	0.093	0.065	26.4
	average	68.8	33.6	21.84	19.9	7.54	1.69	0.54	0.5	154.4

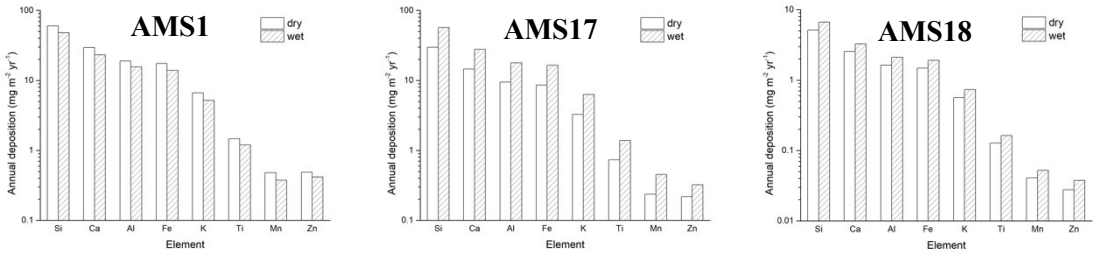

Figure 5.15 The modeled annual dry and wet deposition of the eight elements at three sites for the deposition sensitivity test.

The modeled total dry deposition of the eight elements during the cold season and the warm season

at AMS1 are 82 mg $m^{-2}yr^{-1}$ and 53 mg $m^{-2}yr^{-1}$, respectively. The modeled total wet deposition of the eight elements are 61 mg $m^{-2}yr^{-1}$ and 47 mg $m^{-2}yr^{-1}$ during the cold season and the warm season, respectively. Similar to the base case, the total dry and wet deposition of the eight elements in the deposition case are 1.55 and 1.29 times higher during the cold season than the warm season, respectively, because the constant element emissions throughout the year favour higher element concentrations and deposition in the cold season. The weak vertical mixing under stable atmosphere in the cold season also leads to more elements near surface in the cold season. The total dry deposition of the eight elements are 35% and 12% higher than that total wet deposition in the cold season and the warm season, respectively. These differences are smaller in the warm season than in the cold season due to more precipitations and higher wet deposition in the warm season. These differences are much smaller than those in the base case (35% < 159% in the cold season and 12% < 229% in the warm season). This indicates that the wet deposition accounts more for the removal of elements by using Wang et al. (2014) and Zhang et al. (2001) deposition schemes.

In the deposition sensitivity test, the modeled seasonal dry and wet deposition of individual elements are listed in Table 5.8. Similar to the base case, the modeled dry and wet deposition of the eight elements are 54% and 27% on average higher during the cold season than the warm season (Fig. 5.16), respectively, owing to the constant element emissions in the deposition sensitivity test. The modeled dry deposition of individual elements are higher than the modeled wet deposition by around a factor of 1.4 during the cold season and 1.1 during the warm season (Fig. 5.16), but these discrepancies are much smaller than those in the base case, namely a factor of 2.7 during the cold season and a factor of 3.4 during the warm season. This implies that the replaced dry & wet deposition schemes strengthen the wet deposition in the total deposition. Additionally, compared the deposition sensitivity test to the base case, the modeled dry deposition of the eight elements decrease by 37.2-47.7% during the cold season and 53.4-67.7% during the warm season, respectively, while the modeled wet deposition increase by 9-19.6% during the cold season and 15-33.9% during the warm season, respectively. This suggests the weakening of dry deposition and the strengthening of wet deposition by using Wang et al. (2014) and Zhang et al. (2001) deposition

schemes.

Table 5.8 The modeled seasonal dry and wet deposition (mg $m^{-2}yr^{-1}$) of the eight elements at three stations for the deposition sensitivity test.

Stations	Deposition	Seasons	Elements								Total
			Si	Ca	Al	Fe	K	Ti	Mn	Zn	
AMS1	Dry	cold	37	18	12	11	4	0.89	0.29	0.29	83
		warm	24	12	7.5	6.8	2.6	0.58	0.19	0.2	54
	Wet	cold	27	13	8.7	7.8	2.9	0.67	0.21	0.22	61
		warm	21	10	6.9	6.1	2.2	0.53	0.16	0.2	47
AMS17	Dry	cold	16	8	5.2	4.7	1.8	0.4	0.13	0.12	36
		warm	13	6.5	4.2	3.9	1.5	0.33	0.11	0.094	30
	Wet	cold	28	14	8.8	8.1	3.1	0.68	0.22	0.17	63
		warm	29	14	9	8.3	3.2	0.7	0.23	0.16	65
AMS18	Dry	cold	3.1	1.5	0.98	0.89	0.34	0.077	0.025	0.017	6.9
		warm	2	1	0.64	0.59	0.22	0.05	0.016	0.011	4.5
	Wet	cold	2.5	1.3	0.8	0.73	0.28	0.062	0.02	0.014	5.7
		warm	4.1	2	1.3	1.2	0.45	0.1	0.032	0.023	9.2

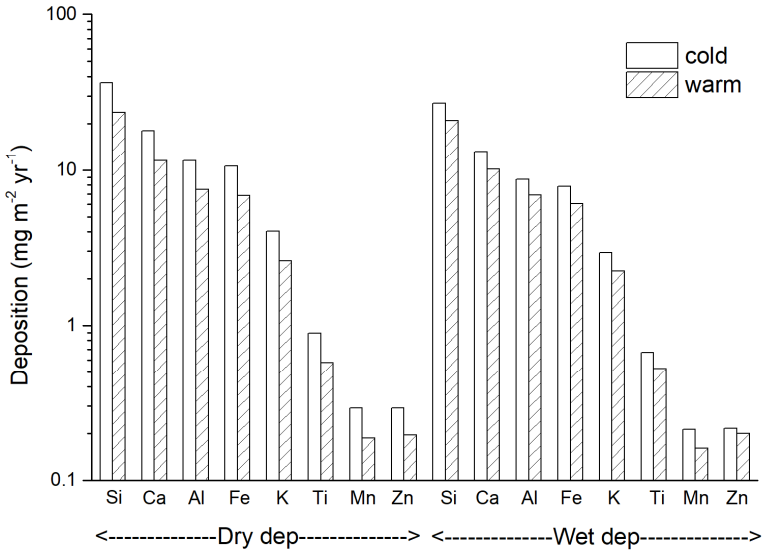

Figure 5.16 The modeled seasonal dry and wet deposition (mg $m^{-2}yr^{-1}$) of the eight elements at AMS1 for the deposition sensitivity test.

The modeled total dry and wet deposition of the eight elements at AMS17 and AMS18 during the cold season and the warm season are shown in Table 5.8. At AMS17, the total dry deposition during the cold season is close to that during the warm season in the base case. However, in the deposition sensitivity test, the total dry deposition is 23% higher during the cold season than the warm season, probably because Zhang et al. (2001) dry deposition scheme produces larger element dry deposition in the cold season. Contrary to the higher total dry deposition than the total wet deposition in the base case, the total wet deposition is higher than the total dry deposition by a factor of 1.71 and 2.15 in the cold season and the warm season, respectively, for the deposition sensitivity test. This indicates that the wet deposition dominates the removal of elements under replaced dry & wet deposition schemes. At AMS18, contrary to the base case, the total wet deposition of the eight elements is 2-fold higher than that total dry deposition during the warm season in the deposition sensitivity test. This is because Wang et al. (2014) below-cloud scavenging formula strengthens the removal of elements by wet deposition.

At AMS17, contrary to similar deposition between the cold and warm seasons in the base case, the

modeled dry deposition of the eight elements are 22-30% higher during the cold season than the warm season (Fig. 5.17) in the deposition sensitivity test due to the strengthening of element dry deposition in the cold season by Zhang et al. (2001) dry deposition scheme. Contrary to the base case, the modeled wet deposition of individual elements are around 1.7 and 2.1 times higher than the modeled dry deposition during the cold season and warm season (Fig. 5.17), respectively, as a result of the enhancement of wet deposition by using Wang et al. (2014) below-cloud scavenging formula. At AMS18, contrary to the higher dry deposition than the wet deposition in the base case, the modeled wet deposition of individual elements are around 2-fold higher than the modeled dry deposition during the warm season (Fig. 5.18). This change suggests that the wet deposition is strengthened by using Wang et al. (2014) below-cloud scavenging formula. Additionally, compared the deposition sensitivity test to the base case, there are decreases of around 63.4% in the cold season and 72.3% in the warm season for the modeled dry deposition of the eight elements at AMS17. There are increases of around 24% in the cold season and 51.6% in the warm season for the modeled wet deposition of the eight elements. At AMS18, the predicted dry deposition of the eight elements decrease by around 55.4% in the cold season and 60.6% in the warm season, while the predicted wet deposition of the eight elements increase by around 53.3% in the cold season and 95% in the warm season. These variations at AMS17 and AMS18 agree with the findings at AMS1 that the replaced dry & wet deposition schemes weaken element dry deposition and strengthen element wet deposition.

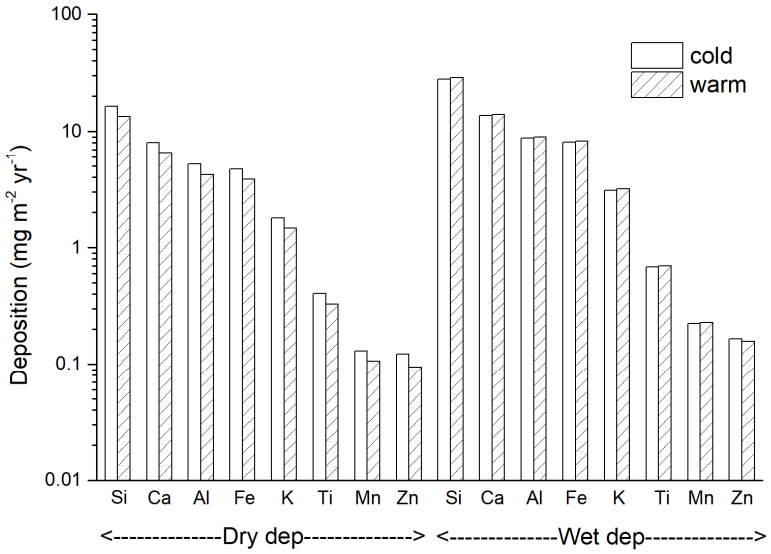

Figure 5.17 The modeled seasonal dry and wet deposition (mg $m^{-2}yr^{-1}$) of the eight elements at AMS17 for the deposition sensitivity test.

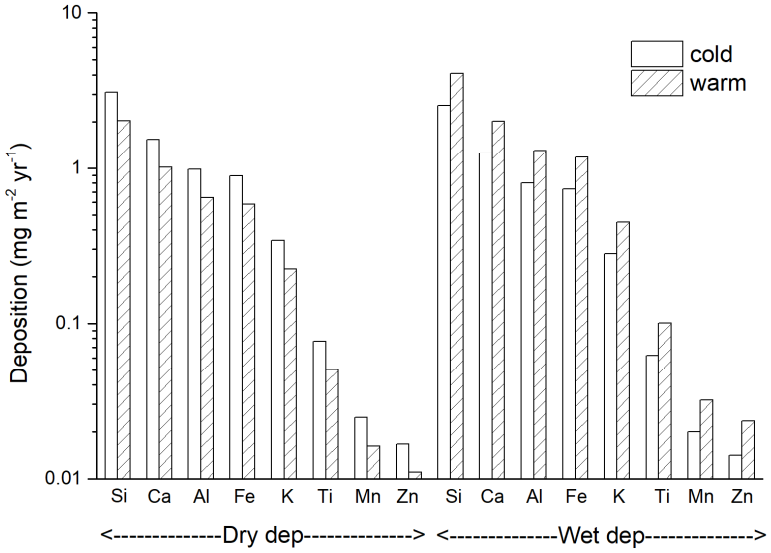

Figure 5.18 The modeled seasonal dry and wet deposition (mg $m^{-2}yr^{-1}$) of the eight elements at AMS18 for the deposition sensitivity test.

Fig. 5.19 shows the spatial distribution for modeled annual total dry and wet deposition of the eight elements in PM_{10}. Despite the use of Wang et al. (2014) and Zhang et al. (2001) deposition schemes, the spatial patterns of total dry and wet deposition are similar to those in the base case (Fig. 4.23). On a yearly basis, the removal of the eight elements from the atmosphere to the surfaces mostly happen within the hotspot of oil sands industry in the AOSR. Both total dry and wet deposition show a decline of around three orders of magnitude from the central area to the remote area, suggesting the substantial contribution to the local environment by the oil sands industry activities. In addition, there is an apparent reduction in the dry deposition because the hotspot region shrinks. The peak values of the wet deposition in the deposition sensitivity test are similar to those in the base case, but they spread over wider regions.

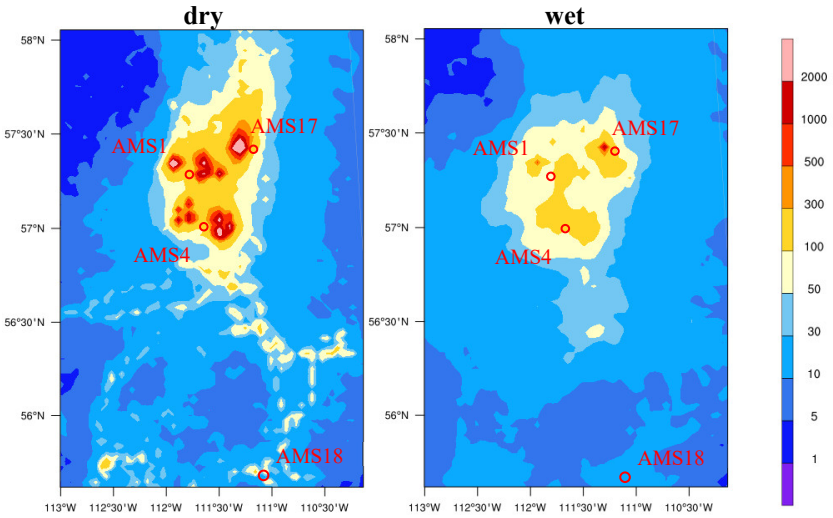

Figure 5.19 Spatial mapping for modeled annual total dry and wet deposition (mg $m^{-2}yr^{-1}$) of all eight elements in PM_{10} for the deposition sensitivity test.

Overall, compared with the base case, there is an impact on the modeled annual dry, wet, and total (dry + wet) deposition of the eight elements (or the eight elements together) by using different dry & wet deposition schemes. The modeled annual total deposition (dry + wet) of the eight elements decrease by on average of 30%, 36%, and 26% at AMS1, AMS17, and AMS18, respectively, and the corresponding decreases for the eight elements together are 28%, 36%, and 26%. The modeled annual total dry deposition

of the eight elements at three sites decrease by 56% on average and the modeled annual total wet deposition increase by 33%, respectively, though the total (dry + wet) deposition only decrease by an average of 31%. At the same time, the use of different dry & wet deposition schemes causes some influences on the modeled dry and wet deposition of the eight elements (or the eight elements together) on the seasonal basis. Compared with the base case, the modeled wet deposition accounts more for the total deposition, and even dominates in the total deposition in the two seasons. However, the spatial distribution of dry and wet deposition is similar under different dry & wet deposition schemes.

6. Conclusions

6.1 Summary

In this study, emission, transport, and deposition processes in WRF-Chem are modified to include eight trace elements. The chemical reactions of elements are not considered because of the limited knowledge on the atmospheric chemistry for these elements. The eight elements are simulated by WRF-Chem in two-way nested domains with the inner domain centered at the AOSR in a two-year period from 2016 to 2017. The annual stack and area emissions for the eight elements are extracted from the Joint Canada-Alberta Implementation Plan for Oil Sands Monitoring air emissions inventory. The annual total emissions are equally split into each month of a year. The emissions from discrete points and area are interpolated into the model grids. The plume rise for stack emissions is considered to avoid the overestimation of the element concentrations near the surface. The modeling results are validated using the measured meteorological data, including surface air temperature, surface wind, and precipitation, at Mildred Lake weather station. The model in general has a good performance on the air temperature and wind, but the monthly precipitation has an error of 55% on average. The overprediction of precipitation may have a positive bias on the wet deposition of trace elements.

On the yearly basis, the comparisons between the model and the observations at three monitoring sites (AMS1, AMS17, and AMS18) reveal that the percentage differences in the concentration of the eight elements are in the range of -6.9% to 76%, -48% to 72%, and -165% to 5.8% at AMS1, AMS17, and AMS18, respectively. The model results in the element concentrations are the best at AMS1 with an averaged difference of 23%, followed by AMS17 (25%) and AMS18 (-56%). The averaged observed concentrations at three sites for Si, Ca, Al, Fe, K, Ti, Mn, and Zn are 489 ng m^{-3}, 228 ng m^{-3}, 200 ng m^{-3}, 108 ng m^{-3}, 69 ng m^{-3}, 9.5 ng m^{-3}, 2.7 ng m^{-3}, and 4.7 ng m^{-3}, respectively. Among these eight elements, the model performance at three sites is the best for Ca with an average difference of 17%, followed by Al (31%), Si (37%), Fe (46%), K (58%), Ti (63%), Mn (66%), and Zn (92%). Additionally, all elements except Al are overpredicted by 29-122% at AMS1, and all elements except K and Zn are overestimated

by 15-113% at AMS17. On the contrary, all elements except Ca are underpredicted by 20-90% at AMS18. These different model performances at the three sites may be caused by some uncertainties in the element emissions. The dramatic drops in the modeled element concentrations with the distance from the emission sources may suggest that the removal of elements by dry & wet deposition is too efficient. The model simulated winds are weaker than the observations that may weaken the transport of elements from the emission sources, potentially leading to the elevated element concentrations near the major oil sands industry area in the model simulations. The uncertainties in the simulated meteorological conditions may also contribute to the errors in the atmospheric deposition of elements. On the seasonal basis, the model predicts higher element concentrations in the cold season than in the warm season. However, the observations show an opposite trend. The modeled total concentrations of the eight elements are overestimated by 82% in the cold season and underestimated by 38% in the warm season on average at the three AMS sites. The flipped model trend is mainly caused by the constant emission rates throughout the year. The industrial activities (thus the emissions) in the cold seasons are less than those in the warm season. The snow cover in the cold season also weakens the element emissions from the dust that is a major emission source in the AOSR. However, these seasonal variations of element emissions are not considered in the model simulation. Physically, the planetary boundary layer is more stable and shallower in the cold season. It suppresses the vertical mixing of elements. Hence, the element concentrations tend to be larger near the surface in the cold season.

Regardless of the monitoring site, Si has the largest modeled annual concentration in PM_{10}, generally followed by Ca, Al, Fe, K, Ti, Mn, and Zn, agreeing with the order of their magnitudes in the emission rates. The modeled annual total concentrations of the eight elements are the highest at AMS1 and AMS4, followed by AMS17 and AMS18. This is because AMS1 and AMS4 are located at the hotspot of oil sands industry while AMS18 is over 150 km away from the hotspot of oil sands industry. On the seasonal basis, the modeled concentrations of the eight elements at AMS1, AMS17, and AMS18 have the same trend as the total concentrations, i.e., higher in the cold season than in the warm season.

The seasonal percentage differences in the modeled concentrations of the eight elements are largest at AMS1, followed by AMS18 and AMS17. On the contrary, the modeled concentrations of the seven elements (Si, Ca, Al, Fe, K, Ti, and Mn) in $PM_{2.5-10}$ at AMS4 are higher during the warm season than the cold season. This is because AMS4 is located downstream of a major emission source. More westerly winds blow from this major emission source to AMS4 in the warm season. Thus, more elements spread from this emission source to AMS4, leading to the higher modeled element concentrations at AMS4.

The modeled annual dry deposition of all eight elements is the highest at AMS1, followed by AMS4, AMS17, and AMS18, similar to the order of modeled annual total element concentrations at the four sites. This implies that the ambient element concentration is a significant factor determining the element dry deposition flux. The modeled annual wet deposition of all elements are the highest at AMS4 and AMS17. Although the modeled annual total element concentrations in PM_{10} at AMS17 are much smaller than that at AMS1 (971 ng m^{-3} < 2860 ng m^{-3}), the modeled annual wet deposition at AMS17 is higher than that at AMS1 (124.1 mg $m^{-2}yr^{-1}$ > 113.9 mg $m^{-2}yr^{-1}$) owing to the higher modeled annual precipitation at AMS17 than at AMS1 (766 mm > 572 mm). This confirms that both the ambient element concentration and the precipitation amount determine the element wet deposition flux. For all elements and at all AMS sites, the modeled annual dry deposition is always larger than the wet deposition, though they are in the same order of magnitudes. The precipitation amount determines the predominance of removal processes being dry or wet deposition. The modeled annual precipitation is only 572-769 mm at the four sites, which may not be sufficient for larger wet deposition. On the seasonal basis, the pattern of modeled dry and wet deposition of elements is different among AMS sites. The dry deposition depends on the modeled element concentration and the modeled dry deposition velocity. The higher dry deposition at AMS1 and AMS18 during the cold season and the higher dry deposition at AMS4 during the warm season are due to their higher modeled element concentrations in the corresponding season. The higher dry deposition at AMS17 during the warm season is owing to the larger dry deposition velocities. Instead, the wet deposition relies on the modeled element concentration and the modeled

precipitation. The higher wet deposition at AMS1 and AMS4 during the cold season are because of their higher modeled element concentrations in the cold season. The wet deposition during the cold season are close to that during the warm season at AMS17 and AMS18, due to more precipitations during the warm season. However, regardless of sites and seasons, the modeled dry deposition either for individual elements or the eight elements in total are always larger than the modeled wet deposition. This is because of 572-769 mm modeled precipitation at AMS sites, which limits the removal of elements by wet deposition.

The longitude-height and latitude-height cross sections show that the modeled wind speed is larger in the cold season than that in the warm season. The potential temperature increases more rapidly with height in the cold season indicating more stable atmosphere in wintertime. The modeled total concentrations of the eight elements near the surface are higher during the cold season than the warm season, and they decrease from around 3 $\mu g\ m^{-3}$ to 0.001 $\mu g\ m^{-3}$ (1 $ng\ m^{-3}$) at the height of around 2 km and 3 km in the cold and warm seasons, respectively. In the cold season, the highly stable atmosphere prevents the vertical mixing of elements and forces elements to move horizontally near the surface, potentially causing serious local environmental impacts. The spatial distribution of modeled concentration and deposition of the eight elements suggests that all elements have a similar spatial pattern with a major spread in N-S direction following the prevailing winds. They are concentrated in the central region of the AOSR where the major oil sands industry facilities are located. The maximum modeled concentration and deposition of eight elements are located around 15 km west of AMS17. In the central region, the modeled domain averaged annual concentrations of Si, Ca, Al, Fe, K, Ti, Mn, and Zn are 2.67 $\mu g\ m^{-3}$, 1.31 $\mu g\ m^{-3}$, 0.83 $\mu g\ m^{-3}$, 0.77 $\mu g\ m^{-3}$, 0.3 $\mu g\ m^{-3}$, 0.065 $\mu g\ m^{-3}$, 0.021 $\mu g\ m^{-3}$, and 0.016 $\mu g\ m^{-3}$, respectively, and the modeled annual total concentration of the eight elements is 5.98 $\mu g\ m^{-3}$. Furthermore, the modeled domain averaged annual total deposition (dry + wet) of Si, Ca, Al, Fe, K, Ti, Mn, and Zn are 385 $mg\ m^{-2}yr^{-1}$, 187 $mg\ m^{-2}yr^{-1}$, 122 $mg\ m^{-2}yr^{-1}$, 111 $mg\ m^{-2}yr^{-1}$, 42 $mg\ m^{-2}yr^{-1}$, 9.4 $mg\ m^{-2}yr^{-1}$, 3.05 $mg\ m^{-2}yr^{-1}$, and 2.62 $mg\ m^{-2}yr^{-1}$, respectively, and the modeled annual total deposition of the

eight elements is 862 mg $m^{-2}yr^{-1}$. Both modeled element concentrations and deposition decline quickly by around three orders of magnitude from the central region to the remote region 150 km away. That indicates oil sands industry makes significant impacts mostly on a local region close to the emission sources.

In the sensitivity tests, one-year simulations in 2017 are conducted to study how seasonal varying emission and different deposition schemes influence the element dispersion and deposition. In the first model sensitivity test, the annual total emissions are reallocated to 70% in the warm season and 30% in the cold season. This seasonally varied element emissions leads to small influence on the modeled annual concentration and deposition of the eight elements. Compared with the base case, the modeled annual concentrations of the eight elements in PM_{10} are reduced by an average of 9.5%, 4.4%, and 8.8% at AMS1, AMS17, and AMS18, respectively. The discrepancies in the modeled annual total deposition (dry + wet) of the eight elements are averaged -3.9%, 1%, and -4.2% at AMS1, AMS17, and AMS18, respectively. The model-measurement percentage differences for the annual concentrations of the eight elements in PM_{10} are similar to the base case. The biggest improvements are in the seasonal results. Compared with the base case, both the modeled concentrations and deposition of the eight elements are increased by around 40% in the warm season, but decreased by around 40% in the cold season, agreeing with 40% change in the element emissions. This indicates that the element concentrations and deposition are strongly proportional to the emission. In addition, the averaged bias in the modeled total concentrations of the eight elements in PM_{10} against the observations is reduced from 45% to 13% in the cold season and from 45% to 24% in the warm season. However, elements in $PM_{2.5}$ are overestimated by 55% and those in $PM_{2.5-10}$ are underestimated by 25% in the whole year. Since elements in PM_{10} dominate the whole spectra, the model performance on the modeled element concentration still becomes better with seasonally varied element emissions.

In the second model sensitivity test, replacing the default dry & wet deposition schemes in WRF-Chem with Zhang et al. (2001) and Wang et al. (2014) deposition schemes results in some impacts on the

modeled annual concentration and deposition of the eight elements. Compared with the base case, the modeled annual concentrations of the eight elements in PM_{10} are elevated by 6.8%, 19.6%, and 17.7% on average at AMS1, AMS17, and AMS18, respectively. On the other hand, the modeled annual total deposition (dry + wet) of the eight elements decreases by 30%, 36%, and 26% on average at AMS1, AMS17, and AMS18, respectively. The annual dry deposition of all eight elements decreases by an average of 56% and annual wet deposition increases by an average of 33% for the three sites, though the annual total (dry + wet) deposition decreases by an average of 31%. This indicates that the use of Zhang et al. (2001) dry deposition scheme and Wang et al. (2014) wet deposition scheme weakens the dry deposition and enhances the wet deposition. The spatial patterns of the dry and wet deposition are similar to the base case. On the seasonal basis, there are also some influences on the modeled concentration and deposition of the eight elements by using different dry & wet deposition schemes. The modeled wet deposition of individual elements are close to the dry deposition, or even dominate over the dry deposition in the two seasons. Compared with the base case, the averaged modeled concentrations of the eight elements in PM_{10} increase by around 14% in the cold season and 16% in the warm season for the three sites. The averaged bias in the modeled total concentrations of the eight elements in PM_{10} from the observations increases from 45% to 66% in the cold season and decreases from 45% to 37% in the warm season. This is because that the modeled element concentrations are overestimated in the cold season and underestimated in the warm season. The increase of modeled element concentrations under the different dry & wet deposition schemes strengthens this overestimation and weakens this underestimation. As a result, the bias in the modeled element concentrations is larger in the cold season and smaller in the warm season.

6.2 Future work

The dispersion and deposition of trace elements are largely controlled by the emission. Thus, the future work should focus on the improvement of emission database, especially anthropogenic sources

and the element speciation. Through sensitivity test, it is expected that the modeling performance on the element concentrations can be further improved under the joint impact by considering time-varying element emissions and using appropriate dry & wet deposition schemes, however, this expectation needs validation by additional model simulations and field measurements. In addition, significant changes in atmospheric deposition of elements by using different deposition schemes suggest that direct measurement of element deposition need to be considered in future field observations. These measurements can be used to validate the numerical deposition schemes. The effect of different terms in the deposition schemes on the atmospheric deposition needs a further investigation. With the aim to verify the predominance of element removal by dry or wet deposition, studies over a region with annual precipitation larger than 1000 mm are required.

Bibliography

Ajilesh, P., Rakesh, V., Sahoo, S.K. and Himesh, S. 2020. Observed and model-simulated thermodynamic processes associated with urban heavy rainfall events over Bangalore, India. Meteorol. Appl. 27, e1854.

Allen, A.G., Nemitz, E., Shi, J.P., Harrison, R.M., and Greenwood, J.C. 2001. Size distributions of trace metals in atmospheric aerosols in the United Kingdom. Atmos. Environ. 35, 4581–4591.

Al-Momani, I.F., Daradkeh, A.S., Haj-Hussein, A.T., Yousef, Y.A., Jaradat, Q.M., and Momani, K.A. 2005. Trace elements in daily collected aerosols in Al-Hashimya, central Jordan. Atmos. Res. 73, 87–100.

Al-Momani, I.F., Ya'qoub, A.-R.A., and Al-Bataineh, B.M. 2002. Atmospheric deposition of major ions and trace metals near an industrial area, Jordan. J. Environ. Monit. 4, 985–989.

Appel, K.W., Pouliot, G.A., Simon, H., Sarwar, G., Pye, H.O.T., Napelenok, S.L., Akhtar, F., and Roselle, S.J. 2013. Evaluation of dust and trace metal estimates from the Community Multiscale Air Quality (CMAQ) model version 5.0. Geosci. Model Dev. 6, 883–899.

Arruti, A., Fernández-Olmo, I., and Irabien, Á. 2010. Evaluation of the contribution of local sources to trace metals levels in urban PM2.5 and PM10 in the Cantabria region (Northern Spain). J. Environ. Monit. 12, 1451–1458.

Balasubramanian, R., and Qian, W.B. 2004. Characterization and source identification of airborne trace metals in Singapore. J. Environ. Monit. 6, 813–818.

Bari, M.A., Kindzierski, W.B., and Cho, S. 2014. A wintertime investigation of atmospheric deposition of metals and polycyclic aromatic hydrocarbons in the Athabasca Oil Sands Region, Canada. Sci. Total Environ. 485–486, 180–192.

Bhanarkar, A., Rao, P., Gajghate, D., and Nema, P. 2005. Inventory of SO_2, PM and toxic metals emissions from industrial sources in Greater Mumbai, India. Atmos. Environ. 39, 3851–3864.

Bilos, C., Colombo, J.C., Skorupka, C.N., and Rodriguez Presa, M.J. 2001. Sources, distribution and variability of airborne trace metals in La Plata City area, Argentina. Environ. Pollut. 111, 149–158.

Binkowski, F.S., and Shankar, U. 1995. The regional particulate matter model: 1. Model description and preliminary results. J. Geophys. Res. 100, 26191–26209.

Birmili, W., Allen, A.G., Bary, F., and Harrison, R.M. 2006. Trace metal concentrations and water solubility in size-fractionated atmospheric particles and influence of road traffic. Environ. Sci. Technol. 40, 1144–1153.

Briggs, G.A. 1969. Plume rise: A critical survey, Air Resources Atmospheric Turbulence and Diffusion Lab., Oak Ridge, Tenn. doi:10.2172/4743102.

Cerro, J.C., Cerdà, V., Caballero, S., Bujosa, C., Alastuey, A., Querol, X., and Pey, J. 2020. Chemistry of dry and wet atmospheric deposition over the Balearic Islands, NW Mediterranean: Source apportionment and African dust areas. Sci. Total Environ. 747, 141187.

Chandra, S., Kulshrestha, M.J., Singh, R., and Singh, N. 2017. Chemical characteristics of trace metals in PM10 and their concentrated weighted trajectory analysis at Central Delhi, India. J. Environ. Sci. 55, 184–196.

Charlesworth, S., Miguel, E.D., and Ordóñez, A. 2011. A review of the distribution of particulate trace elements in urban terrestrial environments and its application to considerations of risk. Environ. Geochem. Health. 33, 103–123.

Chen, F. and Dudhia, J. 2001. Coupling an advanced land-surface/ hydrology model with the Penn State/ NCAR MM5 modeling system. Part I: Model description and implementation. Mon. Wea. Rev. 129, 569–585.

Chen, X., Balasubramanian, R., Zhu, Q., Behera, S.N., Bo, D., Huang, X., Xie, H., and Cheng, J. 2016. Characteristics of atmospheric particulate mercury in size-fractionated particles during haze days in Shanghai. Atmos. Environ. 131, 400–408.

Cheng, I., Al Mamun, A., and Zhang, L. 2021. A synthesis review on atmospheric wet deposition of particulate elements: Scavenging ratios, solubility, and flux measurements. Environ. Rev. 29, 340–353.

Cheng, I., Wen, D., Zhang, L., Wu, Z., Qiu, X., Yang, F., and Harner, T. 2018. Deposition mapping of polycyclic aromatic compounds in the oil sands region of Alberta, Canada and linkages to ecosystem impacts. Environ. Sci. Technol. 52, 12456–12464.

Chou M.D., and Suarez, M.J. 1999. A solar radiation parameterization for atmospheric studies. NASA Tech. Rep. NASA/TM-1999-10460, vol. 15, pp 38.

Cong, Z., Kang, S., Zhang, Y., and Li, X. 2010. Atmospheric wet deposition of trace elements to central Tibetan Plateau. Appl. Geochem. 25, 1415–1421.

Cooke, C.A., Kirk, J.L., Muir, D.C.G., Wiklund, J.A., Wang, X., Gleason, A., and Evans, M.S. 2017. Spatial and temporal patterns in trace element deposition to lakes in the Athabasca oil sands region (Alberta, Canada). Environ. Res. Lett. 12, 124001.

Denkhaus, E. and Salnikow, K. 2002. Nickel essentiality, toxicity, and carcinogenicity. Crit. Rev. Oncol. Hematol. 42, 35–56.

Diaz-De-Quijano, M., Joly, D., Gilbert, D., Toussaint, M.L., Franchi, M., Fallot, J.M., and Bernard, N. 2016. Modelling and mapping trace element accumulation in Sphagnum peatlands at the European scale using a geomatic model of pollutant emissions dispersion. Environ. Pollut. 214, 8–16.

Duan, J., Tan, J., Wang, S., Hao, J., and Chai, F. 2012. Size distributions and sources of elements in particulate matter at curbside, urban and rural sites in Beijing. J. Environ. Sci. 24, 87–94.

Fang, G.C., Lo, C.T., Huang, W.J., Wu, Y.S., and Huang, J.H. 2011. Atmospheric particulates-bound mercury Hg(p) study at five characteristic sampling sites in Taiwan. Environ. Monit. Assess. 181, 273–289.

Fang, G.C., Wu, Y.S., Huang, S.H., and Rau, J.Y. 2004. Dry deposition (downward, upward) concentration study of particulates and heavy metals during daytime, nighttime period at the traffic sampling site of Sha-Lu, Taiwan. Chemosphere. 56, 509–518.

Fomba, K.W., van Pinxteren, D., Müller, K., Spindler, G., and Herrmann, H. 2018. Assessment of trace metal levels in size-resolved particulate matter in the area of Leipzig. Atmos. Environ. 176, 60–70.

Fountoukis, C., Ackermann, L., Ayoub, M.A, Gladich, I., Hoehn, R.D., and Skillern, A. 2016. Impact of atmospheric dust emission schemes on dust production and concentration over the Arabian Peninsula. Model. Earth Syst. Environ. 2, 115.

Galarneau, E., Hollebone, B.P., Yang, Z., and Schuster, J. 2014. Preliminary measurement-based estimates of PAH emissions from oil sands tailings ponds. Atmos. Environ. 97, 332–335.

Gallego, S.M., Pena, L.B., Barcia, R.A., Azpilicueta, C.E., Iannone, M.F., Rosales, E.P., Zawoznik, M.S., Groppa, M.D., and Benavides, M.P. 2012. Unravelling cadmium toxicity and tolerance in plants: Insight into regulatory mechanisms. Environ. Exp. Bot. 83, 33–46.

Gildemeister, A.E., Graney, J., and Keeler, G.J. 2005. Source proximity reflected in spatial and temporal variability in particle and vapour phase Hg concentrations in Detroit, MI. Atmos. Environ. 39, 353–358.

Gopalapillai, Y., Kirk, J.L., Landis, M.S., Muir, D.C.G., Cooke, C.A., Gleason, A., Ho, A., Kelly, E., Schindler, D., Wang, X., and Lawson, G. 2019. Source analysis of pollutant elements in winter air deposition in the athabasca oil sands region: a temporal and spatial study. ACS Earth Space Chem. 3, 1656–1668.

Gratz, L.E., Keeler, G.J., Morishita, M., Barres, J.A., and Dvonch, J.T. 2013. Assessing the emission sources of atmospheric mercury in wet deposition across Illinois. Sci. Total Environ. 448, 120 –131.

Grell, G.A. and Freitas, S.R. 2014. A scale and aerosol aware stochastic convective parameterization for weather and air quality modeling. Atmos. Chem. Phys. 14, 5233–5250.

Griffin, D., Zhao, X., McLinden, C.A., Boersma, F., Bourassa, A., Dammers, E., et al. 2019. High-resolution mapping of nitrogen dioxide with TROPOMI: First results and validation over the Canadian oil sands. Geophys. Res. Lett., 46, 1049–1060.

Gueguen, C., Cuss, C.W., and Cho, S. 2016. Snowpack deposition of trace elements in the Athabasca oil sands region, Canada. Chemosphere. 153, 447–454.

Guo, X., Ji, H., Li, C., Gao, Y., Ding, H., Tang, L., and Feng, J. 2017. The sources of trace element pollution of dry depositions nearby a drinking water source. Environ. Sci. Pollut. Res. 24, 3829–3842.

Harrison, R.M. and Yin, J. 2000. Particulate matter in the atmosphere: which particle properties are important for its effects on health? Sci. Total Environ. 249, 85–101.

Harrison, R.M., Tilling, R., Callén Romero, M.S., Harrad, S., and Jarvis, K. 2003.A study of trace metals and polycyclic aromatic hydrocarbons in the roadside environment. Atmos. Environ. 37, 2391–2402.

Hong, S., Noh, Y., and Dudhia, J. 2006. A New Vertical Diffusion Package with an Explicit Treatment of Entrainment Processes. Mon. Wea. Rev. 134, 2318–2341.

Huang, R.F., McPhedran, K.N., Yang, L.L., and El-Din, M.G. 2016. Characterization and distribution of metal and nonmetal elements in the Alberta oil sands region of Canada. Chemosphere. 147, 218–229.

Hutzell W.T. and Luecken D.J. 2008. Fate and transport of emissions for several trace metals over the United States. Sci. Total Environ. 25, 164–79.

Ioannidou, A. 2011. Activity size distribution of 7Be in association with trace metals in the urban area of the city of Thessaloniki, Greece. Atmos. Environ. 45, 1286–1290.

Jeworrek, J., West, G., and Stull, R., 2021. WRF precipitation performance and predictability for systematically varied parameterizations over complex terrain. Weather Forecast. 36, 893–913.

Kalenderski, S., Stenchikov, G., and Zhao, C. 2013. Modeling a typical winter-time dust event over the Arabian Peninsula and the Red Sea. Atmos. Chem. Phys. 13, 1999–2014.

Kelly, E.N., Schindler, D.W., Hodson, P.V., Short, J.W., Radmanovich, R., and Nielsen, C.C. 2010. Oil sands development contributes elements toxic at low concentrations to the Athabasca River and its tributaries. Proc. Natl. Acad. Sci. 107, 16178–16183.

Kim, P.R., Han, Y.J., Holsen, T.M., and Yi, S.M. 2012. Atmospheric particulate mercury: Concentrations and size distributions. Atmos. Environ. 61, 94–102.

Kirk, J.L., Muir, D.C.G., Gleason, A., Wang, X., Lawson, G., Frank, R.A., Lehnherr, I., and Wrona, F. 2014. Atmospheric deposition of mercury and methylmercury to landscapes and waterbodies of the Athabasca oil sands region. Environ. Sci. Technol. 48, 7374–7383.

Köcher, G., Zinner, T., and Knote, C. 2023. Influence of cloud microphysics schemes on weather model predictions of heavy precipitation. Atmos. Chem. Phys. 23, 6255–6269.

Krewski, D., Yokel, R.A., Nieboer, E., Borchelt, D., Cohen, J., Harry, J., Kacew, S., Lindsay, J., Mahfouz, A.M., and Rondeau, V. 2007. Human health risk assessment for aluminium, aluminium oxide, and aluminium hydroxide. J. Toxicol. Environ. Health Part B. 10, 1–269.

Kyllönen, K., Karlsson, V., and Ruoho-Airola, T. 2009. Trace element deposition and trends during a ten year period in Finland. Sci. Total Environ. 407, 2260–2269.

Landing, W.M., Caffrey, J.M., Nolek, S.D., Gosnell, K.J., and Parker, W.C. 2010. Atmospheric wet deposition of mercury and other trace elements in Pensacola, Florida. Atmos. Chem. Phys. 10, 4867–4877.

Landis, M.S., Edgerton, E.S., White, E.M., Wentworth, G.R., Sullivan, A.P., and Dillner, A.M. 2018. The impact of the 2016 Fort McMurray Horse River Wildfire on ambient air pollution levels in the Athabasca Oil Sands Region, Alberta, Canada. Sci. Total Environ. 618: 1665–1676.

Landis, M.S., Pancras, J.P., Graney, J.R., White, E.M., Edgerton, E.S., Legge, A., and Percy, K.E. 2017. Source apportionment of ambient fine and coarse particulate matter at the Fort McKay community site, in the Athabasca Oil Sands Region, Alberta, Canada. Sci. Total Environ. 584–585, 105–117.

Landis, M.S., Studabaker, W.B., Pancras, J.P., Graney, J.R., White, E.M., and Edgerton, E.S. 2019. Source apportionment of ambient fine and coarse particulate matter polycyclic aromatic hydrocarbons at the Bertha Ganter-Fort McKay community site in the Oil Sands Region of Alberta, Canada. Sci. Total Environ. 666, 540–558.

Lim, J.H., Sabin, L.D., Schiff, K.C., and Stolzenbach, K.D. 2006. Concentration, size distribution, and dry deposition rate of particle-associated metals in the Los Angeles region. Atmos. Environ. 40, 7810–7823.

Liu, S., Zhu, C., Tian, H., Wang, Y., Zhang, K., Wu, B., Liu, X., Hao, Y., Liu, W., Bai, X., Lin, S., Wu, Y., Shao, P., and Liu, H. 2019. Spatiotemporal Variations of Ambient Concentrations of Trace Elements in a Highly Polluted Region of China. J. Geophys. Res. Atmos. 124, 4186–4202.

Lu, R., Turco, R.P., Stolzenbach, K., Friedlander, S.K., Xiong, C., Schiff, K., Tiefenthaler, L., and Wang, G.Y. 2003. Dry deposition of airborne trace metals on the Los Angeles Basin and adjacent coastal waters. J. Geophys. Res. Atmos. 108, D2.

Maddah, M.A. and Mostamandi, S. 2024. WRF prediction of an atmospheric river-related precipitation event: Sensitivity to cumulus parameterization schemes. Meteorol. Appl. 31, e2160.

Makkonen, U., Hellén, H., Anttila, P., and Ferm, M. 2010. Size distribution and chemical composition of airborne particles in south-eastern Finland during different seasons and wildfire episodes in 2006. Sci. Total Environ. 408, 644–651.

Malandrino, M., Casazza, M., Abollino, O., Minero, C., and Maurino, V. 2016. Size resolved metal distribution in the PM matter of the city of Turin (Italy). Chemosphere. 147, 477–489.

Mamun, A.A., Celo, V., Dabek-Zlotorzynska, E., Charland, J.P., Cheng, I., and Zhang, L. 2021. Characterization and source apportionment of airborne particulate elements in the Athabasca oil sands region. Sci. Total Environ. 788, 147748.

Mamun, A.A., Cheng, I., Zhang, L., Celo, V., Dabek-Zlotorzynska, E., Charland, J.P. 2022. Estimation of atmospheric dry and wet deposition of particulate elements at four monitoring sites in the Canadian athabasca oil sands region. J. Geophys. Res. Atmos. 127, e2021JD035787.

Mamun, A.A., Cheng, I., Zhang, L., Dabek-Zlotorzynska, E., and Charland, J.P. 2020. Overview of size distribution, concentration, and dry deposition of airborne particulate elements measured worldwide. Environ. Rev. 28, 77–88.

Mamun, A.A., Zhang, L., Yang, F., Cheng, I., and Qiu, X. 2023. Atmospheric deposition mapping of particulate elements in the Canadian Athabasca oil sands region. Environ. Pollut. 331, 121868.

Masri, S., Kang, C.M., and Koutrakis, P. 2015. Composition and sources of fine and coarse particles collected during 2002–2010 in Boston, MA. J. Air Waste Manage. Assoc. 1995. 65, 287–297.

McLinden, C.A., Adams, C.L.F., Fioletov, V., Griffin, D., Makar, P.A., Zhao, X., Kovachik, A., Dickson, N., Brown, C., Krotkov, N., Li, C., Theys, N., Hedelt, P., and Loyola, D.G. 2020. Inconsistencies in sulfur dioxide emissions from the Canadian oil sands and potential implications. Environ. Res. Lett. 16, 014012.

Mlawer, E.J., Taubman, S.J., Brown, P.D., Iacono, M.J., and Clough, S.A. 1997. Radiative transfer for inhomogeneous atmosphere: RRTM, a validated correlated k model for the longwave. J. Geophys. Res. 102, 16663–16682.

Monin, A.S. and Obukhov, A.M. 1954. Basic laws of turbulent mixing in the surface layer of the atmosphere. Contrib. Geophys. Inst. Acad. Sci. USSR. 24, 163–187.

Montoya-Mayor, R., Fernández-Espinosa, A.J., Seijo-Delgado, I., and Ternero-Rodríguez, M. 2013. Determination of soluble ultra-trace metals and metalloids in rainwater and atmospheric deposition fluxes: a 2-year survey and assessment. Chemosphere, 92, 882–891.

Morrison, H., van Lier-Walqui, M., Fridlind, A.M., Grabowski, W.W., Harrington, J.Y., Hoose, C., Korolev, A., Kumjian, M.R., Milbrandt, J.A., Pawlowska, H., Posselt, D.J., Prat, O.P., Reimel, K.J., Shima, S.I., van Diedenhoven, B., and Xue, L. 2020. Confronting the Challenge of Modeling Cloud and Precipitation Microphysics. J. Adv. Model. Earth Sy. 12, e2019MS001689.

Mooibroek, D., Schaap, M., Weijers, E.P., and Hoogerbrugge, R. 2011. Source apportionment and spatial variability of PM2.5 using measurements at five sites in the Netherlands. Atmos. Environ. 45, 4180–4191.

Moreno, T., Querol, X., Alastuey, A., Reche, C., Cusack, M., Amato, F., Pandolfi, M., Pey, J., Richard, A., Prévôt, A.S.H., Furger, M., and Gibbons, W. 2011. Variations in time and space of trace metal aerosol concentrations in urban areas and their surroundings. Atmos. Chem. Phys. 11, 9415–9430.

Muezzinoglu, A., and Cizmecioglu, S.C. 2006. Deposition of heavy metals in a Mediterranean climate area. Atmos. Res. 81, 1–16.

Nagajyoti, P.C., Lee, K.D., and Sreekanth, T.V.M. 2010. Heavy metals, occurrence and toxicity for plants: a review. Environ. Chem. Lett. 8, 199–216.

Odabasi, M., Muezzinoglu, A., and Bozlaker, A. 2002. Ambient concentrations and dry deposition fluxes of trace elements in Izmir, Turkey. Atmos. Environ. 36, 5841–5851.

Outridge, P.M. and Scheuhammer, A.M. 1993. Bioaccumulation and toxicology of chromium: Implications for wildlife. In Reviews of environmental contamination and toxicology, Ware, G.W. (Ed.), Springer New York, pp. 31–77.

Özsoy, T., and Örnektekin, S. 2009. Trace elements in urban and suburban rainfall, Mersin, Northeastern Mediterranean. Atmos. Res. 94, 203–219.

Pan, Y., Tian, S., Li, X., Sun, Y., Li, Y., Wentworth, G.R., and Wang, Y. 2015. Trace elements in particulate matter from metropolitan regions of Northern China: Sources, concentrations and size distributions. Sci. Total Environ. 537, 9–22.

Pan, Y.P., and Wang, Y.S. 2015. Atmospheric wet and dry deposition of trace elements at 10 sites in Northern China. Atmos. Chem. Phys. 15, 951– 972.

Phillips-Smith, C., Jeong, C.H., Healy, R.M., Dabek-Zlotorzynska, E., Celo, V., Brook, J. R., and Evans, G. 2017. Sources of particulate matter components in the Athabasca oil sands region: investigation through a comparison of trace element measurement methodologies. Atmos. Chem. Phys. 17, 9435–9449.

Rajeevan, M., Kesarkar, A., Thampi, S.B., Rao, T.N., Radhakrishna, B., and Rajasekhar, M. 2010. Sensitivity of WRF cloud microphysics to simulations of a severe thunderstorm event over Southeast India. Ann. Geophys. 28, 603–619.

Reff, A., Bhave, P.V., Simon, H., Pace, T.G., Pouliot, G.A., Mobley, J.D., and Houyoux, M. Emissions inventory of PM2.5 trace elements across the United States, Environ. Sci. Technol. 43, 5790–5796.

Ren, C., Huang, X., Liu, T., Song, Y., Wen, Z., Liu, X., Ding, A., and Zhu. T. 2023. A dynamic ammonia emission model and the online coupling with WRF–Chem (WRF–SoilN–Chem v1.0): development and regional evaluation in China. Geosci. Model Dev. 16, 1641–1659.

Rosseland, B., Eldhuset, T.D., and Staurnes, M. 1990. Environmental effects of aluminium. Environ. Geochem. Health. 12, 17–27.

Sabin, L.D., and Schiff, K.C. 2008. Dry atmospheric deposition rates of metals along a coastal transect in southern California. Atmos. Environ. 42, 6606–6613.

Sakata, M., and Asakura, K. 2011. Atmospheric dry deposition of trace elements at a site on Asian-continent side of Japan. Atmos. Environ. 45, 1075–1083.

Samara, C., and Voutsa, D. 2005. Size distribution of airborne particulate matter and associated heavy metals in the roadside environment. Chemosphere, 59, 1197–1206.

Schuster, J.K., Harner, T., Su, K., Eng, A., Wnorowski, A., and Charland, J.P. 2019. Temporal and spatial trends of polycyclic aromatic compounds in air across the Athabasca oil sands region reflect inputs from open pit mining and forest fires. Environ. Sci. Technol. Lett. 6, 178–183.

Shahin, U., Yi, S.M., Paode, R.D., and Holsen, T. 2000. Long-term elemental dry deposition fluxes measured around Lake Michigan with an auto mated dry deposition sampler. Environ. Sci. Technol. 34, 1887–1892.

Shephard, M.W., McLinden, C.A., Cady-Pereira, K.E., Luo, M., Moussa, S.G., Leithead, A., Liggio, J., Staebler, R.M., Akingunola, A., Makar, P., Lehr, P., Zhang, J., Henze, D.K., Millet, D.B., Bash, J.O., Zhu,

L., Wells, K.C., Capps, S.L., Chaliyakunnel, S., Gordon, M., Hayden, K., Brook, J.R., Wolde, M., and Li, S.M. 2015. Tropospheric emission spectrometer (TES) satellite observations of ammonia, methanol, formic acid, and carbon monoxide over the Canadian oil sands: Validation and model evaluation. Atmos. Meas. Tech. 8, 5189–5211.

Shi, G., Chen, Z., Teng, J., Bi, C., Zhou, D., Sun, C., et al. 2012. Fluxes, variability and sources of cadmium, lead, arsenic and mercury in dry atmospheric depositions in urban, suburban and rural areas. Environ. Res. 113, 28–32.

Shotyk, W., Bicalho, B., Cuss, C.W., Duke, M.J.M., Noernberg, T., Pelletier, R., Steinnes, E., and Zaccone, C. 2016. Dust is the dominant source of "heavy metals" to peat moss (Sphagnum fuscum) in the bogs of the Athabasca Bituminous Sands region of northern Alberta. Environ. Int. 92–93, 494–506.

Singh, M., Jaques, P.A., and Sioutas, C. 2002. Size distribution and diurnal characteristics of particle-bound metals in source and receptor sites of the Los Angeles Basin. Atmos. Environ. 36, 1675–1689.

Slinn, W.G.N. 1984. Precipitation scavenging. In Atmospheric Science and Power Production, ed. D. Randerson. DOE/TIC-27601, p. 466-532, NTIS, Springfield VA.

Song, F. and Gao, Y. 2011. Size distributions of trace elements associated with ambient particular matter in the affinity of a major highway in the New Jersey–New York metropolitan area. Atmos. Environ. 45, 6714–6723.

Subhash, C., Monika, J.K., Ruchi, S., and Nahar, S. 2017. Chemical characteristics of trace metals in PM10 and their concentrated weighted trajectory analysis at Central Delhi, India. J. Environ. Sci. 55, 184–196.

Tasdemir, Y., and Kural, C. 2005. Atmospheric dry deposition fluxes of trace elements measured in Bursa, Turkey. Environ. Pollut. 138, 462–472.

Toscano, G., Moret, I., Gambaro, A., Barbante, C., and Capodaglio, G. 2011. Distribution and seasonal variability of trace elements in atmospheric particulate in the Venice Lagoon. Chemosphere, 85, 1518–1524.

Trzcinka-Ochocka, M., Jakubowski, M., Szymczak, W., Janasik, B., and Brodzka, R. 2010. The effects of low environmental cadmium exposure on bone density. Environ. Res. 110, 286–293.

Tsai, Y.I., Kuo, S.C., and Lin, Y.H. 2003. Temporal characteristics of inhalable mercury and arsenic aerosols in the urban atmosphere in southern Taiwan. Atmos. Environ. 37, 3401–3411.

Wang, J., Pan, Y., Tian, S., Chen, X., Wang, L., and Wang, Y. 2016. Size distributions and health risks of particulate trace elements in rural areas in northeastern China. Atmos. Res. 168, 191–204.

Wang, X., Sato, T., and Xing, B. 2006. Size distribution and anthropogenic sources apportionment of airborne trace metals in Kanazawa, Japan.Chemosphere. 65, 2440–2448.

Wang, X., Zhang, L., and Moran, M.D. 2014. Development of a new semi-empirical parameterization for below-cloud scavenging of size-resolved aerosol particles by both rain and snow. Geosci. Model Dev. 7, 799–819.

Wasiuta, V., Kirk, J.L., Chambers, P.A., Alexander, A.C., Wyatt, F.R., Rooney, R.C., and Cooke, C.A. 2019. Accumulating mercury and methylmercury burdens in watersheds impacted by oil sands pollution. Environ. Sci. Technol. 53, 12856–12864.

Willis, C.E., Kirk, J.L., Louis, V.L., Lehnherr, I., Ariya, P.A., and Rangel-Alvarado, R.B. 2018. Sources of methylmercury to snowpacks of the Alberta oil sands region: A study of in situ methylation and particulates. Environ. Sci. Technol. 52, 531–540.

Wright, L.P., Zhang, L., Cheng, I., Aherne, J., and Wentworth, G.R. 2018. Impacts and effects indicators of atmospheric deposition of major pollutants to various ecosystems – A review. Aerosol and Air Quality Research. 18, 1953–1992.

Wu, Y.C., Zhang, J.P., Ni, Z.X., Liu, S.L., Jiang, Z.J., and Huang, X.P. 2018. Atmospheric deposition of trace elements to Daya bay, South China Sea: fluxes and sources. Mar. Pollut. Bull. 127, 672–683.

Xiu, G., Cai, J., Zhang, W., Zhang, D., Büeler, A., Lee, S., Shen, Y., Xu, L., Huang, X., and Zhang, P. 2009. Speciated mercury in size-fractionated particles in Shanghai ambient air. Atmos. Environ. 43, 3145–3154.

Xu, J.W., Martin, R.V., Henderson, B.H., Meng, J., ¨Oztaner, Y.B., Hand, J.L., Hakami, A., Strum, M., and Phillips, S.B. 2019. Simulation of airborne trace metals in fine particulate matter over North America. Atmos. Environ. 214, 116883.

Xuan, J. 2005. Emission inventory of eight elements, Fe, Al, K, Mg, Mn, Na, Ca, and Ti in dust source region of East Asia. Atmos. Environ. 39, 813–821.

Yan, Q., Kong, S., Yan, Y., Liu, X., Zheng, S., Qin, S., Wu, F. Q., Niu, Z. Z., Zheng, H., Cheng, Y., Zeng, X., Wu, J., Yao, L.Q., Liu, D.T., Shen, G.F., Shen, Z.X., and Qi, S.H. 2022. Emission and spatialized health risks for trace elements from domestic coal burning in China. Environ. Int. 158,107001.

Yang, F., Mamun, A.A., Cheng, I., Qiu, X., and Zhang, L. 2023. Contributions of the oil sands sources to the ambient concentrations and deposition of particulate elements in the Canadian Athabasca oil sands region. Sci. Total Environ. 898, 165519.

Yang, F., Cheng, I., Xiao, R., Qiu, X., and Zhang, L. 2023. Emissions database development and dispersion model predictions of airborne particulate elements in the Canadian Athabasca oil sands region. Environ. Res. 220, 115223.

Yi, S.M., Lee, E.Y., and Holsen, T.M. 2001. Dry deposition fluxes and size distributions of heavy metals in Seoul, Korea during yellow-sand events. Aerosol Sci. Technol. 35, 569–576.

Zaveri, R.A., Easter, R.C., Fast, J.D., and Peters, L.K. 2008. Model for simulating aerosol interactions and chemistry (MOSAIC), J. Geophys. Res. 113, D13204.

Zaveri, R.A. and Peters, L.K. 1999. A new lumped structure photochemical mechanism for large-scale applications. J. Geophys. Res. 104, 30387–30415.

Zeng, Y., Wang, M., Zhao, C., Chen, S., Liu, Z., Huang, X., and Gao, Y. 2020. WRF-Chem v3.9 simulations of the East Asian dust storm in May 2017: Modeling sensitivities to dust emission and dry deposition schemes. Geosci. Model Dev. 13, 2125–2147.

Zhang, L., Fang, G.C., Liu, C.K., Huang, Y.L., Huang, J.H., and Huang, C.S. 2012. Dry deposition fluxes and deposition velocities of seven trace metals peciesat five sites in central Taiwan – a summary of surrogate surface measurements and a comparison with model estimations. Atmos. Chem. Phys. 12, 3405–3417.

Zhang, L., Gong, S., Jacob, P., and Barrie, L. 2001. A size-segregated particle dry deposition scheme for an atmospheric aerosol module. Atmos. Environ. 35, 549–560.

Zhang, L. and He, Z. 2014. Technical note: An empirical algorithm estimating dry deposition velocity of fine, coarse, and giant particles. Atmos. Chem. Phys. 14, 3729–3737.

Zheng, M., Guo, Z., Fang, M., Rahn, K.A., and Kester, D.R. 2005. Dry and wet deposition of elements in Hong Kong. Mar. Chem. 97, 124–139.

Zhu, J., Wang, T., Talbot, R., Mao, H., Yang, X., Fu, C., Sun, J., Zhuang, B., Li, S., Han, Y., and Xie, M. 2014. Characteristics of atmospheric mercury deposition and size-fractionated particulate mercury in urban Nanjing, China. Atmos. Chem. Phys. 14, 2233–2244.

Zwozdziak, A., Gini, M.I., Samek, L., Rogula-Kozlowska, W., Sowka, I., and Eleftheriadis, K. 2017. Implications of the aerosol size distribution modal structure of trace and major elements on human exposure, inhaled dose and relevance to the PM2.5 and PM10 metrics in a European pollution hotspot urban area. J. Aerosol Sci. 103, 38–52.

Appendix: Major modifications to WRF-Chem

1. Addition of elements

Firstly, the eight elements (Al, Ca, Fe, K, Mn, Si, Ti, and Zn) are added in the "registry.chem" where all simulated gaseous and aerosol species are defined. In this file, the name, the dimension, and the unit of species need definitions. As an example of Al, the definition is as below.

```
state real al_dry ikj misc 1 - rh "AL_DRY" "Al aerosol dry mass" "ug m^-3"
state real al_pmf ikj misc 1 - rh "AL_PMF" "Al fine aerosol dry mass" "ug m^-3"
state real al_pmc ikj misc 1 - rh "AL_PMC" "Al coarse aerosol dry mass" "ug m^-3"
state real peal_a01 ikjftb chem 1 - i0{12}rhusdf=(bdy_interp:dt) "peal_a01" "Al aerosol bin 01" "ug/kg-dryair"
state real peal_a02 ikjftb chem 1 - i0{12}rhusdf=(bdy_interp:dt) "peal_a02" "Al aerosol bin 02" "ug/kg-dryair"
state real peal_a03 ikjftb chem 1 - i0{12}rhusdf=(bdy_interp:dt) "peal_a03" "Al aerosol bin 03" "ug/kg-dryair"
state real peal_a04 ikjftb chem 1 - i0{12}rhusdf=(bdy_interp:dt) "peal_a04" "Al aerosol bin 04" "ug/kg-dryair"
state real peal_cw01 ikjftb chem 1 - i0{12}rhusdf=(bdy_interp:dt) "peal_cw01" "Al aerosol in cloud bin 01" "ug/kg-dryair"
state real peal_cw02 ikjftb chem 1 - i0{12}rhusdf=(bdy_interp:dt) "peal_cw02" "Al aerosol in cloud bin 02" "ug/kg-dryair"
state real peal_cw03 ikjftb chem 1 - i0{12}rhusdf=(bdy_interp:dt) "peal_cw03" "Al aerosol in cloud bin 03" "ug/kg-dryair"
state real peal_cw04 ikjftb chem 1 - i0{12}rhusdf=(bdy_interp:dt) "peal_cw04" "Al aerosol in cloud bin 04" "ug/kg-dryair"
```

The definition of anthropogenic emission and atmospheric deposition of eight elements are also added in the "registry.chem", as below (Al as an example).

```
# emission
state real e_pealj i+jf emis_ant 1 Z i5r "E_PEALJ" "EMISSIONS FINE Al AER" "ug/m3 m/s"
state real e_pealc i+jf emis_ant 1 Z i5r "E_PEALC" "EMISSIONS COARSE Al AER" "ug/m3 m/s"

# deposition
state real ddvelo1 ij misc 1 Z rh "DRYD_VELO1" "dry deposition velocity bin 1" "m/s"
state real ddvelo2 ij misc 1 Z rh "DRYD_VELO2" "dry deposition velocity bin 2" "m/s"
```

state	real	ddvelo3	ij	misc	1	Z	rh	"DRYD_VELO3"	"dry deposition velocity bin 3"	"m/s"
state	real	ddvelo4	ij	misc	1	Z	rh	"DRYD_VELO4"	"dry deposition velocity bin 4"	"m/s"
state	real	ddfluxal	ij	misc	1	Z	rh	"DRYD_FL_AL"	"dry deposition flux for Al"	"ng m^-2 s^-1"
state	real	ddfluxalt	ij	misc	1	Z	rh	"DRYD_FL_ALT"	"accumulated dry deposition flux for Al"	"ug m^-2"
state	real	qsrflxal	ij	misc	1	Z	rh	"QSRFLX_AL"	"dry deposition flux for Al"	"ng m^-2 s^-1"

A chemistry package named "chem" and an emission package named "emis_ant" in the "registry.chem" was defined and included all gaseous and aerosol species. In order to simulate the eight elements, these elements are added into the two packages, as yellow highlighted below.

```
# chemistry package definitions

chem:so2,sulf,no2,no,o3,hno3,h2o2,ald,hcho,op1,op2,ora1,ora2,nh3,n2o5,no3,pan,eth,co,ol2,olt,oli,tol,xyl,hono,hno4,ket,mgly,onit,csl,iso,ho,ho2,hcl,ch3o2,ethp,ch3oh,c2h5oh,par,to2,cro,open,op3,c2o3,ro2,ano2,nap,xo2,xpar,isoprd,isopp,isopn,isopo2,so4_a01,no3_a01,cl_a01,nh4_a01,na_a01,oin_a01,oc_a01,bc_a01,hysw_a01,water_a01,num_a01,so4_a02,no3_a02,cl_a02,nh4_a02,na_a02,oin_a02,oc_a02,bc_a02,hysw_a02,water_a02,num_a02,so4_a03,no3_a03,cl_a03,nh4_a03,na_a03,oin_a03,oc_a03,bc_a03,hysw_a03,water_a03,num_a03,so4_a04,no3_a04,cl_a04,nh4_a04,na_a04,oin_a04,oc_a04,bc_a04,hysw_a04,water_a04,num_a04,so4_cw01,no3_cw01,cl_cw01,nh4_cw01,na_cw01,oin_cw01,oc_cw01,bc_cw01,num_cw01,so4_cw02,no3_cw02,cl_cw02,nh4_cw02,na_cw02,oin_cw02,oc_cw02,bc_cw02,num_cw02,so4_cw03,no3_cw03,cl_cw03,nh4_cw03,na_cw03,oin_cw03,oc_cw03,bc_cw03,num_cw03,so4_cw04,no3_cw04,cl_cw04,nh4_cw04,na_cw04,oin_cw04,oc_cw04,bc_cw04,
num_cw04,peal_a01,peal_a02,peal_a03,peal_a04,peal_cw01,peal_cw02,peal_cw03,peal_cw04,peca_a01,peca_a02,peca_a03,peca_a04,peca_cw01,peca_cw02,peca_cw03,peca_cw04,pefe_a01,pefe_a02,pefe_a03,pefe_a04,pefe_cw01,pefe_cw02,pefe_cw03,pefe_cw04,pek_a01,pek_a02,pek_a03,pek_a04,pek_cw01,pek_cw02,pek_cw03,pek_cw04,pemn_a01,pemn_a02,pemn_a03,pemn_a04,pemn_cw01,pemn_cw02,pemn_cw03,pemn_cw04,pesi_a01,pesi_a02,pesi_a03,pesi_a04,pesi_cw01,pesi_cw02,pesi_cw03,pesi_cw04,peti_a01,peti_a02,peti_a03,peti_a04,peti_cw01,peti_cw02,peti_cw03,peti_cw04,pezn_a01,pezn_a02,pezn_a03,pezn_a04,pezn_cw01,pezn_cw02,pezn_cw03,pezn_cw04



#emission package definitions

emis_ant:e_iso,e_so2,e_no,e_co,e_eth,e_hc3,e_hc5,e_hc8,e_xyl,e_ol2,e_olt,e_oli,e_tol,e_csl,e_hcho,e_ald,e_ket,e_ora2,e_nh3,e_no2,e_ch3oh,e_c2h5oh,e_pm25i,e_pm25j,e_eci,e_ecj,e_orgi,e_orgj,e_so4i,e_so4j,e_no3i,e_no3j,e_so4c,e_no3c,e_orgc,e_ecc,e_pm_10,e_pealj,e_pealc,e_pecaj,e_pecac,e_pefej,e_pefec,e_pekj,e_pekc,e_pemnj,e_pemnc,e_pesij,e_pesic,e_petij,e_petic,e_peznj,e_peznc
```

2. Constants for elements

The aerosol chemistry module is determined as the Model for Simulating Aerosol Interactions and Chemistry (MOSAIC). MOSAIC requires some constants for aerosol properties (density, molecular weight,

and hygroscopicity) and their values (Table 2.2) are added in the “module_data_mosaic_asect”, as below (Al as an example).

```
real, parameter :: dens_peal_aer = 2.70        !! density
real, parameter :: mw_peal_aer  = 26.982       !! molecular weight
real, parameter :: hygro_peal_aer = 0.068      !! hygroscopicity
```

3. Emission and deposition

In order to add anthropogenic emissions for the eight elements, the mass and number emissions are modified to include the eight elements in the “module_mosaic_addemiss”, as below (Al as an example).

```
! compute anthropogenic mass emissions [(ug/m3)*m/s] for each species
! using the apportioning fractions
aem_peal= fr_aem_mosaic_f(n)*emis_ant(i,k,j,p_e_pealj)  +  fr_aem_mosaic_c(n)*emis_ant(i,k,j,p_e_pealc)

! compute number emissions
aem_num =   &
            (aem_so4/dens_so4_aer) + (aem_no3/dens_no3_aer) +   &
            (aem_cl /dens_cl_aer ) + (aem_msa/dens_msa_aer) +   &
            (aem_co3/dens_co3_aer) + (aem_nh4/dens_nh4_aer) +   &
            (aem_na /dens_na_aer ) + (aem_ca /dens_ca_aer ) +   &
            (aem_oin/dens_oin_aer) + (aem_oc /dens_oc_aer ) +   &
            (aem_bc /dens_bc_aer ) +   &
            (aem_peal/dens_peal_aer)
```

The dry deposition flux of the eight elements is calculated as a production of modeled element concentration and modeled dry deposition velocity. These dry deposition fluxes are prepared for output in the “dry_dep_driver”, as below (Al as an example). The wet deposition flux of the eight elements is calculated in the “module_wetscav_driver”, as below (Al as an example).

```
! dry deposition fluxes
ddfluxal(i,j)=chem(i,kts,j,lptr_peal_aer(1,1,1))/alt(i,kts,j)*ddvelo1(i,j) + &
              chem(i,kts,j,lptr_peal_aer(2,1,1))/alt(i,kts,j)*ddvelo2(i,j) + &
              chem(i,kts,j,lptr_peal_aer(3,1,1))/alt(i,kts,j)*ddvelo3(i,j) + &
```

```
                chem(i,kts,j,lptr_peal_aer(4,1,1))/alt(i,kts,j)*ddvelo4(i,j)
ddfluxal(i,j)=ddfluxal(i,j)*1000                ! ug/m2/s -> ng/m2/s
ddfluxalt(i,j)=ddfluxalt(i,j)+ddfluxal(i,j)*dtstep*0.001    ! ng/m2 -> ug/m2

! wet deposition fluxes
wdi_peal(ii,jj)  = - qsrflx(ii,jj,lptr_peal_aer(1,1,1))   &
                   - qsrflx(ii,jj,lptr_peal_aer(2,1,1))   &
                   - qsrflx(ii,jj,lptr_peal_aer(3,1,1))   &
                   - qsrflx(ii,jj,lptr_peal_aer(4,1,1))   &
                   - qsrflx(ii,jj,lptr_peal_aer(1,1,2))   &
                   - qsrflx(ii,jj,lptr_peal_aer(2,1,2))   &
                   - qsrflx(ii,jj,lptr_peal_aer(3,1,2))   &
                   - qsrflx(ii,jj,lptr_peal_aer(4,1,2))
wd_peal(ii,jj)   = wd_peal(ii,jj)   + wdi_peal(ii,jj)
```

4. Deposition sensitivity test

In the deposition sensitivity test, a semi-empirical formula (Eq. 2.7-2.9) developed by Wang et al. (2014) is used for wet deposition of the eight elements. This revision to the wet deposition is made in the "module_mosaic_wetscav", as below.

```
!   prepare sigmag_aer, the size distribution
    do ii = 1, ntype_aer
        nbins = nsize_aer(ii)
        dlo_sect(1,ii) = 3.90625e-6
        dhi_sect(nbins,ii) = 10.0e-4
        factor = log( dhi_sect(nbins,ii)/dlo_sect(1,ii) ) / nbins
        do iii = 2, nbins
            dlo_sect(iii,ii) = dlo_sect(1,ii) * exp( (iii-1)*factor )
            dhi_sect(iii-1,ii) = dlo_sect(iii,ii)
        end do
        do iii = 1, nbins
            sigmag_aer(iii,ii) = (dhi_sect(iii,ii)/dlo_sect(iii,ii))**0.289
        end do
    end do
```

```
!   calculate wet volume of one particle (cm^3)
        wet_volu_1p = dry_volu_1p * (wet_volu/dry_volu)
!   calculate wet radius (cm)
        pi = 3.1415926536
        ag0 = ( wet_volu_1p/1.333333/pi )**third



!  compute scavenging (1/s) in Wang et al. (2014)
     scavsumnum = 0.
     scavsumvol = 0.
     scavsumnumbb = 0.
     scavsumvolbb = 0.
     rainrate = pfx_inrain(i,k,j)*3600
     do iii = 1, na
               a = aaerosv(iii)
               dp = a*2.0*1.0E4      ! convert unit to um
               logdp = LOG10(dp)
               if ( dp .le. 2.0e0 ) then
                        LOG_A = a0 + a1*logdp + a2*logdp**2 + a3*logdp**3
                        B     = c0 + c1*logdp
               else
                        LOG_A = b0 + b1*logdp + b2*logdp**2 + b3*logdp**3 + b4*logdp**4 + b5*logdp**5 + b6*logdp**6
                        B     = d0 + d1*logdp + d2*logdp**2 + d3*logdp**3 + d4*logdp**4 + d5*logdp**5 + d6*logdp**6
               end if
               SC = 10**( LOG_A + B * LOG10(rainrate) )          ! SC: scavenging rate (1/s)
               scavsumnumbb = scavsumnumbb + SC*ynumaerosv(iii)
               scavsumvolbb = scavsumvolbb + SC*yvolaerosv(iii)
     end do
     scavsumnum = scavsumnum + scavsumnumbb            ! scavsumnum: scavenging rate (1/s) for number
     scavsumvol = scavsumvol + scavsumvolbb            ! scavsumnum: scavenging rate (1/s) for volume
```